Chemical Vapor Deposition of Aluminium Oxide (Al_2O_3) and Beta Iron Disilicide (β-$FeSi_2$) Thin Films

Von der Fakultät für Ingenieurwissenschaften, Abteilung Maschinenbau der
Universität Duisburg-Essen
zur Erlangung des akademischen Grades

DOKTOR-INGENIEUR

genehmigte Dissertation

von

Ali Eltayeb Muhsin
aus
Zliten / Libyen

Referent: Prof. Dr. rer. nat. habil Burak Atakan
Korreferent: Prof. Dr. Ing. Dieter Hänel
Tag der mündlichen Prüfung: (11.07.2007)

Abstract

Aluminium oxide thin films were deposited by metal-organic chemical vapor deposition (MOCVD) on stainless steel substrates, (AISI 304). The deposition was studied systematically in a hot-wall CVD reactor (HWR) at atmospheric pressure. The used precursors were aluminium acetylacetonate ($Al(acac)_3$) and synthetic air, which are nontoxic and easy to handle. The phase composition, surface morphology and chemical composition of the films were studied by XRD, SEM and EDX, respectively. The deposition starts at 350°C and the maximum growth rate occurs at a substrate temperature of 475°C. Increasing the furnace temperature beyond 500°C leads to depletion of the precursor and thus the maximum deposition rate is shifted towards the gas inlet. Films deposited at 500°C were transparent and amorphous. They consist mainly of Al and O, although the existence of aluminium hydroxides can not be excluded. Annealing at higher temperatures leads to crystallization and phase transformations: at 800°C γ-Al_2O_3 films are obtained and at 1115°C α-Al_2O_3 is formed. The films are stable up to 800°C, at higher temperature they are spalling.

Beta iron disilicide thin films (β-$FeSi_2$) were successfully deposited by low pressure metal-organic chemical vapor deposition (MOCVD) on silicon substrates, Si(100) using ferrocene ($Fe(C_5H_5)_2$) and TMS ($Si(CH_3)_4$) as precursors. These CVD experiments were performed for the first time in a Halogen Lamp CVD Reactor (HLR) designed for this investigation. By this design, a maximum set point temperature of 800°C and any temperature down to room temperature can be easily achieved and controlled. This control allows possible deposition of different films at different deposition temperature within the same experimental run.

Preparation of iron disilicide films by using a direct deposition technique (DDT) and a

step deposition technique (SDT) with later annealing were studied. In DDT ferrocene and TMS were supplied into the CVD chamber at the same time. For SDT each precursor was supplied separately in order to deposit an iron film followed by a silicon film, finally the iron silicide is formed in an annealing step. The phase composition, surface morphology and chemical composition of the films were studied by XRD, SEM and EDX, respectively.

Films deposited by DDT at 785-800°C and 30 mbar were transparent, amorphous, and well adhesive. EDX analysis shows that the films consist of silicon and very small amount of iron. The films prepared by SDT were formed from crystalline iron films deposited on the substrate at 700°C and amorphous silicon films deposited on the surface of the iron films at 800°C. Also, iron films and silicon films were deposited separately on silicon and steel substrates respectively before performing the SDT. It was found that the iron films can not be deposited directly from ferrocene because of the presence of high level of carbon in the film. Therefore, the carbon containing films were treated with hydrogen in order to produce pure films. After purification XRD analyses show that the films are crystalline (α-Fe). Amorphous silicon films were deposited at 800°C and 30 mbar. A mixture of iron disilicide phases, FeSi, $FeSi_2$ and β-$FeSi_2$ can be prepared by annealing the SDT deposited films 2 hr at 900-950°C.

Dedication

TO
My mother, Fatima
My brothers and my sister
My wife and my sons
My daughter Fatima
And in loving memory of my father
Eltayeb Muhsin

Ali Eltayeb Muhsin

Acknowledgments

I wish to express my sincere gratitude to my supervisor Prof. Dr. rer. nat. Burak Atakan , for the may inspirational discussions and guidance throughout this work.

While many other persons have contributed either directly or indirectly to this work, I should like to mention some of them by names: Dr. C. Pflitsch and Dipl. Eng. D. Viefhaus, many thanks for their continued interest and support.

Special thanks to all academic and technical staff of thermodynamics (institute for combustion and gasdynamics) for their many helpful suggestions and technical supports.

Another special gratitude owes to my wife, from whom I always get support and lovely care.

Duisburg, July 2007

Ali Eltayeb Muhsin

Table of Contents

List of Figures

Chapter 1

Introduction

1.1 Thin Films Deposition Processes:

Thin films are extensively used in many industrial applications and can be prepared as resistors, insulators, conductors and semiconductors. They are technologically important, especially in the fields of microelectronics, nanotechnology, optics, and protective coatings. Excellent textbooks and reviews about the fundamentals of thin films deposition and examples of various processes are readily available today [1 to 6]. Various deposition methods such as Physical vapor deposition (PVD) and chemical vapor deposition (CVD) are used to produce thin films. PVD is a process by which a thin film of material is deposited on a substrate by converting the source material of the film into vapor by physical means. The vapor is transported across a region of low pressure from its source to the substrate and the vapor undergoes condensation on the substrate to form the thin film. The most widely used methods of accomplishing PVD of thin films are by evaporation, sputtering and molecular beam epitaxy (MBE). The CVD process is a technique where gases or vapors of chemical compounds of the elements which shall be forming the film are introduced into a reaction chamber; a solid deposit film is obtained via chemical reactions on a substrate.

1.2 Chemical Vapor Deposition:

Chemical vapor deposition is a widely used method for depositing thin and high quality films with well defined chemical composition and structural uniformity. In a

typical chemical vapor deposition process the substrate is exposed to one or more volatile precursors, which react and/or decompose on the substrate surface to produce the desired deposit. The activation energy for the reaction can be overcome by various methods, where the most common approach is to heat the substrate. Volatile byproducts are generally also produced, which are removed by the gas flow through the reaction chamber. The main benefit derived by a chemical vapor deposition process is the resulting uniform, adherent and reproducible films. Often the main disadvantages lie in the need to resort to dangerous and toxic chemicals to obtain the desired deposition along with the high temperatures necessary for some of the reactions. CVD technology opens possibilities to prepare new materials and structures for various applications for many industrial products. With CVD, it is possible to produce most metals, many nonmetallic elements, as well as large number of compounds including carbides, nitrides, oxides, silicides, and many others. This technology is now an essential factor in the coating of tools, bearings, corrosion applications and other wear resistant parts, in the manufacture of semiconductors and other electronic components, and in many optical and optoelectronic applications [1-3].

The most common chemical vapor deposition techniques are thermal chemical vapor deposition (TCVD), plasma-enhanced chemical vapor deposition (PECVD) and laser chemical vapor deposition (LCVD). In TCVD the vapor of the precursor forms a deposit when it comes into contact with a hot substrate. In PECVD the vapor of the precursor is decomposed in a plasma. PECVD process allows depositions at lower substrate temperatures. In LCVD the precursor is decomposed in a photochemical process or by pyrolysis when it comes into contact with a substrate which has been heated by laser [1, 2, 4].

Several versions of the chemical vapor deposition processes are in wide use and are frequently referenced in the literature, such as: Metal-Organic chemical vapor deposition (MOCVD), Atmospheric Pressure chemical vapor deposition (APCVD), Low Pressure chemical vapor deposition (LPCVD), Rapid Thermal chemical vapor deposition (RTCVD), Plasma Enhanced chemical vapor deposition (PECVD), Atomic Layer chemical vapor deposition (ALCVD), Ultra-High Vacuum chemical vapor deposition (UVCVD), laser chemical vapor deposition (LCVD), and so on [1,2].

The characterization of the deposited films is crucial and can be carried out with different methods and devices that allow to identify the film and its properties, such as: film thickness, surface morphology, phase composition and chemical compositions. Optical microscopes, scanning electron microscopes (SEM) with energy dispersive X-ray spectrometers (EDX), X-ray diffractometers (XRD) are among these instruments. Beyond these categories there are individual film properties (e.g. adhesion, hardness, stress, electrical conductivity, mobility etc.), which are specific to particular applications and can be measured by different methods [3].

1.3 Scope of the Present Work:

In summary, the goals of this thesis are as follows: Characterization of the influence of deposition parameters on deposition of aluminum oxide (Al_2O_3) thin films on stainless steel substrates (AISI 304) in a hot wall reactor (HWR) at ambient pressure using aluminium acetylacetonate as a source material. Aluminum oxide, commonly referred to as alumina, is a material of choice wherever hardness, wear resistance and thermal and chemical stability are desired. Attractive mechanical and chemical properties of Al_2O_3 make it possible for use in wide range of engineering fields. Alumina thin films in various forms are used in semiconductors devices as protective

coatings and insulating layer, as wear resistant coatings and as sensors. [1, 2, 8, 28, 29, 34, 35]. Alumina films can be deposited in amorphous, metastable and stable crystalline phases. However, amorphous and metastable phases transform to the thermodynamically stable corundum phase (α-Al_2O_3) which is the hardest phases and chemically very inert [34 to 37].

The second goal was to design and build a halogen lamp reactor (HLR), that utilizes halogen lamps as substrate heaters and use of this reactor for the deposition of beta iron disilicide (β-$FeSi_2$) thin films. β-$FeSi_2$ films are deposited on silicon substrates Si(100) by using ferrocene ($Fe(C_5H_5)_2$) and tetramethylsilane ($Si(CH_3)_4$, TMS) as source materials. Beta iron disilicide has attracted much interest as a semiconductor material in many engineering fields, because it is composed of nontoxic elements that exist in great abundance on earth [54]. Crystalline β-$FeSi_2$ is one of the most attractive materials for thermoelectric devices, solar cells, and optical fiber communication because of its high thermoelectric power, high absorption coefficient of 10^5 cm^{-1}, and suitable energy band gap of about 0.85 eV [56]. Recently, it has been reported that an amorphous phase of iron disilicide ($FeSi_2$) is a promising semiconductor material too [52], it has a similar band gap value of 0.85-0.95 eV [52], and it can be deposited on any surface and hence there is a promising potential for applications of iron disilicide in large electronics and for fabrication of solar cells [54, 56].

1.4 Thesis Outline:

The thesis is organized as follows: In the next chapter, Chapter 2, CVD theory is presented concentrating on CVD processes used in the present work and theory of instruments used for film analysis. In chapter 3 the experimental set-up is described, a HWR used for deposition of Al_2O_3 films and the design and construction of a halogen

lamp reactor used for deposition of β-$FeSi_2$. More attention is given to the design of the halogen lamp heater in section 3.1.3.2. Chapter 4 and 5 will provide information about the earlier studied literature, deposition conditions, results, films analyses and discussions about preparation of Al_2O_3 and β-$FeSi_2$ films, respectively. The thesis ends with conclusions and remarks in Chapter 6.

Chapter 2

Chemical Vapor Deposition Theory

2.1 CVD System:

Several forms of CVD are in wide use and are frequently referenced in the literature; among them is metal-organic chemical vapor deposition (MOCVD). MOCVD is a process used for deposition of thin films using volatile metalorganic or organometallic precursors. This process offers relatively low deposition temperatures and uniform deposition over large areas; both are significant process advantages, while most metals and their compounds are only volatile at very high temperature.

CVD systems may be classified according to the reaction chamber pressure as atmospheric pressure (APCVD) or low pressure (LPCVD). Omitting the usage of expensive vacuum equipment, easy process control, large area uniformity and having a simple continuous process are some advantages of the APCVD process. LPCVD, generally provides deposits with greater uniformity, better step coverage, and improved quality, having pressure as a further independent process variable.

In the present study, the MOCVD technique has been employed to deposit Aluminium oxide (Al_2O_3) and beta iron disilicide (β-$FeSi_2$) thin films. Aluminum acetylacetonate is used as a precursor to deposit Al_2O_3 thin films. The deposition is performed at atmospheric pressure in a hot wall reactor. Tetramethylsilane and ferrocene are chosen as precursors for β-$FeSi_2$ films. The deposition is performed at low pressure in a cold wall reactor using halogen lamps as substrate heaters.

In general, typical CVD systems mainly require chemical sources, controllers for setting film parameters, reaction chamber and energy sources.

2.1.1 Chemical Sources:

Chemical sources may be classified as: Inert gases such as argon and nitrogen, which are used as carrier gases of a precursor vapor. Reactant gases are required such as oxygen for oxidation or hydrogen for hydrogenation or reduction, (producing volatile hydrocarbon compounds). Precursors, the source material of the deposits, which should be thermally stable at room temperature and volatile at low temperatures. They must exhibit sufficient thermal stability to be synthesized, handled and then to be evaporated prior to the deposition process. A low evaporation temperature is especially an important factor for low temperature deposition. Mass flow controllers are used to control and mix the amount of gases fed to the reaction chamber during the deposition process.

2.1.2 Energy Sources:

Sources of energy are required for evaporation of the solid and liquid precursors and heating of the substrate in order to activate the chemical reaction in the CVD processes.

2.1.2.1 Vaporization of Precursors:

One of the essential prerequisite of CVD process is to create an appropriate vapor or gas mixture from the volatile precursors and to flow it over the substrate at an appropriate temperature. If the precursor is a gas, then an appropriate gas mixture can be formed using standard mass flow controllers. If the precursor is a liquid or a solid, an appropriate amount of the precursor is filled in a bubbler. The bubbler is heated if necessary in order to evaporate the precursor. The vapor is transported to the reaction

chamber by passing flow of an inert carrier gas through the bubbler. The inert gas saturated with the vapor while bubbling through the liquid or pass through the solid precursors. The transport line of the source gases should be heated slightly above the vaporization temperature in order to prevent the precursor vapor from recondensation.

A high vapor pressure is necessary in order to provide a high concentration of the species in the vapor phase to produce a reasonable deposition rate. The vapor pressure P_v of the precursor may be calculated from the Clausius-Clapeyron equation:

$$P_v = P_0 e^{-\frac{\Delta H}{R}\left(\frac{1}{T_v}-\frac{1}{T_0}\right)} \qquad (2.1)$$

Where ΔH is the enthalpy of evaporation, P_0 is the vapor pressure at reference temperature T_0, T_v is the vaporization temperature and R is the gas constant.

The partial pressure of the precursor can be calculated if saturation is assumed.

2.1.2.2 Substrate Heaters:

The activation energy for the reaction can be overcome by various methods, where the most common approach is thermal chemical vapor deposition (TCVD). In addition, some other methods are used such as photons from a light source, photo thermal chemical vapor deposition (PTCVD) or from a laser, laser assisted chemical vapor deposition (LCVD) as well as energetic electrons in plasmas, plasma enhanced chemical vapor deposition (PECVD). In TCVD systems, heating the substrate can be accomplished by any one of three heat transfer methods, conduction, convection and radiation. Heating a substrate by convection or conduction heat transfer requires a physical contact between the heating source and the substrate, while radiative heat transfer occurs when a temperature difference exists between the substrate and the heating source without any physical contact. There are two types of TCVD reactors,

classified according to the substrate heating process, a hot wall reactor (HWR) and cold wall reactor (CWR). If the entire reactor is heated, it is a HWR, if only the substrate is heated, it is a CWR. In a HWR, heating of the substrate is most often accomplished by resistive heaters surrounding the CVD chamber. Combinations of several heating elements make it possible to produce various temperature gradients along the CVD chamber, in order to control CVD processes occurring in various zones of the reactor. In a CWR, the substrate is the only intentionally heated area. The reactor walls are kept at lower temperature than the substrate. Heating only the substrate rather than the gas or chamber walls helps to reduce unwanted gas phase reactions that can lead to particle formation. Different heaters such as resistive heaters, ceramic heaters, high frequency induction coils, high intensity radiation lamps (halogen lamps), etc. are commonly used as substrate heating sources for both types of reactors, HWR and CWR. Quartz halogen lamps efficiently convert electrical energy into radiated heat (light), at low 15 to 25 lumens per watt. Easy to adjust and replace the lamps and to control the input power allows flexibility for temperature variability as needed for the process.

Depositing of a film is very dependent on substrate temperature in order to induce an appropriate chemical reaction occurring on the surface of the substrate. Some films require low deposition temperature while others require high deposition temperature, depending on the phase diagram. Also the crystallinity of a film depends on temperature, while an amorphous phase is generally deposited at low temperature a crystalline phase needs higher temperature.

2.2 CVD Process:

CVD is a process by which a thin film of material is deposited on a substrate

according to the following general sequence of steps, see Figure 2.1:

1. Mass transport of the vapor of precursors and reactant gases from the reactor inlet to the deposition zone.
2. Chemical reactions in the gas phase leading to new reactive species and byproducts.
3. Mass transport of the reaction products through the boundary layer to the surface of the substrate.
4. Formation of desired films on the substrate surface from chemical reaction occurs on or near the substrate surface including: adsorption of the reaction products, surface diffusion of the adsorbed products and surface reaction at the substrate surface.
5. Remove of by-product gases from the CVD chamber through the exhaust system.

The transport phenomena and kinetics are the main concepts of CVD theory and the optimal conditions for CVD reactions are based on these concepts.

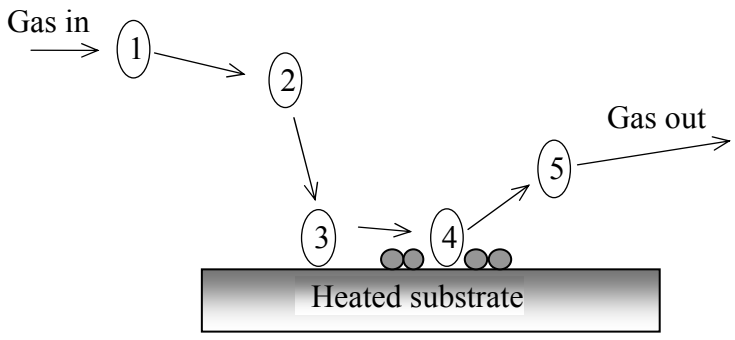

Figure 2.1 Sequence of CVD steps.

2.2.1 Kinetics and mass transport:

The goal in the transport process is to provide a uniform and constant gas phase

supply of the precursor species near the deposition surface. The gas phase transport of the precursor to the deposition site greatly depends on the type and design of the CVD reactor system. The rate of mass transport is dependent on the concentration of the reactants, thickness of the boundary layer and diffusivity of active species. These factors are influenced by the deposition temperature, pressure, gas flow rate, gas property and geometry of the reactor [5].

The CVD processes are carried out from atmospheric pressure to high vacuum. At low pressure CVD, the chemical reactions become more important than the effect of gas flow rates, gas viscosity, and reactor geometry on the growth rate and film composition.

The gas phase reactions either may lead to high purity film through the formation of an active precursor compound or may lead to impure films through unwanted particle formation. These particles, which are relatively large, may cause nonuniformity and poor surface morphology of the deposited films. Adsorption of reaction products, such as carbon and hydrogen because of pyrolysis ligands, onto the surface of the substrate, diffuse to the growth sites, incorporate into the growing film and desorption of its ligand components produce impure films. Gas phase reactions may be minimized by reducing the pressure so that the probability of intermolecular collisions prior to the adsorption on the substrate is strongly reduced.

The deposition temperature varies from one CVD process to another depending on the required decomposition temperature of precursors and the phase of the desired deposited film (amorphous, polycrystalline or crystalline phase).

Fluid flow is often measured by Reynolds number, $Re = (dv\rho/\mu)$, Where: d = characteristic length of the system (diameter of pipe), ρ = density, v = velocity and μ = viscosity of vapor. Laminar flow is often applied in CVD to ensure controllable

transport phenomena in the reaction area, depends strongly on geometry.

The boundary layer (BL) is generally defined as the distance where the velocity of the gas increases from zero at the substrate surface to 99% of the bulk value [5]. The thickness of a boundary layer is related to the Re, where a decrease in Re results in a thicker boundary layer.

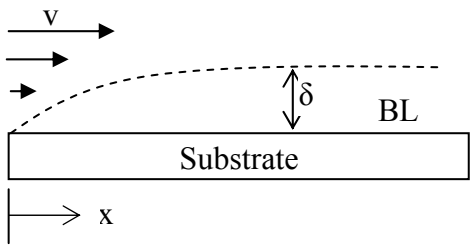

Figure 2.2 A schematic diagram of boundary layer on a substrate surface.

Once the reactants approach the substrate molecules can be adsorbed on the surface and a number of different reactions can occur. The atoms on the surface (produced out of the precursor) diffuse along the substrate surface through the boundary layer and form the desired product. Since the gas flows are continuous, the film thickness will increase with time.

With a high degree of simplification the deposition rate (D_{rate}) of CVD processes, if it is a first order reaction (only decomposition), is related to

$$D_{rate} = k_S \; C_S \tag{2.2}$$

or it is

$$D_{rate} = k \; C_S C_R = k' \; C_S \tag{2.3}$$

with $C_R >> C_S$.

Where k_S and k' is the chemical surface reaction rate constants and C_s is the reactant

concentration. The reaction rate coefficient as described by Arrhenius equation is

$$k_S = k_0 \exp\left(-E_a / RT\right) \qquad (2.4)$$

Where k_0 is a reaction constant, E_a is activation energy of the reaction, R is gas constant and T is the reaction temperature.

If $\ln D_{\text{rate}}$ is plotted versus 1/T (Arrhenius plot), the behavior of Figure 2.3 of deposition rates provides two limiting regions: the surface reaction rate limited region and mass transport limited region. In the surface reaction limited case, the deposition rate is directly proportional to the surface reaction rate and changes rapidly with temperature (temperature dependent), while change in temperature has a small effect on the deposition rate in the mass transport limited case (temperature independent), which is strongly dependent on the inlet gas flow rate.

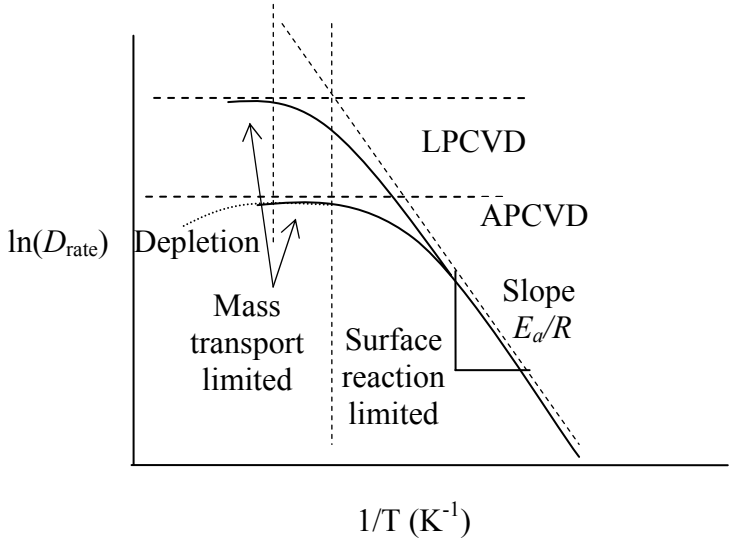

Figure 2.3 Arrhenius plot behavior of deposition rate.

The concentration of the precursor in the reactor is a key factor in both limiting cases. The precursor concentration is equal to the inlet flow concentration when the resident

time is short compared to the time required to consume the species (i.e. condition of high concentration) this condition is related to the surface reaction limited case. The concentration of precursor is much smaller than the inlet concentration when the consumption rate is high (i.e. conditions of slow flow or fast reaction rate) this condition is related to the mass transport limited case. The residence time (dwell time) is the average time that a gas molecule spends in the CVD chamber. It is a function of the reactor and inlet volumetric flow. The consumption time is the average time that a molecule survives before it is incorporated into the deposited film [6].

APCVD is often mass transport limited at high temperatures. Further increasing in the temperature may lead to depletion of the reactants. The concentration of the precursor is a function of deposit position in the reactor, since the gas mixture is initially saturated with precursors but the partial pressure of the reactants is reduced as they are consumed. This factor indicates that the growth rates should be higher closer to the reactor inlet and smaller as the distance from the reactor inlet increases due to strong depletion. Operating of CVD at low pressure increases the surface reaction limited region, Figure 2.3, so higher deposition rates can be achieved as the reduction in pressure would increase diffusion coefficients thus increasing the flux of reactants to the surface where they react quickly

2.3 Analytical Methods:

The deposited film has to be analyzed in order to identify its physical and chemical properties where these properties are important in industrial applications. Morphology, phase composition and chemical composition are investigated in this study using techniques that include X-Ray diffraction (XRD), scanning electron

microscopy (SEM) and energy dispersive X-ray spectroscopy (EDX).

2.3.1 X-Ray Diffraction:

The films may be deposited in amorphous or crystalline phases. The atoms of a crystalline film are arranged in a regular pattern while the atoms of an amorphous film are arranged in a random way. The arranged atoms of a crystalline film form a series of parallel planes separated from one another by a distance *d*, which varies according to the nature of the material. For any crystal, planes exist in a number of different orientations each with its own specific distance *d*. X-Ray Diffraction (XRD) identifies the phase composition of the analyzed films if they are crystalline and polycrystalline. Amorphous films can not be analyzed by this method because of their random arrangement of atoms in the film.

X-ray diffractometers consist of an X-ray generator, a goniometer (angle-measuring device), a sample holder, and an X-ray detector. X-rays are generated within a sealed tube under vacuum. A current is applied that heats a filament within the tube. A high voltage is applied within the tube. This high voltage accelerates the electrons, which then hit a target, often made of copper (λ = 1.5418 Å). When these electrons hit the target, X-rays are produced. The emitted wavelength is characteristic for elements of that target. These X-rays are collimated and directed onto the substrate. The X-ray beam hits the sample and the detector records the X-ray intensity diffracted at the substrate. The distances between the adjacent lattice planes can be calculated by applying Bragg's Law (see Figure 2.4)

$$n\lambda = 2d\sin\theta \qquad (2.5)$$

where n is the order of diffraction (0,1,2,3,…), λ is the wavelength of the incident X-ray beam, d is the distance between adjacent lattice planes, and θ is the angle of

incidence of the X-ray beam. The diffraction angle *2θ* is equal to twice the incident angle *θ*. The goniometer is motorized and moves through a range of *2θ* angle. Each time the Bragg condition is satisfied, the detector measures the intensity of the reflected radiation. An X-Ray detector records the diffracted beam intensity as a function of the angle (2θ). Every crystalline material will give a characteristic diffraction pattern, thus the diffraction pattern acts as a unique "fingerprint". The plot of XRD patterns used to identify the type of material by comparing them with standard XRD patterns database.

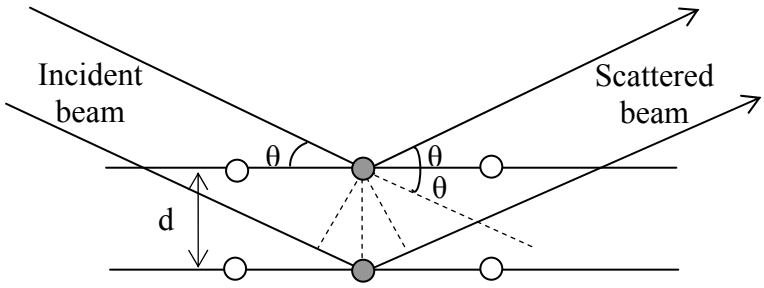

Figure 2.4 Bragg's Law

2.3.2 Scanning Electron Microscopy:

The surfaces morphologies of the films were analyzed by Scanning Electron Microscopy (SEM). The SEM is a microscope that uses electrons rather than light to form an image. There are many advantages of using the SEM instead of a light microscope such as ease of sample observation, higher magnification, larger depth of sharpness and greater resolution. The principle of the SEM is to focus a beam of primary electrons onto a sample, and to collect secondary electrons scattered from the sample. An image is created by scanning the sample surface point by point by the

focused beam of electrons and to reconstruct the image from the scattered intensities. The sample is placed inside a vacuum chamber. After the chamber is evacuated, an electron gun emits a beam of high energy electrons. This beam travels downward through a series of magnetic lenses designed to focus the electrons to a very fine spot. A set of scanning coils moves the focused beam back and forth across the sample, row by row. As the electron beam hits each spot on the sample, secondary electrons are loosed from its surface. A detector counts these electrons and sends the signals to an amplifier. The final image is built up from the number of electrons emitted from each spot on the sample.

2.3.3 Energy Dispersive X-ray Spectroscopy:

The chemical composition of deposited films were analyzed using Energy Dispersive X-ray spectroscopy (EDX) attached to the SEM. EDX is a micro-analytical technique that uses the characteristic spectrum of X-rays emitted by the sample after excitation by high energy electrons to obtain information about its elemental composition. The electron beam of an SEM is used to excite the atoms in the surface of the sample. The auxiliary energy dispersive X-ray detector attachment to an SEM permits the detection and identification of the X-rays produced by the impact of the electron beam on the sample thereby allowing qualitative and quantitative elemental analysis. A quantitative analysis is possible using appropriate calibrations and a suited computer software. Elements of low atomic number are difficult to detect by the EDX such as hydrogen. Some elements contaminated the surface of the film could be also detected by the EDX detector while this method is considered as a near surface elemental analysis technique.

Chapter 3

Experimental Set-up

3.1 CVD Systems:

CVD is a widely used method for depositing thin films of a large variety of materials. In a typical CVD process, reactant gases are transported to the substrate surface where a thermal reaction/deposition occurs. Reaction byproducts are then exhausted out of the system. This process required source chemical materials such as inert and reactant gases. Thermal evaporation system is required if the precursor is not a gas. An appropriate used flow of the reactant gases are controlled by mass flow controller and feed into to the reaction chamber through a feed line system. The film is deposited on a substrate placed on a reaction chamber where the pressure varies from atmospheric to vacuum. In order to activate the chemical reaction the substrate is heated. The substrate temperature is controlled and monitored using temperature sensors. Vacuum pump is used in low pressure process and pressure gages are used to control the pressure in the reactor. Figure 3.1 and 3.2 show the schematic diagrams of the two different used CVD systems.

Depositions of aluminium oxide (Al_2O_3) and beta iron disilicide (β-$FeSi_2$) thin films were investigated. Al_2O_3 films were deposited from aluminum acetylacetonate on stainless steel substrate in a HWR by atmospheric pressure CVD process, Figure 3.1. β-$FeSi_2$ films were deposited from tetramethylsilane and ferrocene on silicon substrates in a CWR, using a bank of halogen lamps as a substrate heater by low pressure CVD process, Figure 3.2.

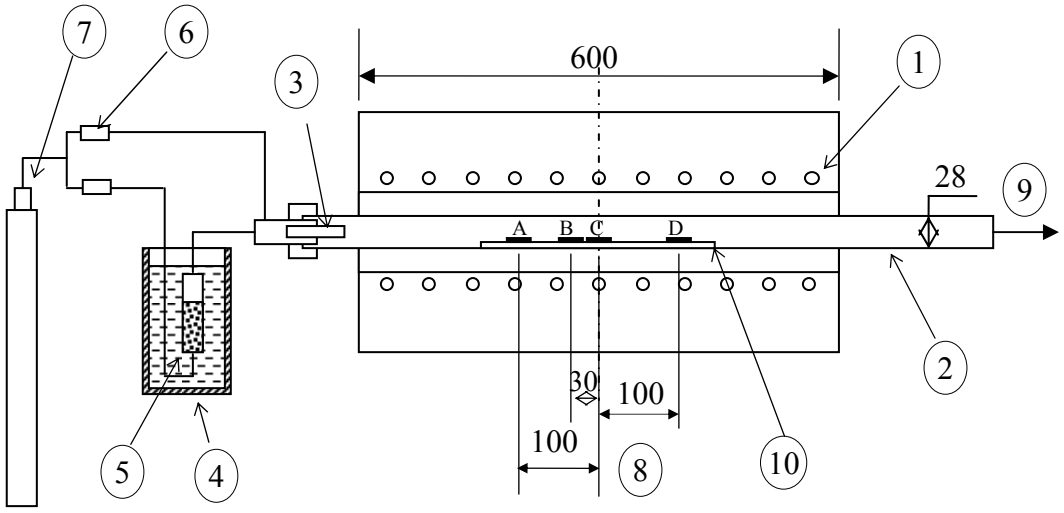

Figure 3.1 A schematic diagram of CVD-HWR system used for deposition of Al_2O_3 thin films: (1) heating coils, (2) reaction chamber, (3) nozzle, (4) thermo bath, (5) $Al(acac)_3$ evaporator, (6) mass flow controller, (7) synthetic air, (8) substrates positions, (9) exhaust and A,B,C and D are the substrates positions, (10) stainless steel bar.

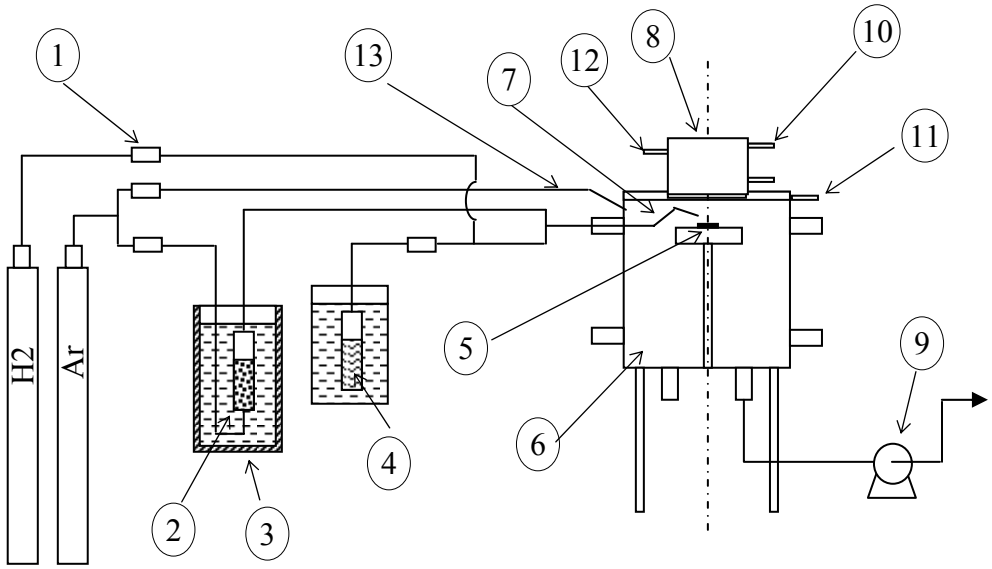

Figure 3.2 A schematic diagram of HLR-CVD system used for deposition of β-$FeSi_2$ thin films: (1) mass flow controller, (2) ferrocene evaporator, (3) thermo bath, (4) TMS evaporator, (5) substrate position, (6) reaction chamber, (8) halogen lamp heater, (9) vacuum pump, (10) N_2 flow cooling lamps connection, (11) chilled air cooling window connection, (12) reflector cooling water connection, (13) Argon flow to the window protection nozzle.

3.1.1 Precursors:

Three metalorganic precursors are used in the present work, aluminum acetylacetonate ($Al(acac)_3$, $Al(C_5H_7O_2)_3$) to create aluminum oxide films (Al_2O_3), ferrocene ($Fe(C_5H_5)_2$) to create iron (Fe), tetramethylsilane ($Si(CH_3)_4$, TMS) to create silicon films (Si). The growth of some films may requires more than one precursor, both $Fe(C_5H_5)_2$ and TMS are used for deposition of beta iron disilicide films (β-$FeSi_2$). Aluminum acetylacetonate, (purity 99%, Strem Chemicals Inc.), is a white solid powder at room temperature and has a melting point of 192°C [39]. It decomposes at temperature around 247°C [40]. It is commercially available, inexpensive, easy to handle and stable under atmospheric conditions. Different vapor pressures are reported in literature, e.g. 4.35 mbar at 150°C [41] and 0.3 mbar at 132°C [43]. Also reported, the enthalpy of sublimation at standard conditions is varying between 23.4 kJ/mol and 121.7 kJ/mol [42].

Ferrocene, $Fe(C_5H_5)_2$, is a solid orange/yellow powder stable in air and non toxic. It has a vapor pressure of 0.0133 mbar at 30°C [76]. Enthalpies of sublimation at different temperatures are available from the NIST webbook (72.5 kJ/mol at 292-300 K and 70.3 kJ/mol at 294-302 K) [42] and were also reported by Siddiqi as (72.659 ± 800 kJ/mol at 295-325 K) [50]. A high vaporizing temperature is required for increasing the vapor pressure. Since it is thermally stable, relatively high pyrolysis temperatures of up to 500°C are needed at which auto-catalytic decomposition reaction occurs in the gas phase and leads to the formation of a black powder, which primarily consists of iron contamination by graphitic carbon and iron carbide Fe_3C [76].

Tetramethylsilane, TMS, is a colorless liquid material, harmful for skin, eye and respiratory irritant. It has a low boiling temperature of around 26°C [42] and a high

vapor pressure of 785 mbar at 20°C. TMS is not corrosive compared with silicon chloride and needs less transport and less care compared with silane; silicon chloride and silane being the alternative precursors for the preparation of silicon films.

Aluminum acetylacetonate and ferrocene were sublimated in a fluidized bed evaporator at specific temperatures in order to increase their vapor pressures. TMS was filled into a glass bubbler and freezed by immersing the bubbler into a container filled with liquid nitrogen. Freezing of TMS was done in order to evacuate the bubbler so that while thawing, the remaining air in the TMS was pumped off. TMS was evaporated at room temperature. The amount of precursor vapor used during the deposition process is controlled by a digital mass flow controller in the range of standard liter per minute (slm) or standard cubic centimeter per minute (sccm), as required.

3.1.2 Substrates:

Two different kinds of substrates were used. Stainless steel pieces 20 x 30 mm in size and 1 mm in thickness cut from a stainless steel, (AISI 304, DIN 1.4301), sheet. Silicon pieces 20 x 30 mm in size or smaller and 0.5 mm in thickness cut from a (100)-oriented silicon wafer. The substrates were carefully cleaned by ethanol and supersonically in a water bath then dried and weighed before deposition.

3.1.3 CVD Reactors:

Description of a conventional HWR used for deposition of Al_2O_3 films and design of a halogen lamp reactor HLR used for deposition of β-$FeSi_2$ films are presented in the next sections.

3.1.3.1 Hot-Wall Reactor (HWR):

The furnace of the HWR described in this section was purchased from Heraeus (Type RE 1.1, 230 V, 14.2 A, 3.3 kW). The reactor was home build also as part of this work. It was used for deposition of Al_2O_3 films at atmospheric pressure. The schematic diagram of the reactor is shown in Figure 3.1. It is a horizontal electrically heated tube furnace with a length of 600 mm. The CVD chamber is a ceramic tube with an inner diameter of 28 mm and 1000 mm length embedded in the heated tube furnace. The supply tubes for the flow of precursor vapor and the reactant gases are stainless steel tubes with inner diameters of 4 mm. The nozzle is simply a ceramic tube with inner diameter of 10 mm connected to one end of the CVD chamber, the other end of the tube is connected to an exhaust gas line.

3.1.3.2 Temperature Distribution in the HWR:

The furnace control temperature is monitored and controlled by K type thermocouples. The maximum design temperature of the furnace is 1000°C. The temperature within the reactor is not constant over the whole heated length, but has a typical temperature profile of a single zone tube furnace. The actual furnace temperature distribution profile was measured at atmospheric pressure and different furnace control temperatures of 400, 500 and 600°C without any flow supplied to the reactor and plotted versus the furnace length in Figure 3.3. The second measurement was done with supplying a synthetic air flow of 2.0 standard liters per minute (slm), this amount was also used later for deposition of Al_2O_3 (chapter 4). The result was illustrated in Figure 3.4. The temperature distribution has a parabolic profile with a maximum furnace temperature at the center of the furnace, (isothermal zone). The gas flow changed the temperature profile only slightly, the maximum temperature

dropped by approximately 10°C. The conclusions is that the actual furnace temperatures profiles which are directly related to the deposition temperatures or to the substrates temperatures are slightly below the furnace control temperatures, (e.g. at position 300 mm, air flow of 2.0 slm and 500°C furnace control temperature the actual furnace temperature is 482°C).

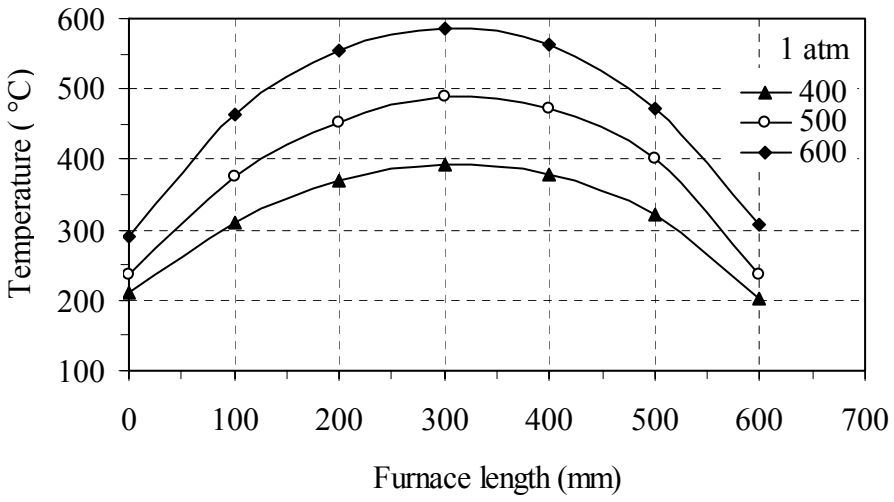

Figure 3.3 Actual furnace temperatures profiles at furnace control temperatures of 400, 500 and 600°C, atmospheric pressure and no gas flow.

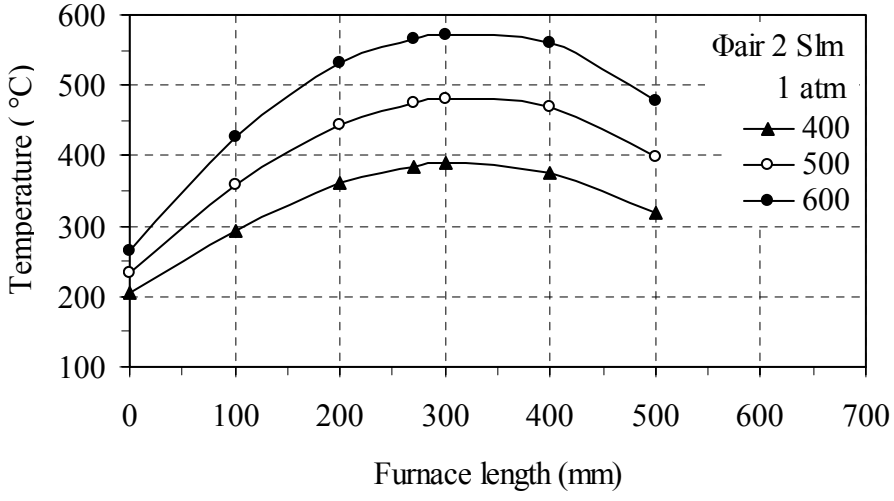

Figure 3.4 Actual furnace temperatures profiles at furnace control temperatures of 400, 500 and 600°C, atmospheric pressure and 2.0 slm synthetic air flow.

3.1.3.3 Halogen Lamp Reactor (HLR):

One of the most important applications of using halogen lamps in thin films processes is a heating substrate source in rapid thermal processes such as oxidation, annealing, and chemical vapor deposition. Heating by halogen lamps provide a convenient, efficient and clean environment thermal source. Energy saving can be achieved by taking advantage of the capability to focus the light on a small area that needs to be heated. A halogen lamp is a diffuse emitter, but by combining the lamps with a reflector, the radiation could be directed and focused on specific areas. Halogen lamps and aluminum reflector system are successfully used and offer unique benefits in many industrial heating requirements. The reflector collects the lamp radiation and produces a high intensity spot in front of it. This method also needs absorbing substrates so that a substrate high absorptivity can absorb a high percentage of the radiation emitted by the lamps. By using more than one halogen lamp in the system, a higher heat flux and thus a higher substrate temperature can be obtained. The substrate temperature might be varied from ambient to temperatures above 1000K, by designing a good heater system, by controlling the lamp input electrical power and by limiting the distance between the heating system and the substrate. The high heat flux capability of halogen lamp heater systems allows to heat the substrate much faster than in many other heating processes. Depending on the applications, either, both front and back sides of the substrate are heated or only one side. Different reflector geometries may be applied such as a horizontal or a parabolic geometry. Numerous numerical simulation and experimental studies have been presented in literature reviews concentrating on studying of: lamp heating system design [Turner 1994, Fiory 2000, Pettersson 2000, Sweetland 2001, Hung 2005], substrate temperature uniformity and control [Norman 1991, Pushkar 1991, Moralesi 1998, Choi 2001,

Logerais 2005, Bouteville 2005], deposition of thin films by CVD [Chang 2001, Lindstam 2001, Lindstam 2002].

3.1.3.3.1 HLR Design and Construction:

A halogen lamp reactor (HLR) was designed that utilizes tungsten halogen lamps as a radiant heat source to heat up the substrate and build as a part of this research. All designed parts were produced in the mechanical engineering workshop and constructed in a CVD laboratory at University of Duisburg-Essen, campus Duisburg. Mechanical engineering drawings for the components of the reactor are attached in appendix A. The reactor is a vertical reactor and consists of four main parts: a CVD chamber, a halogen lamp heater, a light entrance window, and a substrate holder. The descriptions of each part and a proof of the achievable using this design are presented in the next sections. Figure 3.5 shows a schematic diagram of the designed HLR components and Figure 3.2 shows the schematic diagram of the HLR-CVD system used for deposition of β-$FeSi_2$.

3.1.3.3.1.1 CVD Chamber:

The CVD chamber is a vertical cylinder made from a stainless steel (AISI 304, DN 250) with height of 200 mm. Both top and bottom flanges are standard CF flanges sealed with copper gaskets, (DN 250 CF). Several KF standard flanges, (KF50, KF40, and KF25) are placed at different positions at the wall, at the top and at the bottom flanges for gas tube feedings, exhaust gases, vacuum connections, nozzle holder, thermal connections and temperature measurements. A KF100 flange is constructed at the chamber wall for loading the substrate and maintenance. All KF standard flanges are sealed with viton O-ring gasket such that the users can carry out maintenance

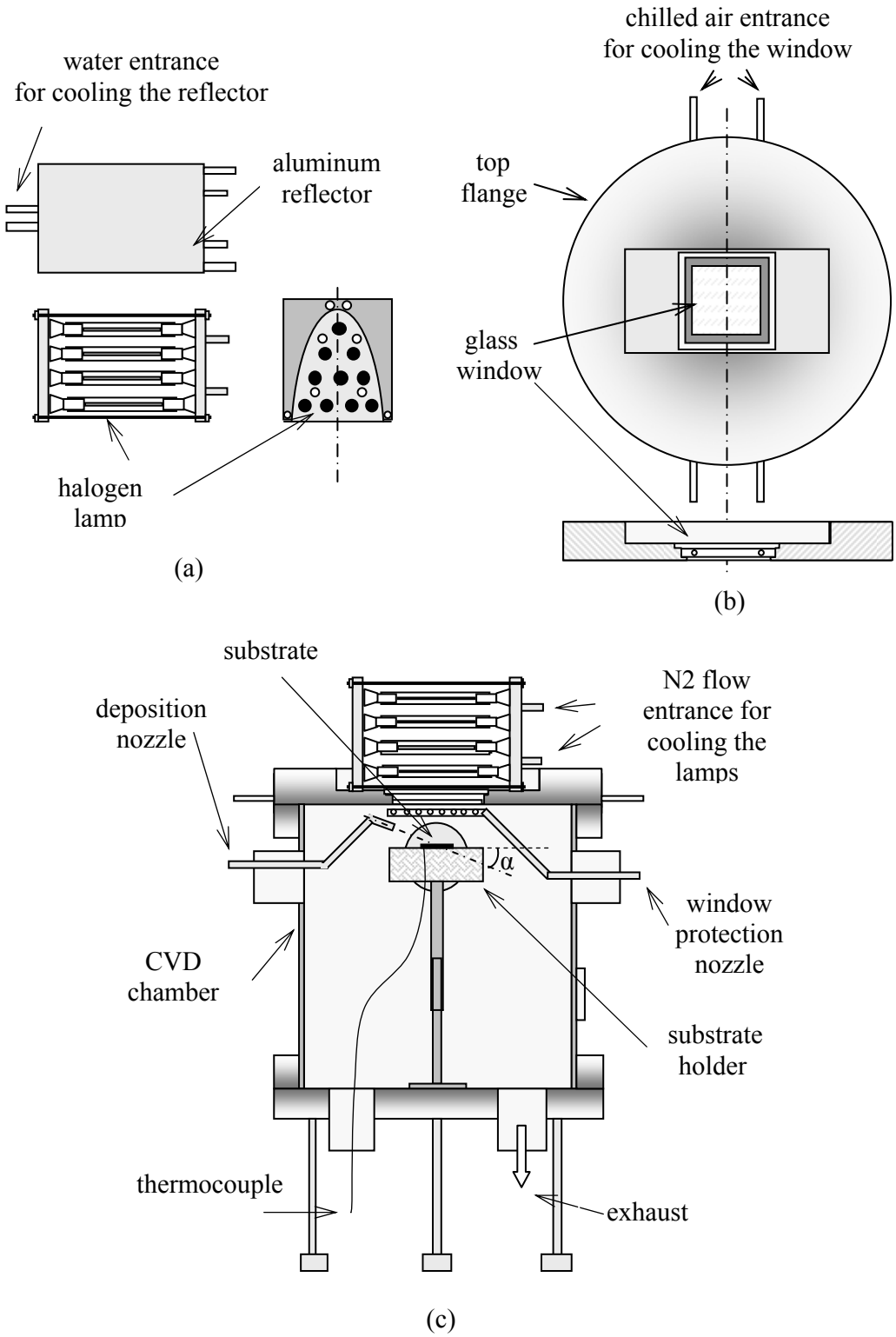

Figure 3.5 A schematic diagram of HLR components: (a) halogen lamp heater, (b) glass window, (c) CVD chamber and substrate holder.

operations and substrate replacements easily. Furthermore, there are additional flanges in the CVD chamber, which enable the user to add new components into the system. Two nozzles are installed inside the CVD chamber, a deposition nozzle and a window protection nozzle. The deposition nozzle has an inner diameter of 4 mm and is installed in the chamber with an angle ($\alpha = 20°$) measured from the horizontal surface of the substrate holder as shown in Figure 3.5 (c). Precursors and gases needed for a deposition process are introduced through this nozzle. The window protection nozzle is designed as a linear tube shower nozzle and installed horizontally under one side of the window. A flow of inert gas (argon) is introduced through this nozzle in order to protect the window from deposition of species during the deposition process. The glass has to be clean so that the required light from the lamps for specific substrate temperature can be transmitted through the glass continuously during the deposition period. This is important also at the same time, while the glass absorbs some light and getting hotter, the deposition might be occurred on the glass surface as well. So, the argon flow will transfer all the products after the precursor decomposed away from the surface of the glass window.

3.1.3.3.1.2 Substrate Halogen Lamp Heater:

The substrate heater designed for this investigation is a front side substrate heating system. The substrate is heated by means of a radiation from conventional tungsten halogen lamps with a total electrical power input of 5 kW. The heating system consists of 10 tungsten halogen lamps and an aluminum reflector. The single halogen lamps are type of double ended linear sources (R7S), 118 mm in length, 500 Watt rated power, ultraviolet free, 9500 Lumen, 230 Volt and radiation output of ~20%. A polished parabolic aluminum reflector is used to reflect and direct the amount of light

flux incident on the substrate. The reflector and lamp housing are continuously cooled by the water cooling system. The heating system was build so that it can be easily moved away from the surface of the window. This design allows easy replacement of the lamps and maintenance of the system. The lamps were arranged under the parabolic aluminum reflector as shown in Figure 3.5 (a). The bulb and the socket of the lamp are cooled by a nitrogen flow. The environmental temperature within the lamp is kept as low as 350°C for lamp damage protection. The lamp input electrical power may be set manually by switching on and off each lamp or each lamp zone. It may also be controlled continuously depending on the result of a measurement of the substrate temperature. A thermocouple, type K is attached to the back side of the substrate to measure and monitor the substrate temperature. The lamp power controller receives the feedback signal through this thermocouple.

3.1.3.3.1.3 Light Entrance Window:

Since the halogen lamp heating system used to heat the substrate was placed outside the CVD system chamber, a specific design of the top flange is required. A borosilicate glass window is constructed on the top flange to transmit the radiation from the heating system. This glass is relatively cheap compared to quartz glass. 90% of visible light and infrared radiation spectrum up to 2 micrometer is transmitted from 2 to 5 mm thickness (Hecker Glastechnik, www.hecker.de, ID-Nr 936803). The area of the window was designed as 76 by 76 mm, and build from two glass plates, each 3.3 mm in thickness, separated by a 5 mm air gap as shown in the schematic diagram Figure 3.5 (b). The bottom glass plate, 86 x 86 mm, is glued into the flange surface with high temperature glue. This glue is chosen to allow the thermal expansion of the glass during the heating process and to its resistance to high temperature (high

temperature glue, LOCTITE 5399 US, -8 to 275°C, peak of 350°C). The top glass plate, 96 x 96 mm, is placed free above the bottom glass plate level. A 5 mm air gap is allowed between the two glass plates for window cooling purposes. A forced chilled air flow is provided to protect the glass and the glue from over heating. The exhaust air temperature is monitored by a thermocouple placed inside the air gap and kept always below 175°C.

3.1.3.3.1.4 Substrate Holder:

The system should be constructed for target substrate temperature of at least 800°C. To achieve these high temperatures a substrate holder was designed for this purpose it consists of a small stainless steel cylinder with inner diameter of 82 mm and height of 30 mm, as shown in Figure 3.6.

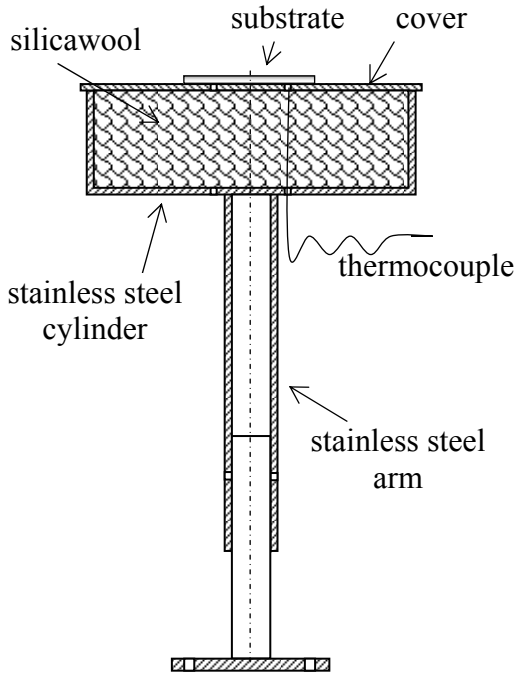

Figure 3.6 A schematic diagram of the substrate holder.

It is filled with silicawool 125, (Silica, www.silca-online.de), an isolation material having a density of 128 kg/m^3 and a thermal conductivity of 0.21 (W/m K) at 800°C and covered with a stainless steel cover of 2 mm thick. This cylinder is fixed on a stainless steel arm, which may be elevated to control the distance between the halogen lamp heater and the substrate, later referred to as heater/substrate distance. The holder is positioned in the center of the CVD chamber directly below the window as seen in Figure 3.5 (c).

The substrate temperature was measured by a thermocouple connected to the backside of the substrate as shown in Figure 3.6. A uniform temperature distribution might be assumed across the substrate at any time during a transient process, while the Biot number, which relates the conduction heat transfer resistance of the substrate (R_{cond}) to the convection heat transfer resistance (R_{conv}), ($Bi = R_{cond} / R_{conv}$) is much smaller than unity, ($Bi << 1$).

3.1.3.3.2 Substrate Temperature Optimization:

3.1.3.3.2.1 Theoretical Results:

Before selecting the final geometry of the reactor, the radiative power from halogen lamps required to heat the substrate was investigated. The radiation spectrum of a halogen lamp (E_λ) at filament lamp temperature of 3000K was calculated from Planck distribution equation and plotted in Figure 3.7. This temperature is given by the supplier (Qsram, www.osram.com).

There are several parameters, which had to be considered during the evaluation of the substrate temperature. These parameters are area and material of the substrate, design of the substrate holder, distance between the lamp and the substrate (heater/substrate distance), geometry of the reflector, selections of the halogen lamps, the glass of the

window and the ambient conditions.

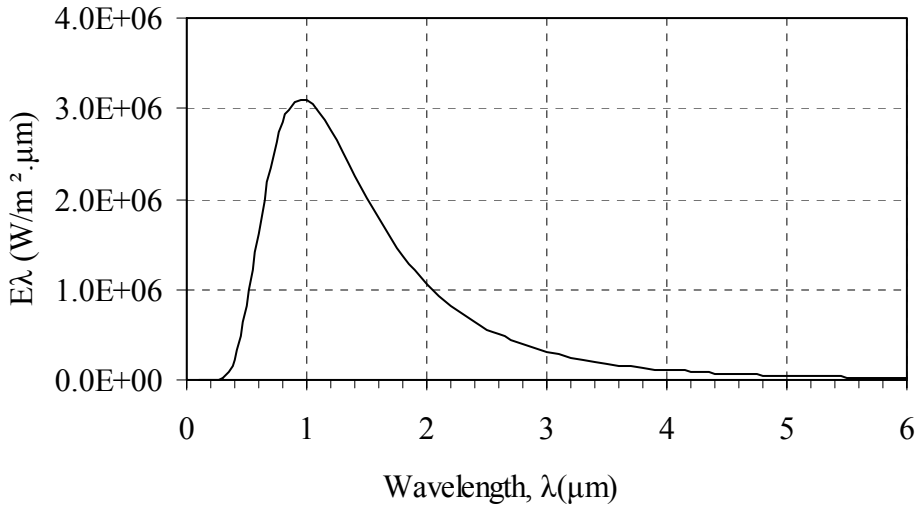

Figure 3.7 Halogen lamp radiation spectrum at filament temperature of 3000K.

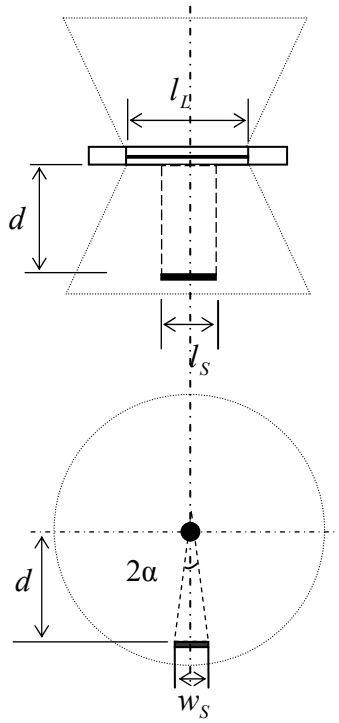

Figure 3.8 A schematic diagram of shining substrate with one halogen lamp where (l_L) is a lamp length, (d) is a distance between the lamp and the substrate; (l_S and w_S) are the length and the width of the substrate, (2α) is a plane angle.

The portion of radiation emitted from the halogen lamp and absorbed by the substrate might be computed from:

$$\dot{Q}_S = \alpha \ \dot{Q}_L \tag{3.1}$$

$$\dot{Q}_L = \varphi \ F \ G_L \tag{3.2}$$

$$\varphi = \frac{\dot{W}_L}{G_L} \tag{3.3}$$

$$F = \left(\frac{l_S}{l_L}\right)\left(\frac{2\tan^{-1}\left(w_S / 2d\right)}{2\pi}\right) \tag{3.4}$$

Where the subscripts L and S related to the lamp and substrate respectively, and α is the substrate absorptivity, G_L is the input electrical lamp power, $\dot{W}_L$ is the equivalent light power (9500 Lumen for every single of the used lamps), φ is the lamp efficiency and F is the geometry factor depending on substrate size (length l_S and width w_S), heater/substrate distance d, the lamp length l_L. Figure 3.8 shows a schematic diagram of shining substrate with one halogen lamp.

The quantity of lamp radiation emitted to the substrate surface was calculated from equation (3.2), where the substrate absorptivity is assumed to be unity, a black body, and by taking in account the influence of the design geometry factor F as presented in equation (3.4) and light efficiency of ~20 % as in equation (3.3). The result was plotted in Figure 3.9 as a function of lamp/substrate distance for lamps input electrical power of 500 W for one lamp and 5000 W for the whole system of 10 lamps as a single lamp source.

The radiatively emitted power from the substrate surface might be calculated from the Stefan- Boltzmann law:

$$\dot{Q} = \varepsilon \sigma A T^4 \tag{3.5}$$

Where, ε is the emissivity of the substrate, A is the substrate area, σ is the Stefan-Boltzmann constant (5.67×10^{-8} W/m^2.K^4) and T is the absolute substrate temperature. As the radiant power of the substrate is primarily a function of the surface temperature, small temperature increases result in large power increases. Performing an energy balance on the substrate where, the amount of radiation absorbed by the substrate surface is equal to the radiation emitted by the substrate surface.

$$\left|\dot{Q}_{in}\right| = \left|\dot{Q}_{out}\right| \tag{3.6}$$

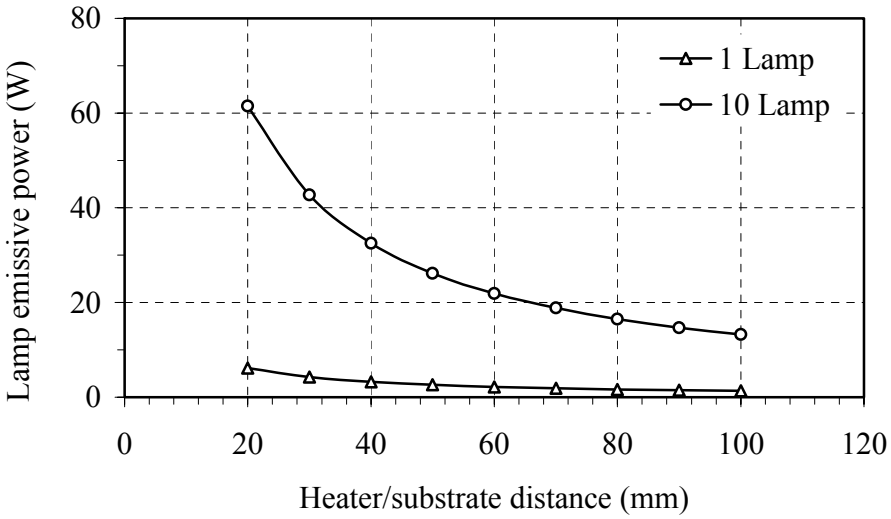

Figure 3.9 Calculated amount of halogen lamp radiation emitted to the substrate based on substrate area (30 x 20) mm^2 and lamp/substrate distance for: (a) 500W and (b) 5000W as a single lamp source.

The total heat transfer from the surface of the substrate was calculated from equation (3.7) based on the design of the substrate holder, the radiative heat transfer from the front side and the conductive heat transfer from the back side of the substrate.

$$\dot{Q}_{out} = \varepsilon \sigma A T^4 + k A \left(\frac{\Delta T}{L} \right) \tag{3.7}$$

Where k and L are a thermal conductivity and a thickness of the isolating material respectively, ΔT is the temperature difference between the top and the bottom of the substrate holder.

To evaluate this model some assumption were made: one dimensional steady state condition, negligible convection heat transfer, substrate emissivity and absorptivity are equal, (0.6). Therefore, the required power for heating the substrate to a specific temperature could be estimated from this simple calculation. Figure 3.10 shows the relation between the required heat transfer rate by a radiation and the substrate temperature. The comparison between the theoretical substrate temperature and experimentally measured temperature as a function of heater/substrate distance is shown in Figure 3.11. The real measured temperatures at heater/substrate distance of 50 and 60 mm are slightly below the calculated temperatures curve. The absorbed heat by the substrate should be improved by using the aluminum reflector. It seems that the effectiveness of the used reflector in this set-up is quite low; it is approximately 10%, perhaps due to thermal degradation of the surface of the reflector.

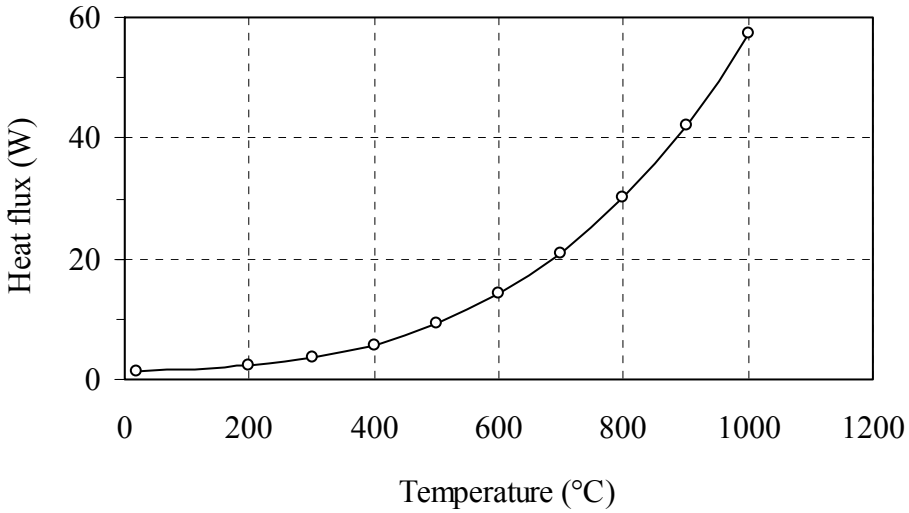

Figure 3.10 The required absorbed heat flux by the substrate as a function of substrate temperature, calculated using equation 3.7.

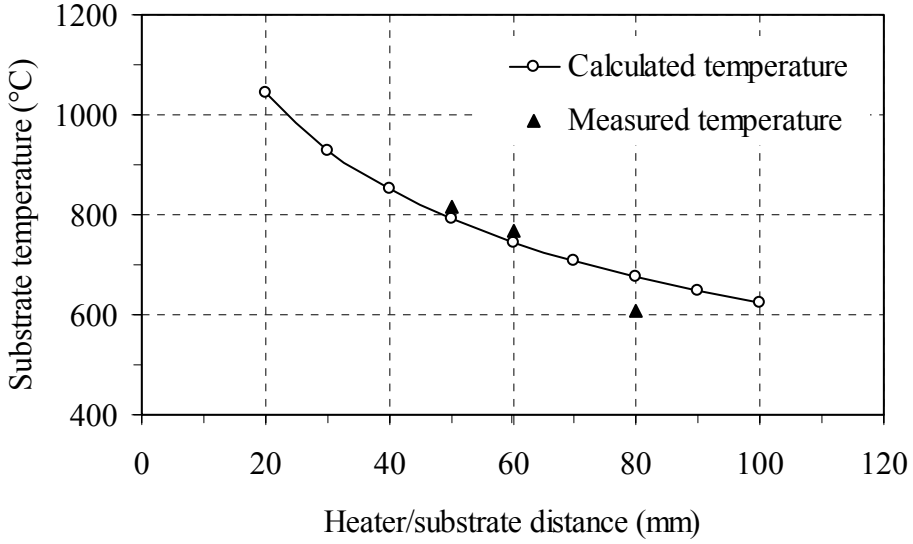

Figure 3.11 Measured and calculated substrate temperature as a function of heater/substrate distance.

3.1.3.3.2.2 Validation of the HLR Design:

After choosing the geometry of the HLR reactor and constructing the reactor, the heating rate and the achievable maximum temperature of substrate were tested. The substrates used for this investigation were pieces of silicon wafers, Si(100), having a thickness of 0.5 mm. The substrates, (20 x 30 mm) were introduced into the chamber manually and placed horizontally on the substrate holder, Figure 3.6. Water, chilled air and nitrogen flows were provided from the conventional flow system in the laboratory in order to cool and protect the aluminum reflector, the window and the halogen lamps respectively. The valves of the cooling systems were opened before the halogen lamp heater is switched on. The substrate temperature was measured and monitored by the thermocouple attached to the backside of the substrate.

To optimize the reactor for the designed maximum substrate temperature of 800°C, the reactor was tested at atmospheric and low pressure (30 mbar), and the substrate holder was adjusted at two heater/substrate distances: 60 and 50 mm. The

experimental runs were performed by applying the maximum electrical power (5 kW) to the lamps and waiting long enough for the substrate to reach the stationary state. The maximum substrate temperature reaches 750°C at 60 mm and 830°C at 50 mm after approximately 360 seconds. After that, the lamp power was controlled according to the thermocouple feed back to the set point temperature of 800°C and the substrate temperatures were acquired every 30 seconds. The average substrate heating rate profiles are illustrated in Figures 3.12 at 1 atm and Figure 3.13 at 30 mbar reactor pressures. Curves (a) and (b) show the substrate heating rates profiles at 50 mm and 60 mm heater/substrate distance, respectively. The values of the transient substrate temperatures illustrated by curves (a) and (b) were fitted to an exponential function, $(T_0+(T_{max}-T_0)(1-e^{(-kt)}))$. The time constant k is: (k = 0.01 at 60 mm , k = 0.012 at 50 mm), t is the heating time, T_0 is the room temperature and T_{max} is the maximum substrate temperature related to each case, (800°C at 50 mm, 770°C at 60 mm).

The set point temperature, which is 800°C, can not be reached at 60 mm heater/substrate distance as the maximum radiation absorbed by the substrate is not enough to increase the substrate temperature to the set point temperature. The maximum temperatures, achieved in this case are 737°C at 1 atm and 772°C at 30 mbar after 840 seconds heating time. But, it is successfully reached and well controlled at 50 mm heater/substrate distance after 360 seconds, where the absorbed radiation by the substrate is enough in this case to increase the temperature to the designed control set point. These results are presented by curves (a) and (b) in Figure 3.12 and 3.13. The slightly change in the value of temperature appears in curve (a) after 360 seconds is due to the controller hysteresis.

Different set point temperatures below 800°C were also tested (not shown here) and successfully applied for the deposition of thin films.

After the heater was switched off, the cooling rate of the substrate was measured; this temperature profile is shown in Figure 3.14. The cooling rate was a function of (T_0+ (T_{max}-T_0) $e^{(-kt)}$) having constant time of (k = 0.17) until reaching of 350°C, after that the cooling rate was delayed because of the presence of the isolation material.

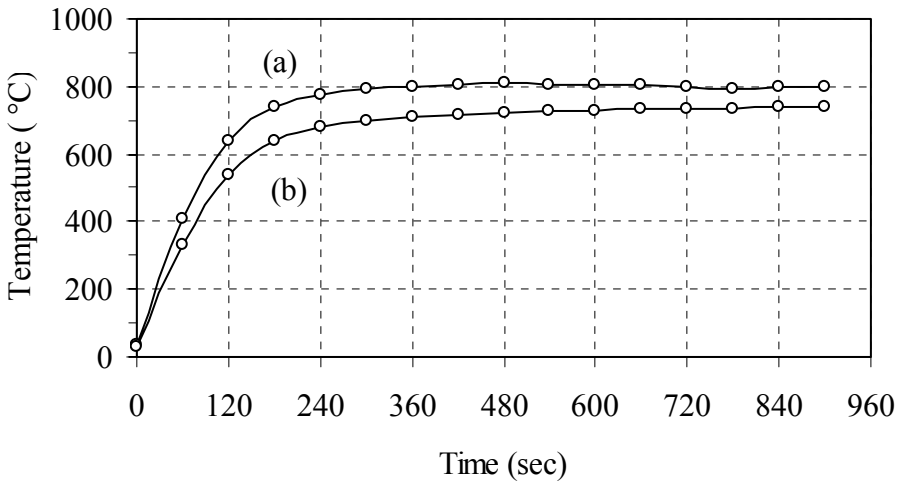

Figure 3.12 Average heating rate of the substrate at 1 atm and substrate temperature set point of 800°C, for heater/substrate distance of (a) 50 mm and (b) 60 mm.

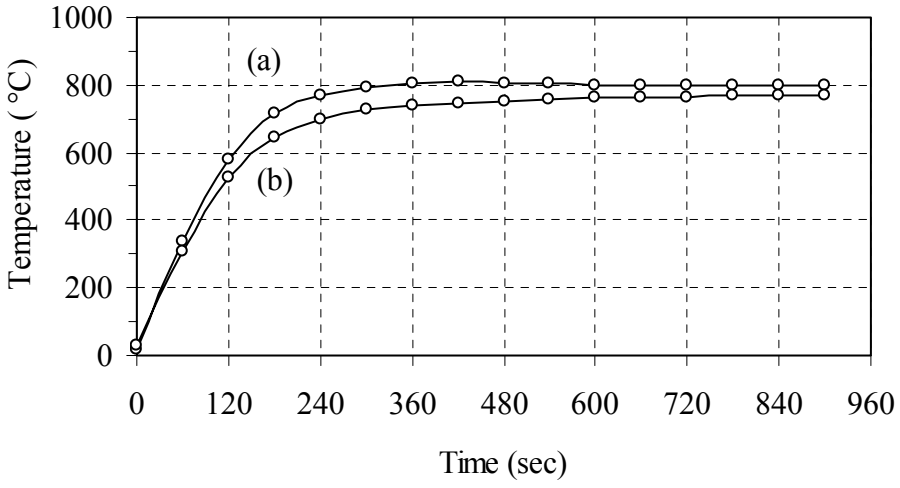

Figure 3.13 Average heating rate of the substrate at 30 mbar and substrate temperature set point of 800°C for heater/substrate distance of (a) 50 mm and (b) 60 mm.

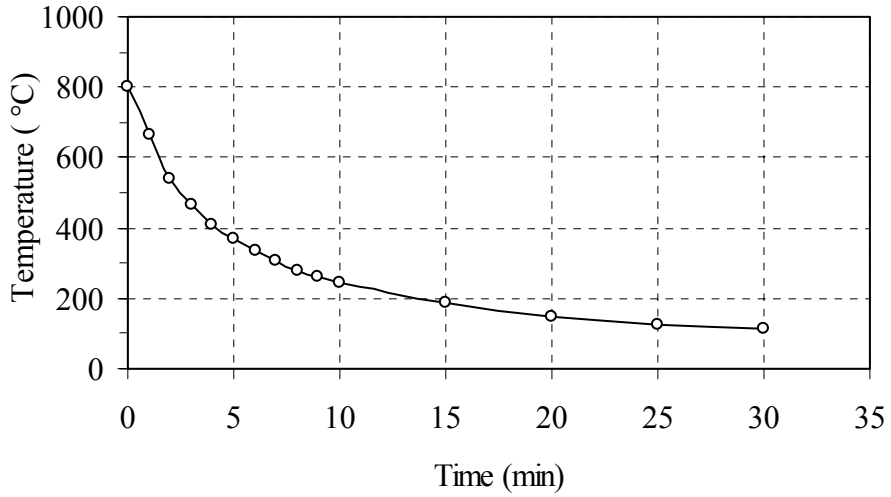

Figure 3.14 Average substrate temperature profile during the substrate cooling process, (Halogen lamp heater was switched off).

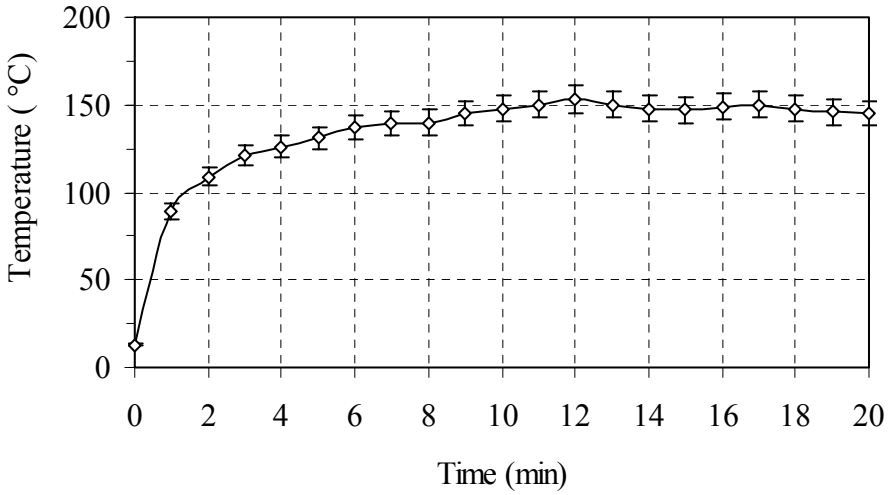

Figure 3.15 Window temperature profile during heating process at substrate temperature set point of 800°C.

Figure 3.15 shows the temperature profile measured within the air cooling system of the window. The temperature of the window rises to a maximum value of 155°C, which is still much lower than the long-term normal working temperature of the glue and the glass as well. Appropriate design of cooling system made the use of glued

borosilicate glass windows possible.

The HLR described in this work was successfully used for deposition of thin films, such as iron, iron carbide, silicon and iron disilicide thin films. This non-contact substrate heater gives several advantages to the CVD system compared to the contact heater such as: substrate fast heating ramp-up and cool-down (saving time), low thermal budget, reduced contamination, possibility of deposition of different films at different deposition temperatures within the same experimental run. The limit of the substrate temperature which can be achieved with this substrate heater was 800°C as needed for the present experiments, but this is not a fundamental limitation and could be expanded. By this design a maximum set point temperature of 800°C and any temperature below are easily achieved and controlled.

3.2 Film analysis:

After having deposited a film it has to be analyzed. Morphology, phase composition and chemical composition are of key interest. These can be investigated using X-Ray diffraction (XRD), optical and scanning electronic microscopes (SEM), energy dispersive X-ray method (EDX).

A Bruker D8 Advance X-ray diffractometer equipped with a copper tube (λ = 1.5418 Å) and with grazing incidence optics was used for phase composition analysis. Environmental scanning electron microscope, ESEM, Quanta 400, continuously acceleration voltage 200 V to 30 kV equipped with EDX analysis system Genesis 4000, Campus Essen and Full computer controlled FESEM with patented GEMINI objective lens acceleration voltage from 100 to 30 kV equipped with an EDX analysis system, Campus Duisburg, were used for surface morphology and chemical composition analyses.

Chapter 4

Deposition of Aluminium Oxide (Al_2O_3) Thin Films

4.1 Introduction

Alumina thin films have attracted much interest in recent years due to their interesting mechanical and electrical properties and possible applications in several engineering fields [38, 47]. These properties are strongly influenced by the phase composition. In most cases, amorphous films are deposited at low temperatures, while metastable and stable crystalline phases require higher deposition temperatures. The range of deposition temperatures reported in the literature review by Maruyama et al., Huntz et al. and Pranhan et al. for amorphous films was between 250 and 550°C [31, 33, 35]. Crystalline phases started to grow above this temperature; up to 900°C the metastable gamma phases was obtained. The thermodynamically stable alpha phase was grown at temperature between 900 and 1200°C as reported by Huntz et al., Bahlawana et al. and Muller et al. [33, 34, 36]. Also Maruyama et al. reported that amorphous films may contain or not (OH) groups depending on deposition conditions. Usually, crystalline alumina films tend to be harder than amorphous films therefore the crystalline phases are favored for the application as hard coating. The hardest phase (corundum) is α-Al_2O_3, which has an excellent thermal stability. Figure 4.1 shows the phase diagram of Al-O as presented in Landolt-Bornstein [47].

Metalorganic chemical vapor deposition has become one of the most widely used methods to deposit Al_2O_3 films. Different CVD setups were applied during deposition

processes, such as atmospheric pressure CVD (APCVD) [31, 33] and low pressure CVD (LPCVD) [34-37]. Several precursors were used as source material of Al_2O_3, among them $AlCl_3$ with a mixture of H_2 and CO_2 [34, 36]. The main disadvantage of this process is the byproduct HCl, which is corrosive and very aggressive. In advantages of MOCVD, low deposition temperatures and possible high deposition rates, several metalorganic chemicals were used as alumina films precursors, such as aluminium tri-isopropoxide (ATI) [28, 33, 34, 37] and aluminium acetylacetonate $Al(acac)_3$ [31, 35, 39].

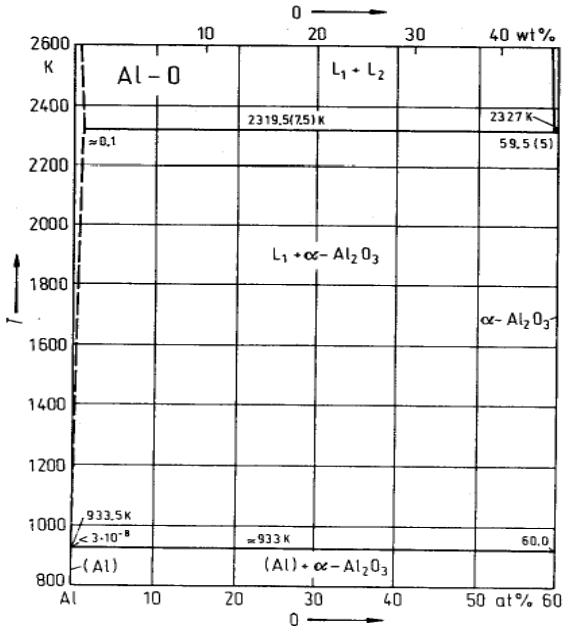

Figure 4.1 Al-O phase diagram (printed from reference [47]).

Maruyama et al. [31] have used $Al(acac)_3$ as single precursor, no oxygen was employed, to deposit Al_2O_3 films at atmospheric pressure, the range of deposition temperature was between 250°C and 600°C. The deposited films were amorphous and contaminated with carbon. Singh et al. [39] observed small alumina crystallites in amorphous films at 600°C. The deposition was carried out at low pressure using $Al(acac)_3$ in the absence of an oxidant gas. The films contain carbon, too. Pradhan et

al. [35] reported that at low pressure and range of deposition temperature between 350°C and 950°C, amorphous, semi-crystalline and crystalline films were deposited from $Al(acac)_3$ without employing any reaction gases.

So far there is no published work on deposition of alumina films at atmospheric pressure using $Al(acac)_3$ together with synthetic air as an oxidant gas. Aluminium acetylacetonate ($Al(acac)_3$) and synthetic air (20.5 % oxygen in nitrogen) are used as precursor and oxidant gas for depositing thin Al_2O_3 films, respectively. In this study, experiments were performed in a HWR running at ambient pressure. Low operation costs have been achieved by using relatively inexpensive precursors and a very simple experimental setup.

4.2 Experimental Procedures:

A complete description of the HWR-CVD system used for deposition of Al_2O_3 thin films was described earlier in chapter 3. Its schematic diagram was shown in Figure 3.1. The temperature distribution in the HWR was presented in chapter 3; the result shows that the temperature within the reactor was not constant over the whole heated length. The actual furnace temperatures distribution profiles were plotted in Figure 3.4 at operating ambient pressure and 2.0 slm synthetic air for 400, 500 and 600°C furnace control temperatures which were also most relevant for the following study. Thus, e.g., the actual substrate temperatures at selected positions (A, B, C and D) in the reactor shown in Figure 3.1 and at 500°C furnace control temperature are: 445°C, 476°C , 482°C and 469°C at positions A, B, C and D respectively.

Aluminium acetylacetonate ($Al(acac)_3$) was sublimated in a fluidized bed evaporator at a constant temperature of 140°C. Besides the data mentioned in chapter 3, the vapor pressure and the enthalpy of sublimation of the used $Al(acac)_3$, (purity 99%, Strem

Chemicals Inc.), were measured in the laboratory by thermogravimetric measurements. The vapor pressure was found 0.3 mbar at 132°C and the enthalpy of sublimation is 100 kJ/mol [43]. Therefore, the vapor pressure at 140°C can be calculated by the Clausius-Clapeyron equation to be 0.53 mbar. The vapor was subsequently transported to the nozzle with a carrier gas flow of 0.6 slm synthetic air (20.5% oxygen in nitrogen). Additionally 1.4 slm synthetic air was fed in, in order to increase the flow velocity. The nozzle and the feed pipes were heated to 155°C in order to prevent recondensation of the $Al(acac)_3$ vapor. All experiments were carried out at ambient pressure around 1013 mbar. Thus, the gas mixture in the reactor consisted of 79.487 mol % N_2, 20.497 mol % O_2, and 0.016 mol % $Al(acac)_3$.

The substrates used in this study were stainless steel (AISI 304) foils, 30 x 20 mm. The substrates were first cleaned by ethanol and then supersonically for 30 minutes in a water bath. After drying, each substrate was with a high precision balance before loading them into the reactor. The substrate temperature depends on its position in side the reactor because of the parabolic profile of the actual furnace temperatures, Figure 3.4. As the deposition of the films are strongly influenced by the substrate temperature. Therefore, four different substrate positions along the flow direction were chosen related to the furnace length in order to study the local deposition rate. Figure 3.1 shows the selected substrates positions: position A (200 mm) in the region of increasing temperature, position B (270 mm) and C (300 mm) in the isothermal zone, and position D (400 mm) in the region of decreasing temperature. In every experimental run, the four substrates were loaded on a stainless steel bar, which acted as a substrates holder, into the chamber. The steel bar was positioned parallel to the gas flow in the radial centre of the reactor, see Figure 3.1.

Several Al_2O_3 films were deposited at different furnace control temperatures of 400,

450, 500, 550 and 600°C. The deposition time was 2 hours for each run. The mass of the film was measured by weighing the substrate with a high precision balance before and after deposition. The deposition rate was calculated from this result based on the known substrate surface area and deposition time, ($mg/cm^2.hr$). The growth rate was also calculated, (μm/hr), considering the density of amorphous alumina phase, (3.40 g/cm^3) [33]. However, this calculation may introduce some small error to the reported linear growth rates, because the film structure is not completely clear and it may consist of hydroxide phases too which have slightly different (2.977, 3.07, 3.37 g/cm^3) densities [47]. In addition, the mass change of the substrate due to oxidation was also considered, as was measured independently in experiments without $Al(acac)_3$; it is around 0.01 mg/cm^2. hr after oxidation at 500°C in pure synthetic air, and thus negligible.

After deposition, the substrates were kept at atmospheric conditions and subsequently analyzed. Due to high oxygen content of the reaction mixture, similar to air, no influence of the ambient air is expected. Films were characterized using scanning electron microscopy (SEM) and energy-dispersive X-ray (EDX) analysis. Phases were determined using X-ray diffraction method (XRD).

4.3 Deposition Results:

4.3.1 Observations:

The depositions were carried out at different furnace control temperatures of 400, 450, 500, 550 and 600°C. The depositions below 500°C were quite homogenous and increase with increasing temperature in all positions A, B, C and D. At 500°C, the maximum deposition was measured at position B, in the center of the furnace where

the actual substrate temperature around 475°C. The amount of deposit increased as the temperature rises to 550°C at position A where the actual substrate temperature is around 490°C, as seen in Figure 4.2 and 4.3. Further increasing of the temperature to 600°C shifted the deposition even closer to the gas entrance. The film thickness depends on the substrate temperature and might also be influenced by the reaction time which is directly related to the substrate positions in the reactor. Local deposition rates at all substrate position A, B, C and D increase with the substrate temperature until they reach a maximum, afterwards they gradually decrease, see Figures 4.2 and 4.3. The deposited films at all locations are homogeneous and cover the entire substrate surfaces without any cracks and spalling. They are well adhering and are rainbow colored, This interference indicates that the films are transparent and have thicknesses of the order of magnitude of the wavelength of visible light; some pictures of the films are shown in appendix C.

The effects of the furnace control temperature and the substrate temperature as well as the dwell time on the deposits phase and growth rate are discussed in the next sections.

4.3.2 Growth rates:

Deposition rates and growth rates at the positions A, B, C and D were analyzed and plotted in Figure 4.2 as a function of the furnace control temperature, Figure 4.3 as a function of the substrate temperature, Figure 4.4 as a function of the substrate position and Figure 4.5 as a function of the dwell time. The depositions performed at 400 and 450°C were quit homogenous in about 200 mm in the center of the furnace and increased with increasing temperature at all positions A, B, C and D, Figure 4.2 and 4.4. This result agrees with the assumption that the precursor is decomposing to a

minor amount below 450°C [49]. The deposition rates at 500°C were also higher except at position D. It seems that the precursor concentration is mainly reduced between position B and C as the highest deposition rate was measured at 270 mm.

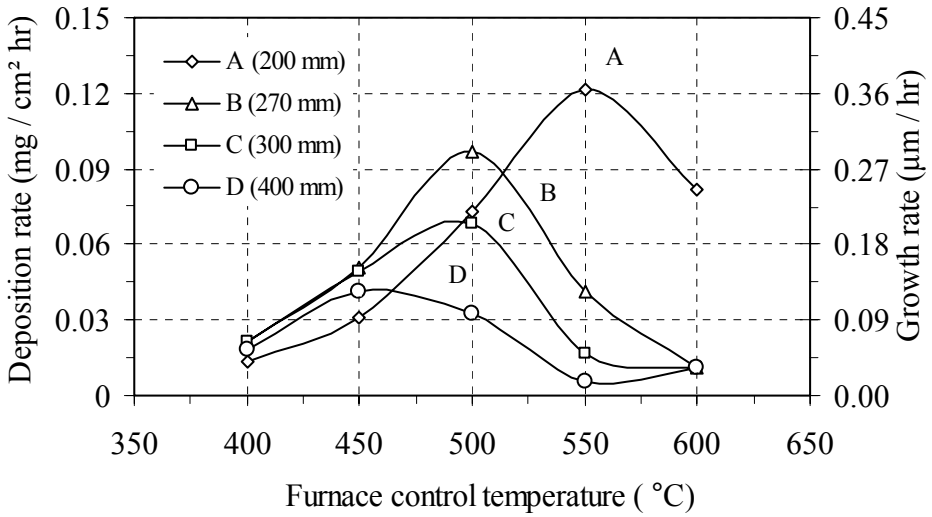

Figure 4.2 Deposition rate and growth rate of thin aluminium oxide films deposited on steel (AISI 304) substrate in HWR at atmospheric pressure and different substrate positions in the reactor plotted as a function of furnace control temperatures.

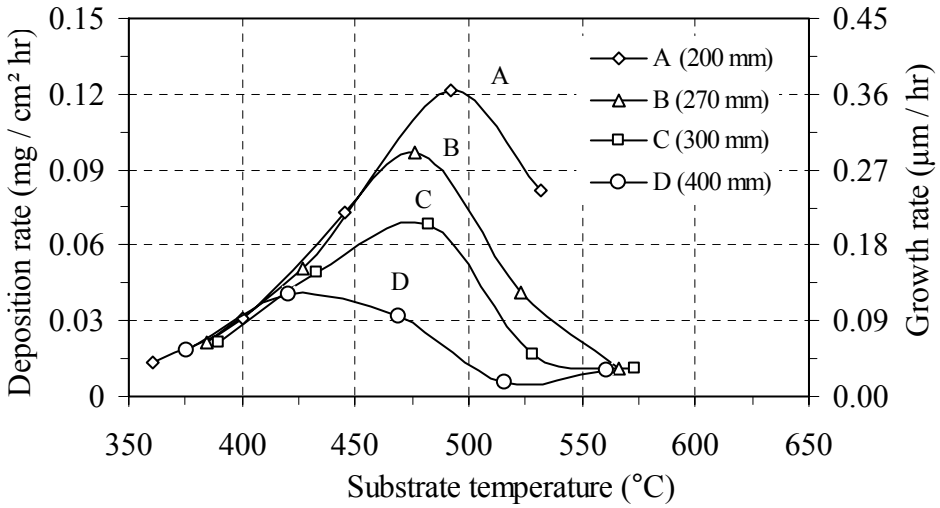

Figure 4.3 Deposition rate and growth rate of thin aluminium oxide films deposited on steel (AISI 304) substrate in HWR at atmospheric pressure and different furnace control temperatures plotted as a function of the substrate temperature.

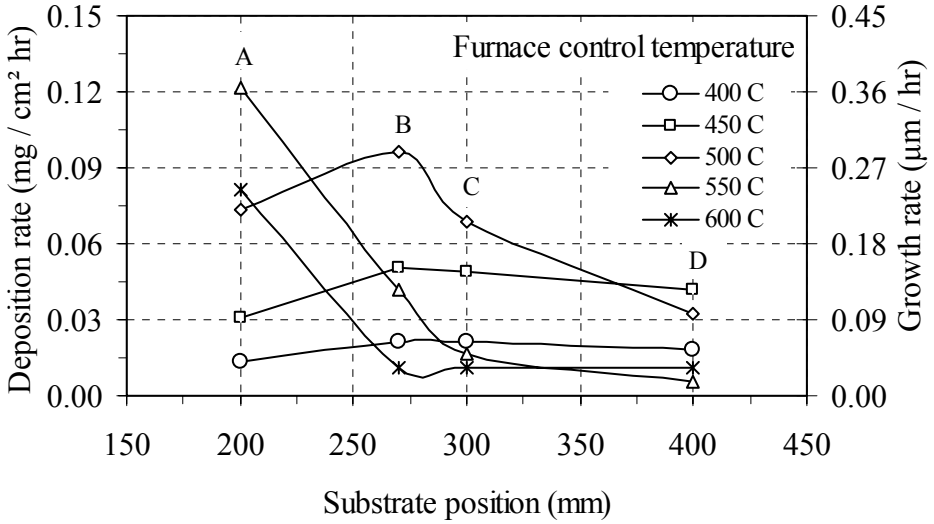

Figure 4.4 Deposition rate and growth rate of thin aluminium oxide films deposited on steel (AISI 304) substrate in HWR at atmospheric pressure and different furnace control temperatures plotted as a function of the substrate position in the reactor.

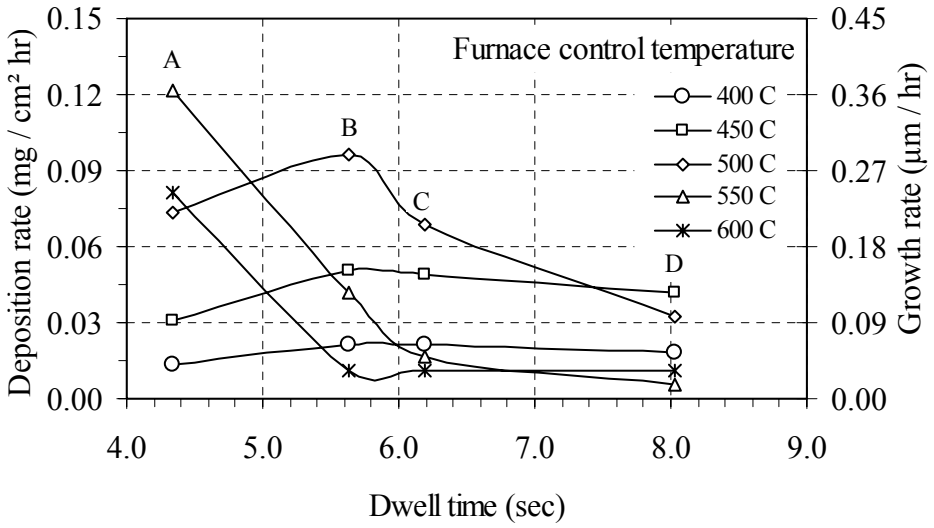

Figure 4.5 Deposition rate and growth rate of thin aluminium oxide films deposited on steel (AISI 304) substrate in HWR at atmospheric pressure and different furnace control temperatures plotted as a function of the dwell time of the precursor within the reactor.

Further increasing the furnace control temperature to 550°C and 600°C shifts the high deposition zone towards the entrance, position A at 550°C and even close to the inlet

at 600°C. The significant reduction in the deposition rates in the positions behind the position of the highest deposition rates, (C and D at 500°C and B, C and D at 550°C and 600°C) are due to the depletion of the precursor.

The concentration of the precursor in the gas phase as a function of substrate temperature was evaluated by a mathematical simulation using Maple. The experimental data used for deposition were used as input for the simulation program assuming a plug flow reactor.

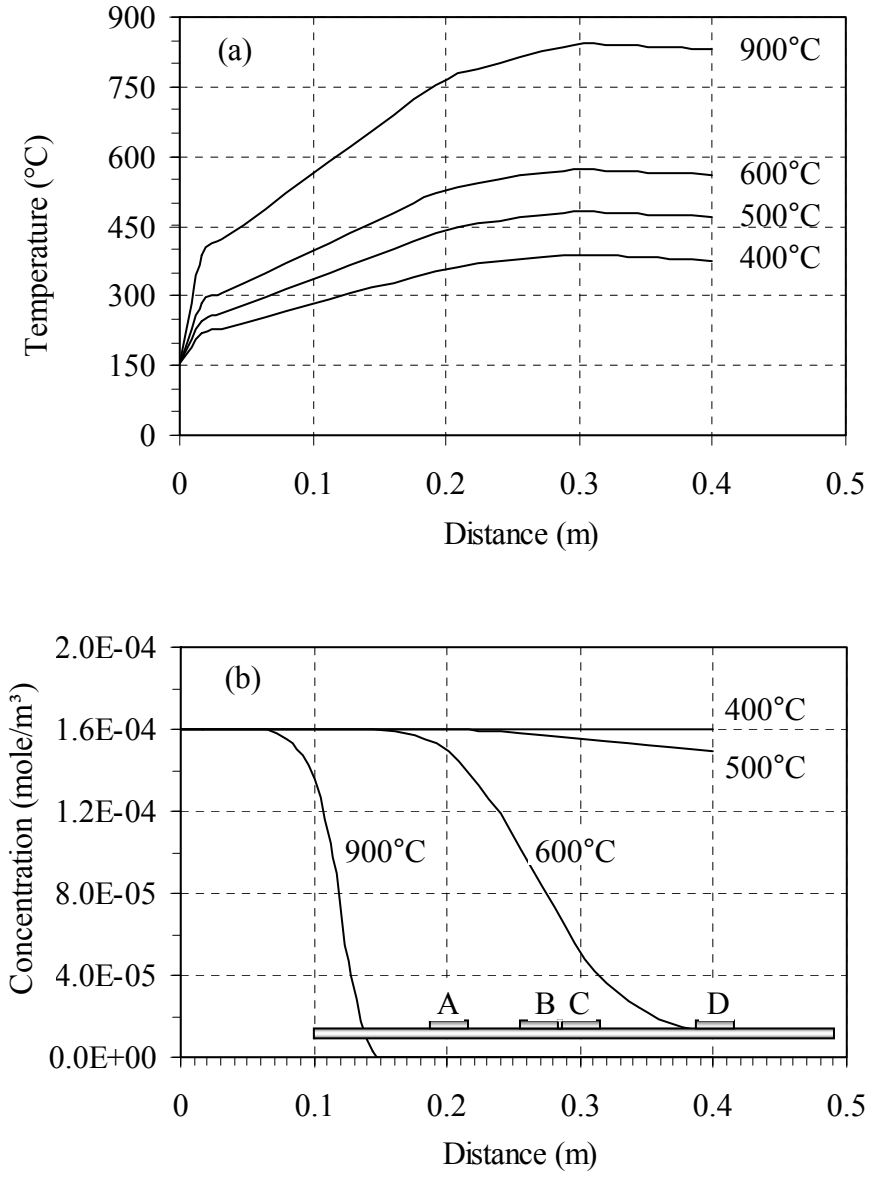

Figure 4.6 Simulation results showing: (a) temperature distribution and (b) the position of the depletion of the precursor in the reactor.

The rate coefficient needed for mathematical calculation was calculated from equation 2.4. The activation energy and the reaction constant were estimated (E_a=2.2 kJ/mole and K_0=10^{14} 1/sec). The concentration of the precursor in the supply tube is a constant while no reaction occurs at low temperature, which is 155°C. As the temperature rises in the reactor as presented in Figure 4.6 (a), the effect of the temperature is expected. Therefore, the change in the precursor concentration was studied from the flow entrance (0.0 m) to 0.4 m long in side the reactor. The positions of the substrates in the reactor as they are used during the deposition process were shown in Figure 4.6 (b). The results were plotted in Figure 4.6 (b) for the furnace control temperatures of 400, 500, 600 and 900°C. The results are in good agreement with that obtained from experimental runs. The depletion in the precursor starts at 500°C in the centre of the rector and shifts towards the inlet gas as the temperature increases.

A comparison between experimental and modeling is easier if Figure 4.3 and 4.6 are regarded. The lowest deposition temperature indicating the beginning of a film growth was around 360°C at position A, Figure 4.3. It seems that the precursor starts to decompose at this temperature; this result fits quite well to the detected CO_2 fraction from $Al(acac)_3$ in the gas phase starting near 305°C at longer dwell times [49]. The maximum deposition was measured at position B, when the substrate temperature is 475°C and at position A when substrate temperature is around 490°C, Figure 4.3. Because the $Al(acac)_3$ is decomposing so fast at this temperature, the deposition just shifts from the furnace center towards the position where the substrate temperature around 475-490°C which means towards the gas inlet. The absolute values of the deposition rates increase during this shift (position B: 0.097 mg/cm^2 hr at 475°C, position A: 0.122 mg/cm^2 hr at 490°C), Also the heterogeneous reaction of $Al(acac)_3$ with oxygen has an activation energy leading to a high growth rate at positions with

high temperature and high precursor concentration. The depletion of the precursor controls the deposition rates at all positions behind the position of highest deposition rate.

The homogeneity of the deposition with changing furnace control temperature can also be well understood regarding Figure 4.2 and 4.4. Up to 450°C furnace control temperature, the deposition is quite homogeneous overall at the measured length of 200 mm between positions A and D as expected for the surface kinetically controlled regime. The slight increase between positions A and B is presumably due to the rising in substrate temperature in that region. It seems that the reaction of the precursor with oxygen is slow enough at this low temperature that no depletion occurs within the dwell time of the precursor in the reactor. Increasing furnace control temperature further shifts and produces high deposition rates starting from substrate position B at 500°C then A at 550°C and even closer to the gas inlet region at 600°C.

4.3.3 Deposits Phase:

The deposited films were amorphous at all deposition temperatures as analyzed by XRD. In order to deposit crystalline film, a higher deposition temperature is required. However, it is not useful to increase the furnace control temperature using this setup. As the furnace control temperature increases above 500°C, the decomposition of the $Al(acac)_3$ becomes too fast, therefore, no $Al(acac)_3$ arrives at the substrate but it is pyrolyzed earlier. This result leads to shift the deposition to the colder part of the furnace in front of the nozzle at the position where the substrate temperature between 475 and 490°C. Figure 4.3 shows the deposition rates as a function of the substrate temperature. It seems to be necessary to reduce the dwell time of the precursor within the hot zone to increase its temperature above 500°C. The obvious approach of using

a higher flow velocity was not promising in this case, because the used gas flow of 2 slm was already high and had to be increased exponentially, since the chemical kinetics is following the Arrhenius law. A different setup is required in order to reach extremely short dwell time of the precursor in the hot zone, and thus a significant higher deposition temperature. Such a new setup is behind the scope of this work. Therefore, crystalline films were prepared from deposited amorphous Al_2O_3 films by heat treatment after deposition. Several films were annealed for 2 hours in vacuum (~1 mbar) and in atmospheric pressure at temperatures of 800, 970 and 1115°C with heating and cooling rate of 4 K/min. The films were analyzed and the results are presented in section 4.4.

It should be mentioned that by using this setup, the deposition of Al_2O_3 films is a very promising and well producible process. Moreover, thicker films can be also deposited by increasing the deposition time. Several experimental runs were performed at

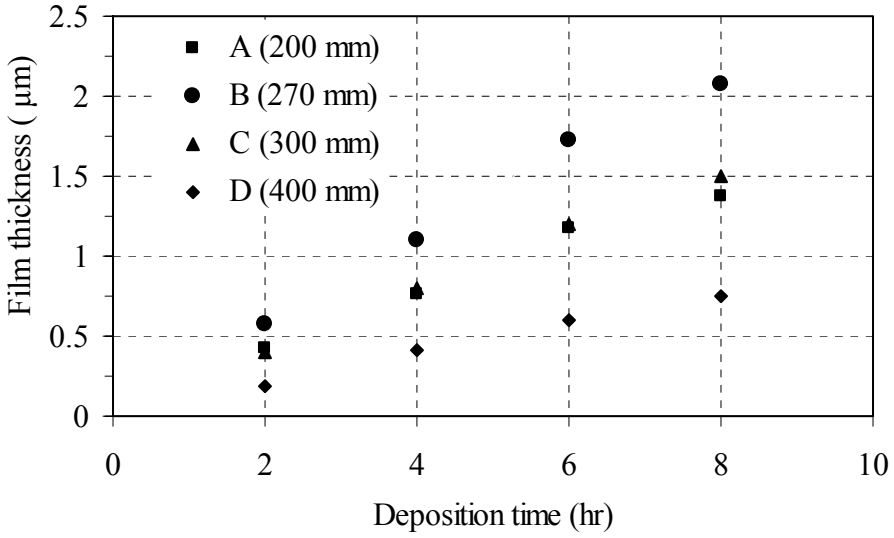

Figure 4.7 Thickness of thin aluminium oxide films deposited on steel (ASI 304) substrate at 500°C furnace control temperature plotted as a function of deposition time.

furnace control temperature of 500°C and deposition times of 2, 4, 6 and 8 hr. As mentioned earlier, the thickest film has been produced at position B, Figure 4.7 shows the relationship between the film thickness at this position and the studied deposition times. The film thickness at 2 hr deposition time is ~0.6 µm and ~2.1µm at 8 hr.

4.4 Film Analysis:

4.4.1 Phase Composition:

As-deposited and annealed films were analyzed by X-ray diffraction (XRD). Figure 4.8 shows the XRD-pattern of the clean substrate, as a reference, as-deposited film and films after annealing at 800°C, 970°C and 1115°C. The diffraction peaks reflecting the typical structure of the stainless steel substrate is shown in Figure 4.8 (a). After 2 hours of deposition at furnace control temperature of 500°C, the reflections of the substrate are still visible and no reflections of Al_2O_3 film appeared, indicating that the as-deposited film is an amorphous film. However, after annealing an as-deposited film at 800°C for 2 hr, the film structure starts to change and some broad reflections of γ-Al_2O_3 appear as well as the reflections of the substrate as seen in Figure 4.8 (c). If further heated, the film gradually crystallizes from amorphous to γ-Al_2O_3 then to α-Al_2O_3 at higher annealing temperatures. Figure 4.8 (d) shows that reflections of γ-Al_2O_3 and of the substrate are still observed after annealing the film at 970°C. Now additional reflections related to corroded stainless steel such as Cr_2O_3, $FeCr_2O_4$ appear. The corrosion may take place at the uncovered areas of the substrate surface due to film spalling, where the unprotected parts of the substrate are oxidized at high temperature. After annealing the films at 1115°C, the XRD-pattern appears in Figure 4.8 (e); indicate of the presence of α-Al_2O_3 and Cr_2O_3. As observed, a phase

transformation of the film occurs between 970°C and 1115°C, from γ-Al_2O_3 to α-Al_2O_3. This result had been confirmed by analyzing many annealed films.

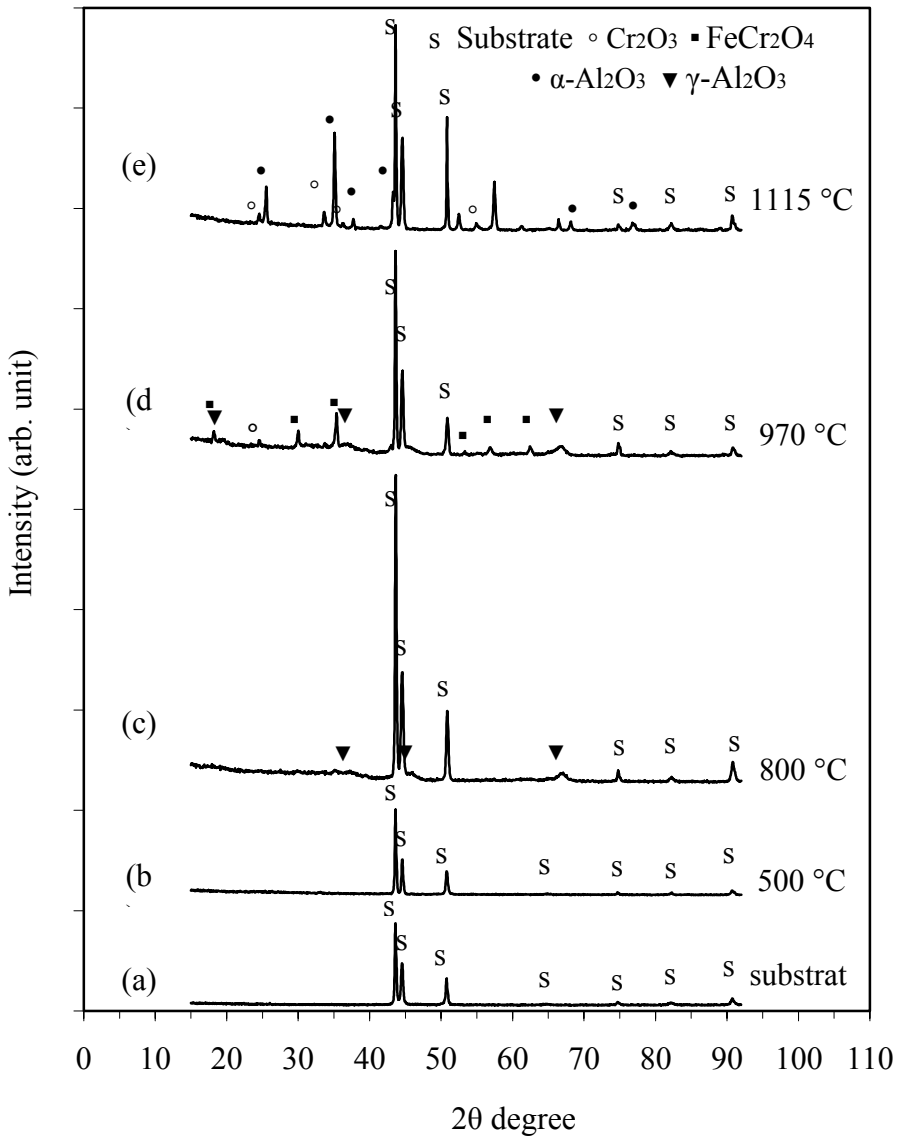

Figure 4.8 XRD spectrums of as-deposited and annealed Al_2O_3 films deposited at furnace control temperature of 500°C and ambient pressure in a HWR compared to XRD spectrum of a clean substrate, (a). (b) as-deposited film, (c), (d) and (e) annealed films at 800, 970 and 1115°C respectively.

4.4.2 Surface Morphology:

Figure 4.9 (b) shows a SEM image of a thin aluminium oxide film deposited within 2 hours on a stainless steel substrate at position B by using a furnace control temperature of 500°C. As a reference, an image of the clean substrate is shown in Figure 4.9 (a). Both images show top views of the samples; they were taken under an angle of 75 degrees to the surface normal. However, before deposition the clean

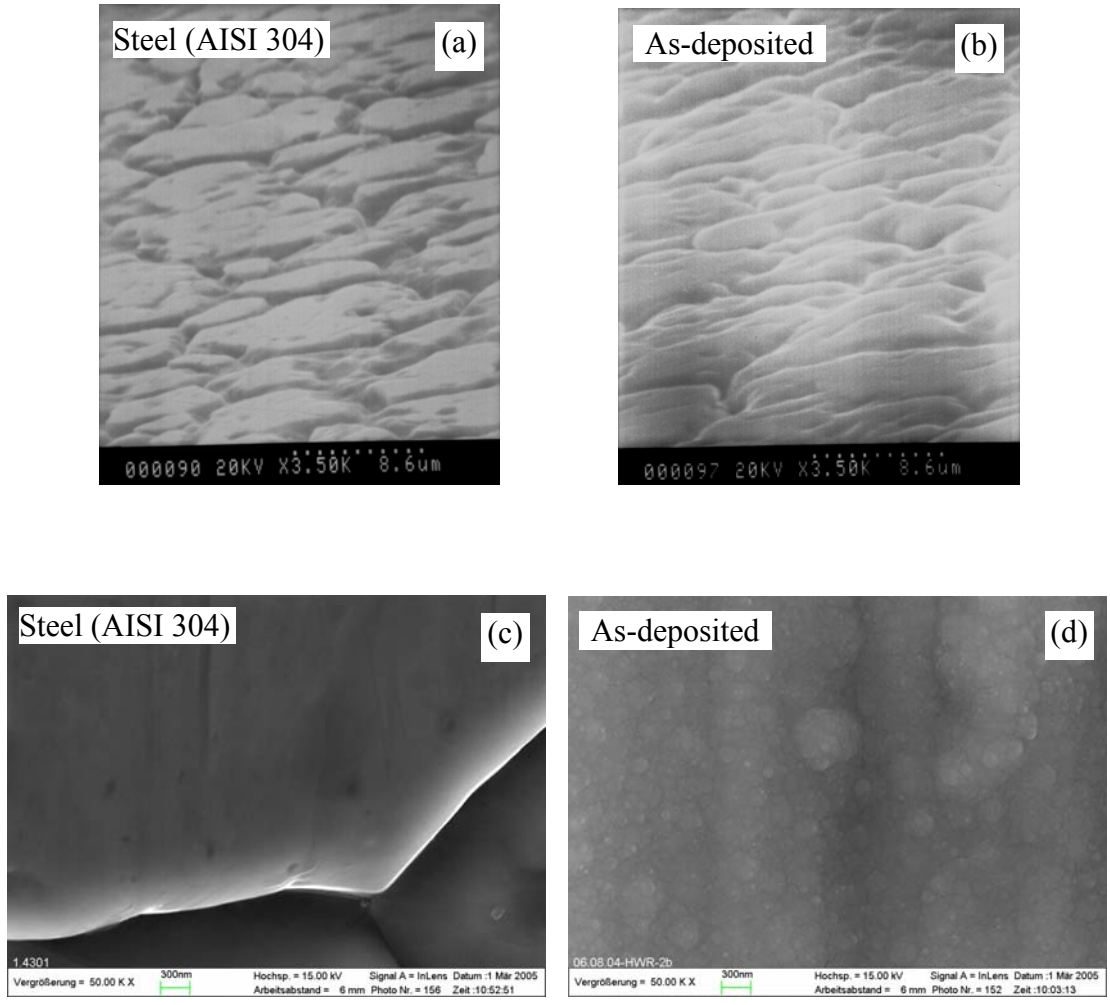

Figure 4.9 SEM image of thin aluminium oxide film deposited on St(304) at furnace control temperature of 500 °C for 2 hr. (a) and (b) views of 70° show a clean stainless steel substrate and as-deposited film, (c) and (d) top view image of a clean stainless steel substrate and as-deposited film at higher magnification.

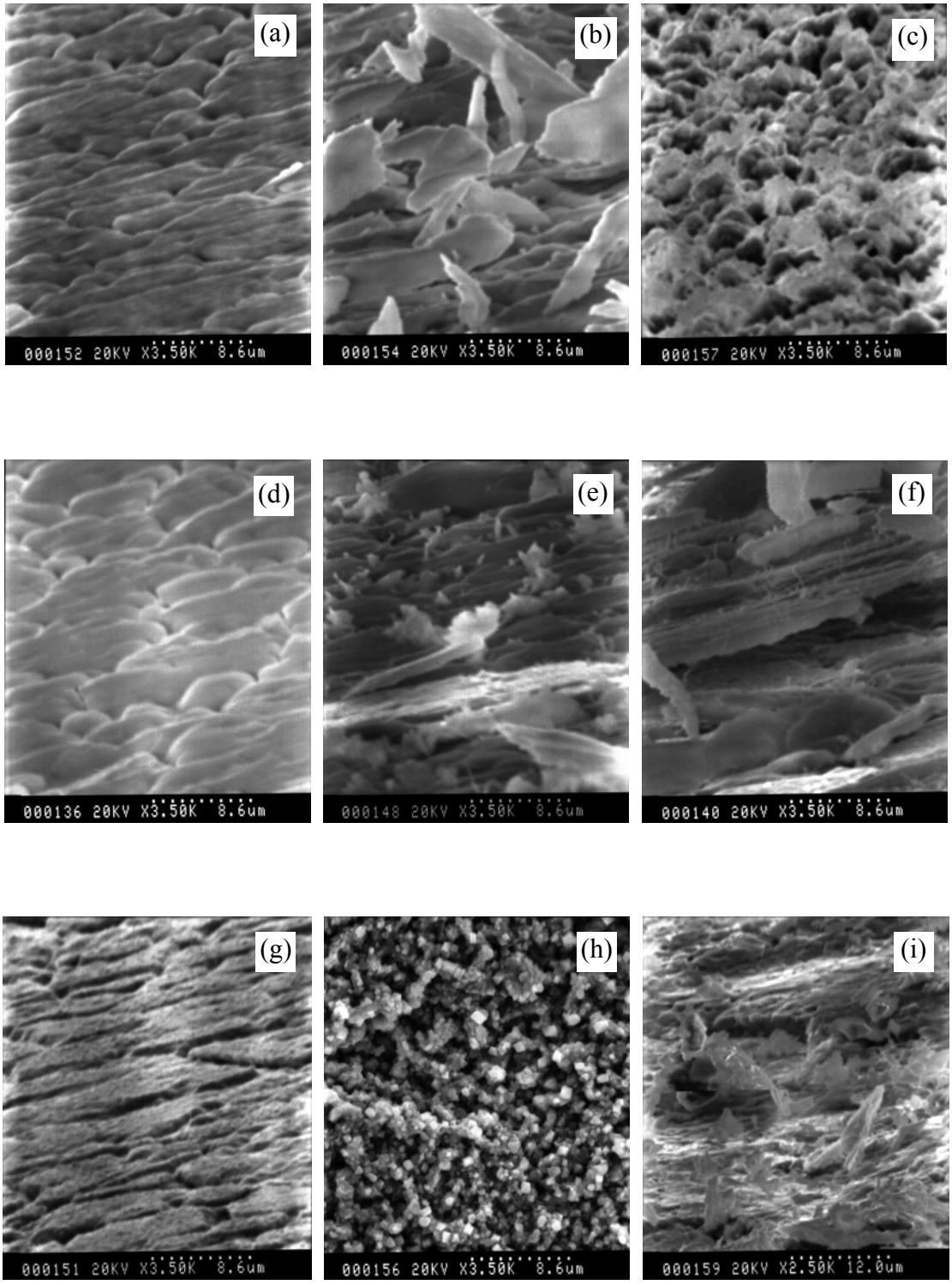

Figure 4.10 SEM images of annealed Al_2O_3 films deposited at furnace control temperature of 500°C and ambient pressure in a HWR: (a), (b) and (c), films annealed in atmospheric pressure, (d), (e) and (f) films annealed in vacuum, the annealing temperatures are 800, 970 and 1115°C respectively. Images (g), (h) and (i) images of a clean substrate annealed at same temperatures, respectively.

stainless steel substrate has a shining silver colored surface and by using a high magnification, one can resolve abreast islands with a diameter of around 5-20 μm which are distributed rather uniformly over the whole area. The islands themselves have a smooth surface, presumably due to the manufacturing of the substrate, and they are separated by small trenches of 1-2 μm depth as seen in Figure 4.9 (c). After deposition, the color of the substrate changed to rainbow colored interferences as it is expected for a transparent film. On the SEM image of the film, Figure 4.9 (b), only slight changes compared to the clean substrate are recognized, the film seems to adapt well to the substrate morphology, although, the trenches between the islands became a little smaller and the edges are less sharp.

The top view image at high magnification (50000X) of the deposited film, Figure 4.9 (d), shows that the film has grown on the substrate surface homogeneously by covering the smooth substrate surface and the surface inside the trenches as well.

The existence of the film can be better resolved after subsequent annealing of a film deposited at position B using a furnace control temperature of 500°C for ~ 4 hr deposition time. The film heat treatment was performed at atmospheric pressure and in vacuum at 800, 970 and 1115°C, respectively. Figure 4.10 shows the SEM images of annealed films at those temperatures in atmospheric (a), (b), (c) and in vacuum (d), (e), (f) pressures compared with SEM images of a clean substrate annealed at same conditions (g), (h), (i). The film breaks off at temperatures higher than 800°C and its fragments stick out of the surface.

The film thickness can be evaluated from these pictures. It is about 0.9 μm, which is in good agreement with the thickness of 0.8 μm obtained from the calculation of film thickness considering the change in mass of the substrate and 3.99 g/cm^3 density of α-Al_2O_3 film. It is worth mentioning that these experiments were well reproducible and

that a destruction of the film could be also observed after annealing the sample at lower temperatures, namely 970°C. After annealing at 800°C the film was still well adhesive, and thus, it is stable up to this temperature.

4.4.3 Chemical Composition:

Only some films could be analyzed in terms of the chemical composition. Figure 4.12 shows the EDX spectrum of a film deposited at 500°C furnace control temperature for two hours at position B was analyzed by energy-dispersive x-ray spectroscopy (EDX). The atomic concentrations of composition of the detected elements in the film are also presented in the Figure 4.12. As a reference, the EDX spectrum of the clean substrate and the atomic concentrations of composition of stainless steel elements are presented in Figure 4.11, 71.80 % Fe, 19.07 % Cr, 6.65 % Ni and traces of Si and Mn. The spectrum of the film clearly differs from the spectrum of the substrate. The concentrations of the substrate elements are reduced due to the shielding produced by the deposited film, 17.42 % Fe, 5.86 % Cr and 1.48 % Ni. The ratio of Fe to Ni and Cr

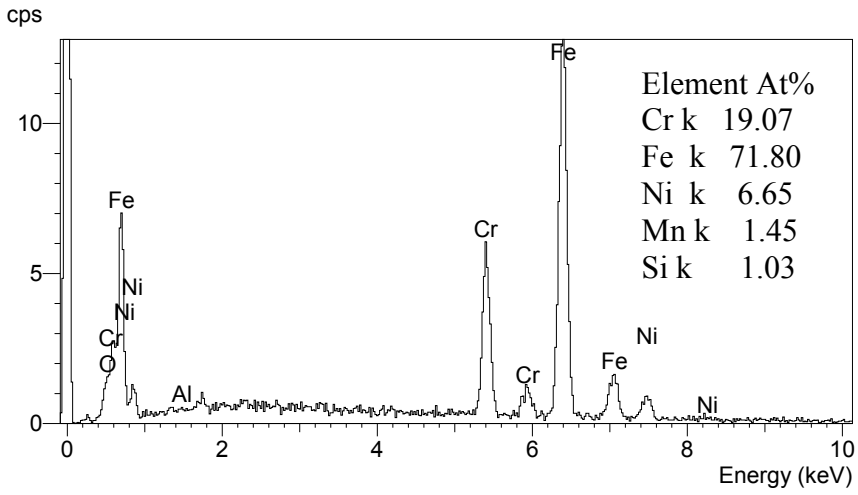

Figure 4.11 EDX spectrum of a clean stainless steel substrate.

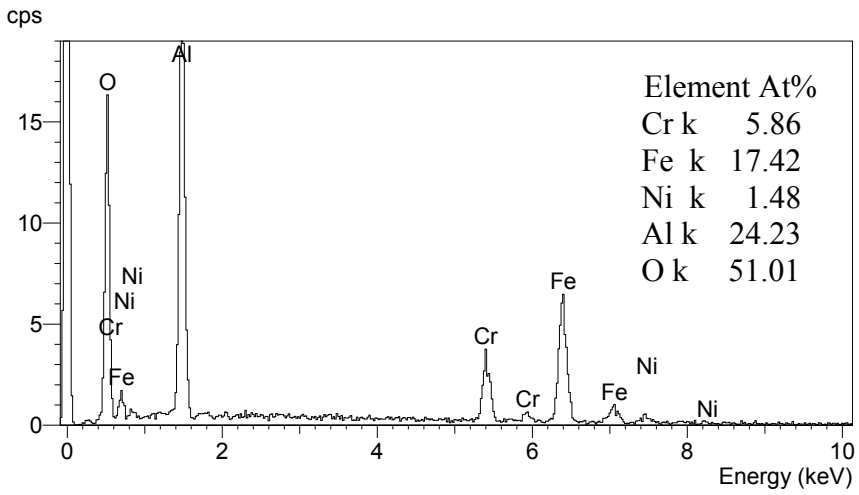

Figure 4.12 EDX spectrum of an aluminium oxide film deposited on a stainless steel substrate in a HWR at ambient pressure.

are nearly the same as in the pure substrate. In addition, peaks of aluminium and oxygen appear, indicating their presence in the deposited film. The atomic concentration of aluminium is 24.23 % and the one of oxygen 51.01 %. Thus, the ratio of oxygen to aluminum is about 2 to 1, which is too high for a pure Al_2O_3 film. Due to this result one can not exclude that probably at least parts of the film consist of aluminium hydroxides. This expectation was also reported by Huntz et al., that films deposited at 450°C consisted probably of amorphous hydrated alumina AlO(OH) [33, 48]. This could explain the high amount of oxygen detected in this film.

4.5 Summary

A low cost CVD setup was used for deposition of thin Al_2O_3 films. Relatively cheap aluminium acetylacetonate and synthetic air were used as precursors. The depositions were carried out at ambient pressure in a conventional HWR, which avoids the usage of expensive vacuum equipments. The film deposition starts at temperatures around 360°C and becomes faster with increasing temperature. The highest deposition rate

was achieved at a temperature of 475°C with the used setup and the used deposition conditions. Higher deposition rates were not possible, because the deposition zone is just shifted towards the gas inlet with increasing temperature due to the depletion of the precursor. Nevertheless, producing thicker films was possible by increasing the deposition time, as the film thickness increases nearly linearly with respect to deposition time. However, it is not possible to deposit crystalline alumina films as higher temperatures are required for crystallization. The deposition at a temperature of 500°C was nearly homogenous over a wide area within the furnace. Therefore, depositing on larger substrate areas will be possible if the CVD system is scaled up. Films deposited at 500°C were well adhesive, completely closed, and looked multicolored, as it is expected for a thin transparent film. They were amorphous and consist of aluminium and oxygen. The films were mechanically and chemically stable up to annealing temperature of 800°C but above this temperature the film can not survive, it is spalling. Annealing at higher temperatures leads to a crystallization: at 800°C, the films became γ-Al_2O_3, and at 1115°C α-Al_2O_3 was observed.

Chapter 5

Deposition of Beta Iron Disilicide (β-$FeSi_2$) Thin Films

5.1 Introduction:

Beta-iron disilicide (β-$FeSi_2$) films grown on silicon substrates were studied because this material is interesting for the following possible applications: Semiconducting β-$FeSi_2$ has been considered to be one of the most promising thermoelectric materials because of its low cost, excellent oxidation resistance up to 900°C and high thermoelectric power [54, 55]. It is applicable for future generation photovoltaic devices and solar cells, based on theoretical prediction of a photovoltaic efficiency of 23%, a high absorption coefficient with about 50 times higher compared to crystalline silicon and a suitable energy band gap of 0.83-0.87eV [52, 56, 61, 62, 66]. Optoelectronic and thermoelectric applications, thin film sensors: for the measurement of heat energy, irradiation measurement and surface temperature thermopiles [53, 54].

Recently, several growth techniques have been applied to prepare β-$FeSi_2$ thin films, including co-evaporation [57, 58], RF magnetron sputtering [59], solid phase epitaxy (SPE) on hot silicon substrates [62, 63], reactive deposition epitaxy (RDE) [64] and molecular beam epitaxy [65].

There are only few published papers on the CVD of β-$FeSi_2$ thin films [66 to 72]. As precursors for CVD β-$FeSi_2$ films, Cyolopentadienyliron (ferrocene, $Fe(C_5H_5)_2$), iron-pentacarbonyl ($Fe(CO)_5$) and iron chloride ($FeCl_3$) were reported as source materials

of iron. Among them, only ferrocene is stable in air, non-toxic and non-corrosive, so it used in this study. Silane (SiH_4), silicon chloride ($SiCl_4$) and tetramethylsilane ($Si(CH_3)_4$) are conceivable as source materials of silicon. Silicon chloride is very corrosive and silane is very reactive and difficult to handle. TMS is a liquid silicon source, which evaporates at ambient conditions as presented earlier in chapter 3. Si and C atoms can be supplied from TMS at a relatively low cracking temperature without forming corrosive or contaminant by-products [75]. The usage of TMS as a CVD precursor of β-$FeSi_2$ is not well studied, only very few reports were published [71, 72]. Therefore, TMS is selected as a silicon precursor for CVD β-$FeSi_2$ films investigated in this study.

Mukaida et al. [71, 72] reported that β-$FeSi_2$ film could be formed by CVD on graphite substrate from SiH_4 and $Fe(C_5H_5)_2$ whereas Fe_2Si_5 and SiC films were deposited from TMS and $Fe(C_5H_5)_2$ on the same substrate. Akiyama et al. [66], reported that he succeeded for first time, in preparing a high-quality β-$FeSi_2$ epitaxial films on a Si(111) substrate at 750 °C by MOCVD using $Fe(CO)_5$ and SiH_4 as source materials. Akiyama et al. [69] also presented a comparison between two films deposited by simultaneous supply of ($Fe(CO)_5$ and SiH_4) and ($Fe(C_5H_5)_2$ and SiH_4). The film deposited from $Fe(CO)_5$ and SiH_4 consisted of a single phase of β-$FeSi_2$ film, while the film deposited from $Fe(C_5H_5)_2$ and SiH_4 consisted of SiC and ε-$FeSi_2$.

In the present work, ferrocene and TMS were selected as precursors for chemical vapor deposition of β-$FeSi_2$ thin films on Si(100) substrate. A CVD reactor with a substrate halogen lamp heater was used for film preparation. The design and construction details of the reactor were already described in chapter 3. Two different techniques of film deposition were practiced: a Direct Deposition Technique (DDT) and a Step Deposition technique (SDT). In DDT: a film was deposited by supplying

ferrocene and TMS vapors into a CVD chamber at the same time. In SDT: an alternating supply of the precursors was chosen; an iron film is deposited on a silicon substrate and a silicon film is deposited on the iron film by supplying of ferrocene and TMS vapors into a CVD chamber separately. Afterwards the films were annealed.

5.2 Experimental Procedures:

A schematic diagram of the HLR-CVD system used for deposition is shown in Figure 3.5. Silicon, Si(100), pieces of approximately 20 x 30 mm or smaller size and stainless steel, (AISI 304), pieces 20 x 30 mm were used as substrates. Every substrate was cleaned by ethanol and by an ultrasonic cleaner in a water bath, for 30 minutes prior to deposition. Finally, the substrate was dried and weighed with a high-precision balance before it was loaded into the reactor.

Ferrocene (purity > 98%) purchased from Fluka and TMS purchased from Merck were used as iron and silicon sources, respectively. Ferrocene, a solid powder, was filled in a glass evaporator and sublimated by immersing the evaporator in a high temperature water bath. Based on the data mentioned in chapter 3 the ferrocene vapor pressure is 0.0133 mbar at 30°C and the enthalpy of sublimation at same temperature is 72.5 kJ/mol, the vapor pressure at 70°C can be estimated by the Clausius-Clapeyron equation to be 0.38 mbar. The supply line of ferrocene vapor and the nozzle inside the reactor were heated by resistive wire heaters wrapped around the tube in order to prevent the source vapor from recondensing. A high purity argon gas (99.999 %, Messer) controlled by mass flow controller was used as a carrier gas for the ferrocene vapor. Liquid TMS was filled in a glass bubbler and freezed in liquid nitrogen then connected to the reactor before evacuation. In order to keep the TMS in a constant room temperature as much as possible, the bubbler was immersed in a room

temperature water bath during deposition process. The flow rate of TMS vapor was controlled by mass flow controller. A flow of hydrogen (99.999 %, Messer), as a reactant gas, was introduced into the reactor through a mass flow controller. Hydrogen was used to reduce the amount of deposited carbon. All required vapors and gases were mixed in the nozzle section.

The temperature of the substrate was monitored and controlled by using K-type thermocouples inserted in the substrate holder and attached to the backside of the substrate. The reactor was evacuated by a vacuum pump from Pfeiffer Vacuum Company (model DBP 050-4 / PK T11808). The pressure of the reactor was measured with a baratron capacitance manometer.

After filling the bubblers with the precursors and loading the substrate, the reactor was evacuated, the halogen lamp substrate heater was switched on and an argon flow of 200 sccm was supplied into the CVD chamber through the window protected nozzle in order to protect the glass from deposited species. Every experiment was performed at specific condition deposition parameters: CVD chamber pressure and deposition temperature were not changed within a run. At the end of the deposition period, the substrate was kept under vacuum condition until the temperature cooled down to nearly room temperature, after that the reactor was pressurized and the deposited film was taken out for analyses.

The mass of the deposited film was calculated from subtracting the weight of the clean substrate from the deposited one. The phase composition, morphology and chemical composition of the films were analyzed by X-ray diffraction (XRD), scanning electron microscope (SEM) and energy dispersive X-ray method (EDX).

Those steps of experimental procedures have been followed always during the deposition techniques unless other experimental procedures are mentioned. The

specific condition of each film deposition process will be mentioned in the appropriate section of the text.

5.3 Deposition Techniques:

The depositing of β-$FeSi_2$ films was investigated using the two techniques, direct deposition technique (DDT) and step deposition technique (SDT) as explained in next sections.

5.3.1 Direct Deposition Technique (DDT):

Experimental runs were performed in the HLR-CVD system. Argon gas carrying ferrocene vapor and TMS vapor and hydrogen (reactant gas) were supplied into the CVD reactor at the same time. They were controlled by mass flow controller and mixed in the nozzle section before reaching the orifice. Ferrocene was sublimated at 70°C and transported by an argon flow of 50 sccm. TMS was evaporated at room temperature, 10 to 20 sccm of the vapor was supplied into the reactor. The transport gas line was heated to temperature of 120°C in order to prevent ferrocene vapor from recondensation. The hydrogen flow rate was 50 sccm. The films were deposited at 30 mbar and 785-800°C for 60 minutes. Thus, the gas mixture in the reactor, as the flow of TMS vapor increases from 10 to 20 sccm, consisted of (44.793-41.060 mol % Ar), (45.455-41.667 mol % H_2), (0.661-0.606 mol % Ferrocene) and (9.091-16.667 mol % TMS).

5.3.1.1 Deposition Results:

After one-hour deposition time, only a black powder was detected on the silicon

substrates between deposition temperatures of 650 to 750°C. The substrate color was changed to rainbow color after increasing the substrate temperature to 785°C and 800°C. The deposited film was an adhered transparent film. It seems that only ferrocene decomposes and forms a black powder below 785°C, which consists of iron, carbon and iron carbide while TMS started to decompose at 785°C. This result is in well agreement with what K.C. Kim [75] reported TMS begins to decompose at about 800°C. The average deposition rate was calculated from the change in substrate weight and the substrate area after 1 hour deposition time (0.06 mg/cm^2.hr at TMS flow rate of 10 sccm and 0.1 mg/cm^2.hr at TMS flow rate of 20 sccm). The film thickness was estimated from the mass of the film using the density of bulk $FeSi_2$ (6170 mg/cm^3); it is between 100 nm and 160 nm at 785°C.

5.3.1.1 Film Analysis:

XRD patters of the films deposited at substrate temperature of 800°C were compared to typical XRD patterns of a clean Si(100) substrate, as a reference, in Figure 5.1 (a and b). XRD analyses show no crystalline film, only the reflection of Si(100) substrate is visible; a sharp peak at 2θ = 55.20° and a broad peak at 2θ between 55.5° to 56°. Therefore, one can conclude that as-deposited film was an amorphous film. However, after annealing several films at annealing temperatures between 900 and 950 °C for 2 hr in vacuum (1.4 mbar) and 100 sccm N_2 flow in a HWR, a peak corresponding to $FeSi_2$ at 2θ = 47.76° can be observed clearly in Figure 5.1 (c). Films deposited on steel substrates were transparent films too. XRD patterns, Figure 5.2 (a, b, c), were compared a clean steel substrate with as-deposited and annealed films. No peaks of iron disilicide were detected even after annealing. Sharp peaks at 2θ of 43.65°, 44.55°, 50.80° and some other weak peaks correspond to the steel substrate

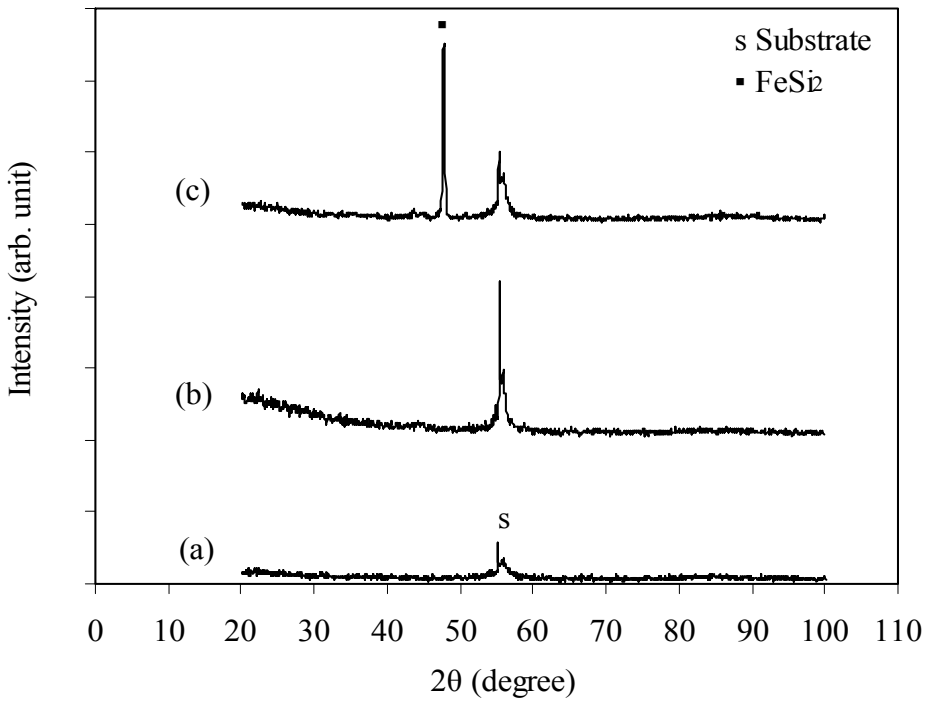

Figure 5.1 XRD patterns of a film deposited from ferrocene and TMS on Si(100) substrate using DDT: (a) clean Si(100), (b) as-deposited film, (c) annealed film.

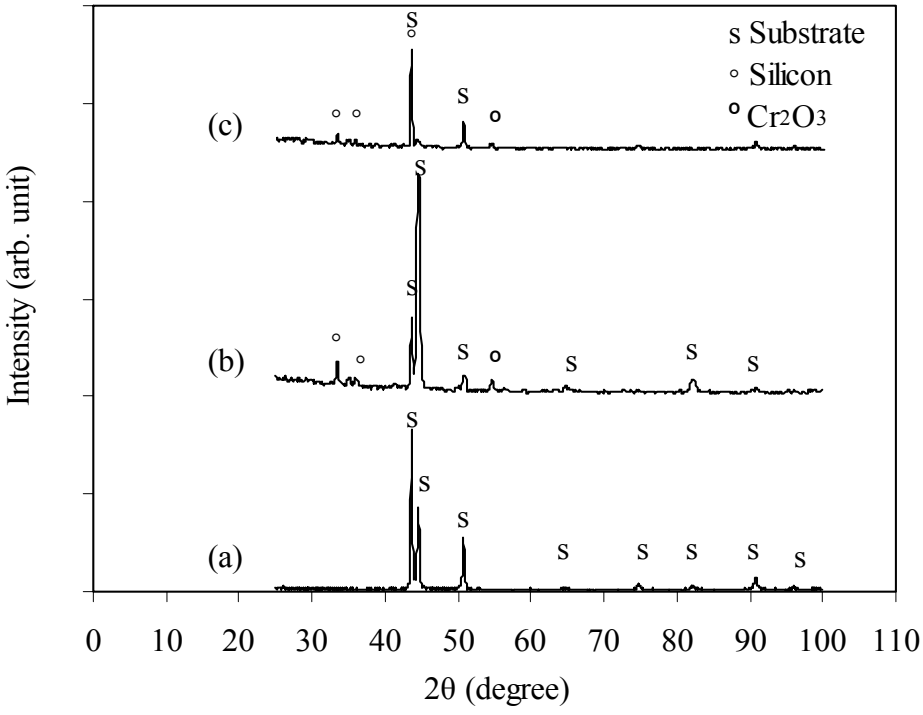

Figure 5.2 XRD patterns of a film deposited from ferrocene and TMS on steel substrate using DDT: (a) clean stainless steel, (b) as-deposited film, (c) annealed film.

were clearly visible in Figure 5.2 (a). Beside the peaks of the steel substrate there are some weak peaks of Cr_2O_3 and silicon, Figure 5.2 (b, c).

Top view SEM images of as-deposited films on silicon and steel substrates were shown in Figure 5.3 and 5.4 respectively. The films deposited on silicon substrate were dense films consisting of fine grains of several nanometers in diameters some of them having diameters of 200 to 500 nm. Films grown on steel substrates consisted of fine balls with diameters of 100 to 300 nm. The films could be easily recognized in Figure 5.4 in comparison to the clean substrate morphology and seem to be well adapted to the substrate surface.

EDX spectra of films deposited on silicon and steel substrates were shown in Figure 5.5 and 5.6 respectively. The atomic percentages of the elements within the films were calculated by the spectrometer software. Films deposited on silicon substrate had an iron atomic percentage of 1.24 % which might be considered a very low amount of iron in the film. The atomic percentage of carbon in the film deposited on silicon substrate was 28.65 %. The atomic percentage of silicon deposited on steel substrate was 9.47 %. The content of oxygen (16.77 % to 28.12 %) in the films deposited on both silicon and steel substrates might be due to atmospheric contamination after deposition.

From this discussion, one can conclude that as-deposited films from ferrocene and TMS precursors using the direct deposition technique were amorphous and consisted of a small amount of iron in the film. In order to increase the amount of iron in the deposited film, the ferrocene sublimation temperature was raised up to 80°C. The result was a thinner transparent film with some black powder on its surface. Therefore, the ferrocene sublimation temperature of 70°C is chosen as an optimum sublimation temperature of ferrocene in this investigation. Based on these

experimental results, a step deposition technique (SDT) was designed as an alternative technique to deposit the crystalline beta phase of iron disilicide.

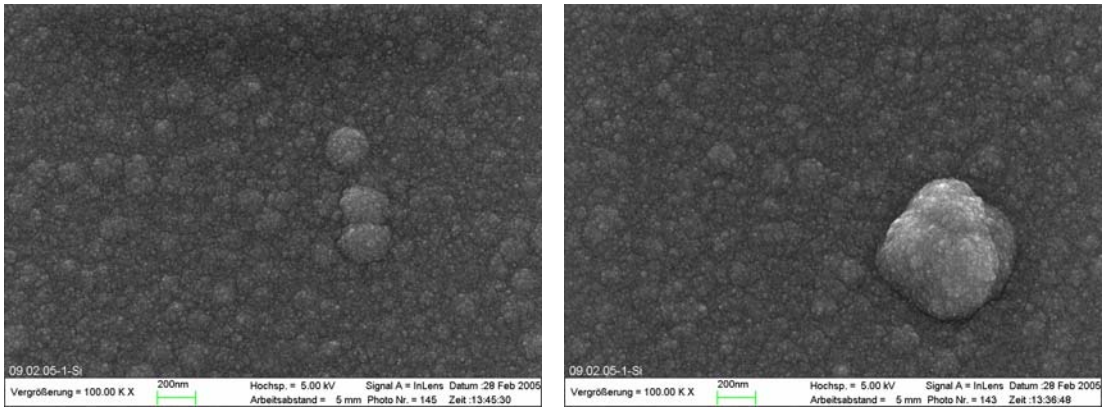

Figure 5.3 SEM image of a film deposited from ferrocene and TMS on Si(100) substrate using DDT.

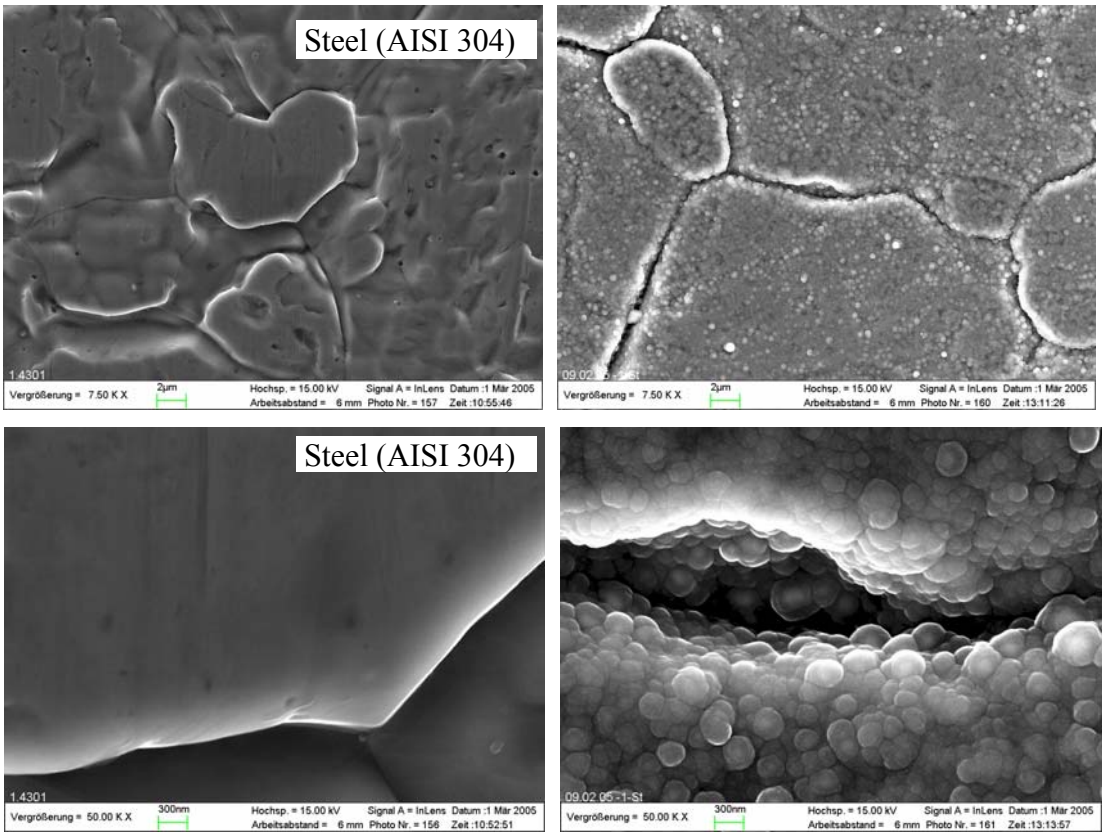

Figure 5.4 SEM images of a clean stainless steel substrate and a film deposited from ferrocene and TMS using DDT.

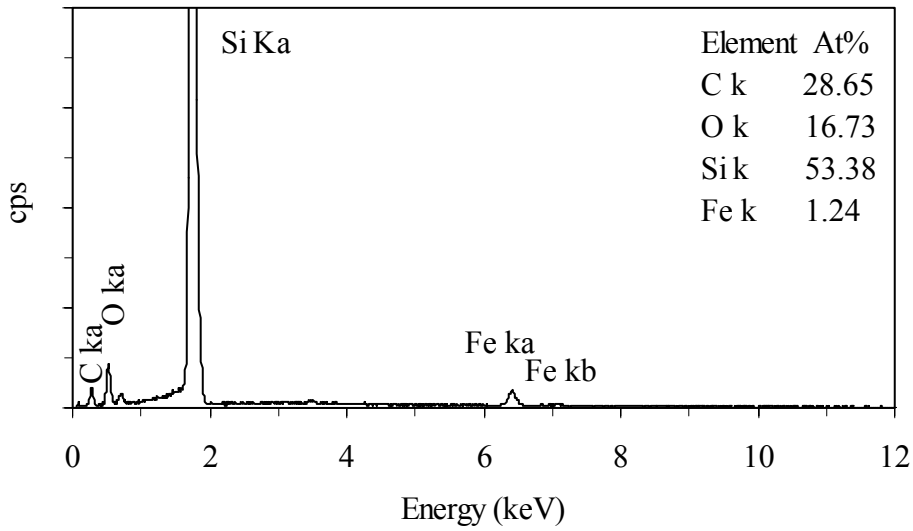

Figure 5.5 EDX spectrum of a film deposited from ferrocene and TMS on Si(100) substrate using DDT.

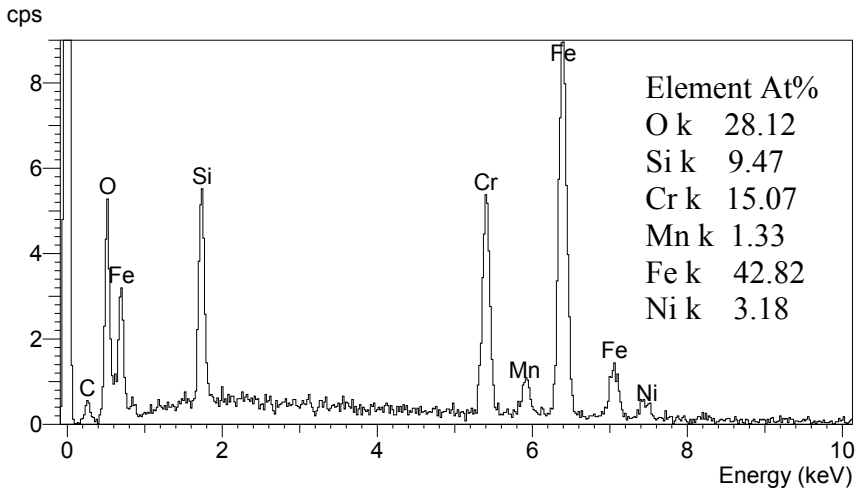

Figure 5.6 EDX spectrum of a film deposited from ferrocene and TMS on stainless steel substrate using DDT.

5.3.2 Step Deposition Technique (SDT):

Ferrocene and TMS precursors were separately supplied to the CVD chamber. An iron film was deposited on the substrate surface; then a silicon film was deposited on the surface of the deposited iron film. Before practicing this technique, iron and

silicon films were prepared separately and analyzed by XRD, SEM and EDX.

5.3.2.1 Deposition of Iron Films:

Steel and silicon substrates were used in each experimental run for investigating the growth of iron films. The same preparations of the substrates and the HLR-CVD system introduced in the experimental procedure section have been followed. Effects of deposition as a function of substrate temperature, ferrocene sublimation temperature and hydrogen flow rate as a reactant gas were studied.

5.3.2.1.1 Effect of Substrate Temperature:

CVD experiments were carried out at different substrate temperature of 650, 700, 750 and 800°C. The reactor pressure was kept constant at 30 mbar and the deposition time was 60 min for each run. The ferrocene powder was sublimated at temperature of 70°C and transported to the CVD chamber by 50 sccm argon flow. Thus, the gas mixture in the reactor consisted of 98.549 mol % Argon and 1.451 mol % Ferrocene. After 10 min, a black powder layer started to cover the substrate and the substrate holder. This result was observed at all studied deposition temperatures. The mass of the film was obtained by subtracting the weight of the substrate before deposition from the weight after deposition. The grown film on silicon substrate was a black powder layer. At substrate temperature of 650°C, the black layer covered a small surface area of the substrate and at of 700 and 750°C, the layers were very dense and covered the entire substrates surfaces homogeneously, while at 800°C, it was a thin very fine black powder layer. The black powder layer was a non adhering film; it can be scratched easily from the substrate surface. Films grown on steel substrates consisted of well adhering gray films covered with small amounts of black powder. At

650°C large amount of black powder was observed on the surface of the gray film while at higher temperature the amount of the powder is negligible. Also, this powder can be easily removed from the surface of the film. XRD analyses of the black powder and the gray film show that the gray film was an iron carbide film, Figure 5.12 (b), and the black powder consisted of iron, carbon and iron carbide compounds, Figure 5.13 (b).

Figure 5.7 shows the growth rate of the films on silicon and steel substrates. The deposition temperature seems to modify the growth rates of the deposited films as well as the substrate material (silicon or stainless steel). The opposite devaluation of the two curves could be related to the material of the surface. At 700°C, the mass of the films on both substrates are almost the same, while the films are completely different. A possible explanation could be that iron and carbon atoms in the gas phase react with the iron in the steel substrate and produce well adhering iron carbide films, while no strong iron silicon bonds are formed on the surface and the formed iron is blown away.

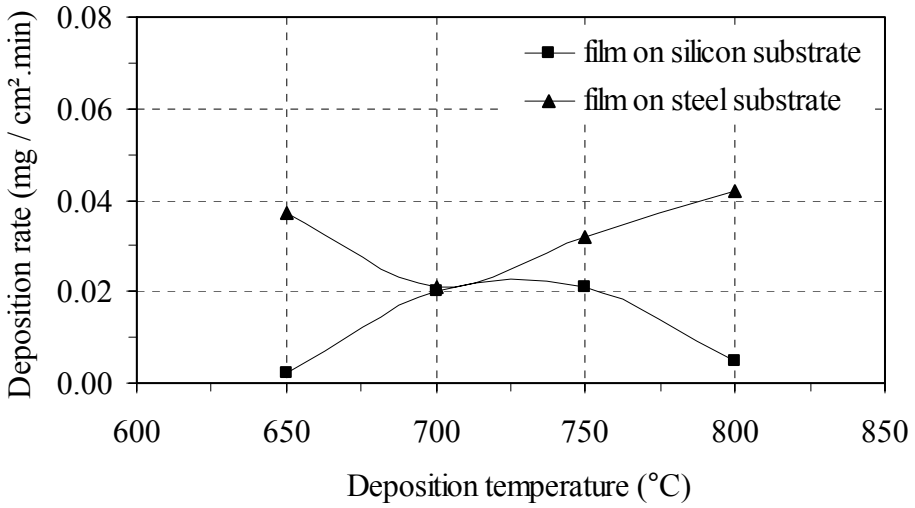

Figure 5.7 Average deposition rates of the deposited films from ferrocene on silicon and steel substrates at various deposition temperatures.

5.3.2.1.2 Effect of Ferrocene Sublimation Temperature:

In order to study the effect of the amount of ferrocene vapor in the gas phase, which is directly related to the ferrocene sublimation temperature, experimental runs were performed at 700°C substrate temperature, 50 sccm of argon flow and ferrocene sublimation temperature of 60°C and 80°C. A hill of a black powder was observed on the silicon substrate in front of the nozzle when the experiment was performed at ferrocene sublimation temperature of 80°C. At 60°C, less amount of black powder was produced in the same deposition time. Changing the sublimation temperature changes the vapor phase concentration of ferrocene and thus leads to the production of less or more black powder in the gas phase but no pure iron film was deposited.

5.3.2.1.3 Effect of Hydrogen Flow:

In order to reduce the amount of carbon in the deposited film, the effect of hydrogen flow on film deposition was studied during the deposition process at the deposition temperature of 700°C. Hydrogen flow rates of 0, 25, 100, 300 and 500 sccm were applied at 35 mbar and 100 mbar reactor pressures. The ferrocene sublimation temperature was kept constant at 70°C and the argon flow carrying ferrocene vapor was fixed to 50 sccm. In all cases black powder was deposited on silicon substrates and gray films covered with some black powder were deposited on the steel substrates. Every substrate was weighed before and after deposition, the deposition rate was calculated as a function of substrate area and 60 min deposition time. Results were plotted in Figures 5.8 and 5.9 for films deposited on silicon and steel substrates, respectively. On silicon at 35 mbar, the deposition rate decreases continuously to almost no film on the substrate at 500 sccm. However, when the pressure is 100 mbar, the deposited mass first increases at 25 sccm H_2 flow, after that it decreases while

further increasing the H_2 flow, as presented in Figure 5.8. The effect of increased H_2 flow at 35 mbar and 100 mbar on deposited films on steel substrates is a slight increase in the deposited mass compared to hydrogen free experiments and may be considered as nearly constant for hydrogen flows from 25 to 500 sccm. When the two Figures 5.8 and 5.9 compared, it seems that the surface adhesion and the material of the substrate are more important for the deposited mass than the change in hydrogen flow, the poorly adhering films and powders on silicon are blown away, while the well adhering films on steel can not blown away by increased flow.

From XRD and EDX analyses, one can conclude that no pure iron films can be deposited directly on both silicon and steel substrates by changing the substrate temperature or ferrocene sublimation temperature or supplying a different amount of hydrogen during the deposition process.

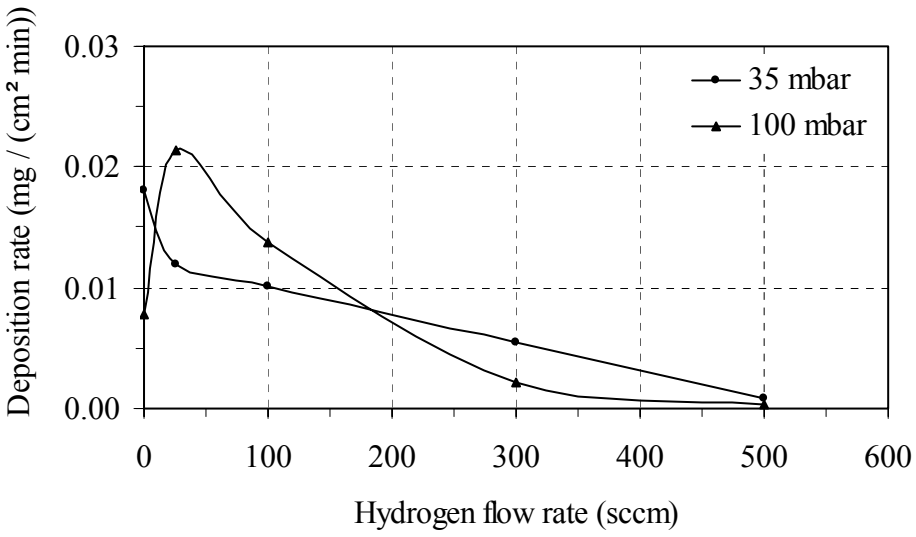

Figure 5.8 Relationship between deposition rates of films deposited on silicon substrate at 700°C and hydrogen flow at 35 and 100 mbar of depositing pressures.

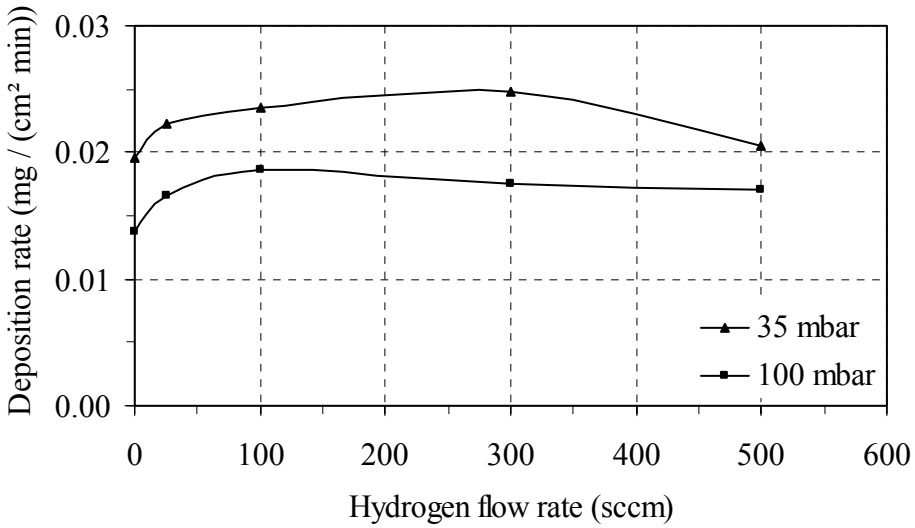

Figure 5.9 Relationship between deposition rates of films deposited on stainless steel substrate at 700°C and hydrogen flow at 35 and 100 mbar of depositing pressures.

5.3.2.1.4 Treatment of As-deposited Films with Hydrogen flow:

As concluded from last section no pure iron film could be deposited under the designed deposition conditions. However, treatment with hydrogen flow of as-deposited films which are black powder and gray films on silicon and steel substrates were investigated to grow pure iron films. The films deposited at 700°C were chosen for this investigation. At this deposition temperature, the deposition rate is independent of the chosen substrate as shown in Figure 5.7. As-deposited films grown on both silicon and steel substrates were analyzed by XRD before the treatment with hydrogen. Results illustrated in Figure 4.12 (b) show that the film grown on silicon substrates consisted of carbon, iron and iron carbide compounds. The as-deposited films on steel substrates, which were gray films, consisted of iron carbide compound as shown by the XRD analyses in Figure 5.13 (b). The studied films were treated with hydrogen flows of 300 to 500 sccm and annealing temperatures equal to the

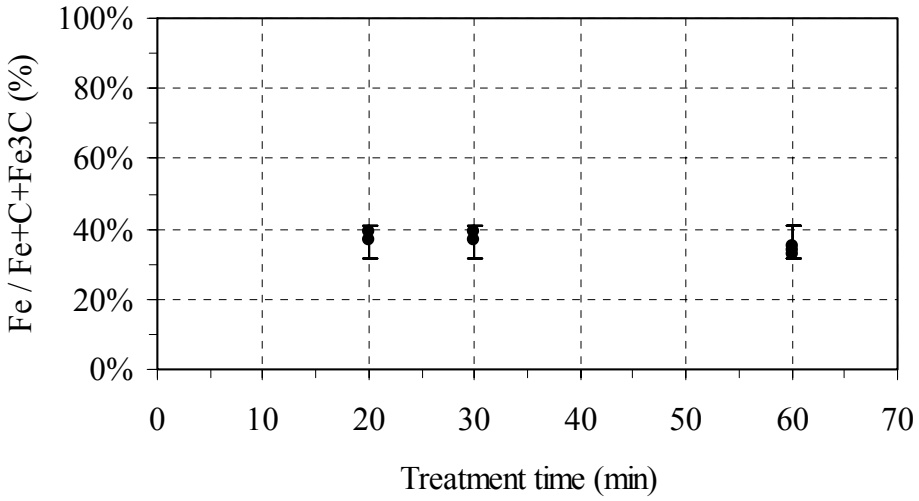

Figure 5.10 Mass of iron in as-deposited film (Fe+C+Fe3C) on silicon substrate at 700°C and different hydrogen treatment time.

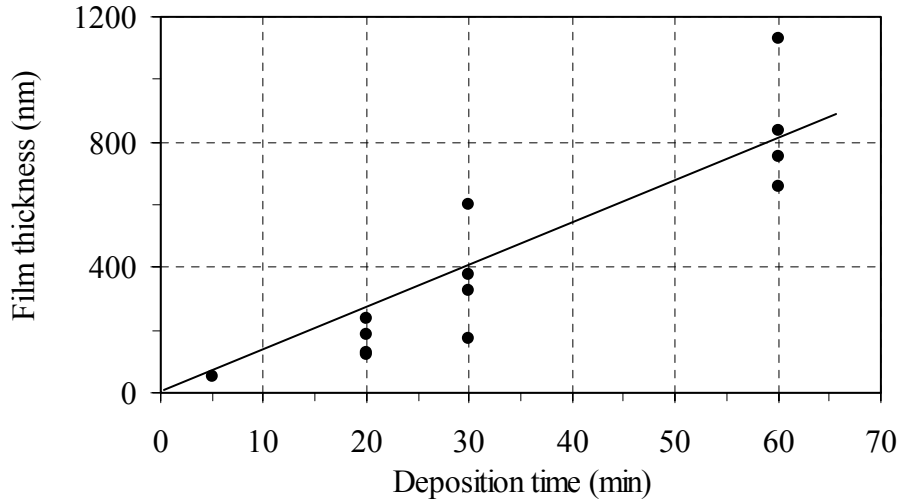

Figure 5.11 Relationship between thicknesses of the pure iron films deposited on silicon substrate at 700°C and deposition time.

deposition temperature, which is 700°C. All treatments were carried out at 100 mbar reactor pressure. Numbers of as-deposited films prepared at various deposition times of 20, 30 and 60 min on silicon substrates were treated with hydrogen for 20, 30 and 60 min respectively. During the treatment process, it was observed that the black

powder was changing from black to gray color. Every substrate was weighed before and after treatment. The mass percentage of iron in the as-deposited films was calculated by dividing the mass of the film after treatment over the mass of the film before treatment. Results illustrated in Figure 5.10, show that the percentage of mass of iron film was approximately constant. Between 35% to 40 % of the black powder was iron and the rest was evaporated during the treatment period for every studied film. The film thickness was calculated from the change in mass and the density of bulk iron (7.87 g/cm^3) [7]. Figure 5.11 shows a linear relationship between the thickness of the iron films and the deposition time. In addition, pure iron films were prepared on steel substrates after performing the same treatment of as-deposited films with hydrogen flow.

5.3.2.1.5 Film Analysis:

The structure, surface morphology and chemical composition of the films were analyzed by XRD, SEM and EDX respectively. The phase composition of the films deposited at 650, 700, 750, 800°C were analyzed by XRD. The XRD patterns show that all films, which consisted of black powders, were iron contaminated by graphitic carbon and iron carbide. Figure 5.12 (b) shows the XRD patterns of a black powder film on silicon substrate at 700°C. Peaks of carbon, iron carbide, Fe_3C, and iron are clearly observed. Films deposited on steel substrates consisted of only iron carbide, Fe_3C. Figure 5.13 (b) shows the XRD patterns of a film on steel substrate deposited at 700°C. XRD patterns of the hydrogen treated films on silicon and steel substrates are presented in Figure 5.12 (c) and 5.13 (c) respectively and compared with films before treatment; all peaks of carbon and iron carbide disappeared. Only sharp diffraction peaks of iron were obtained, for both, hydrogen treated films on silicon and steel

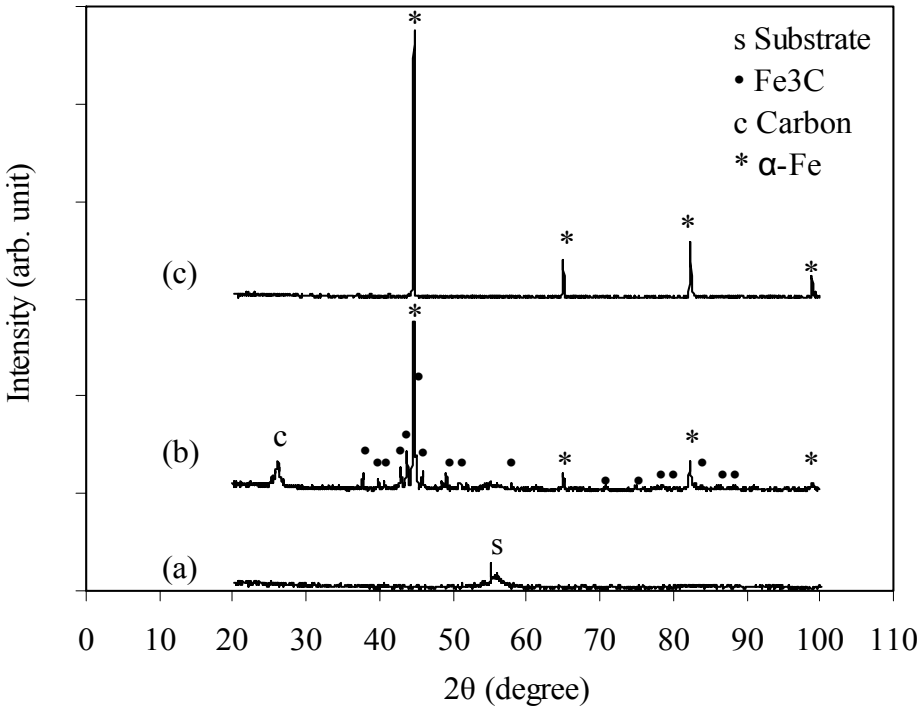

Figure 5.12 XRD patterns of films deposited on silicon substrate at 700°C: (a) Clean silicon substrate, (b) as-deposited film, (c) film after treatment with H_2.

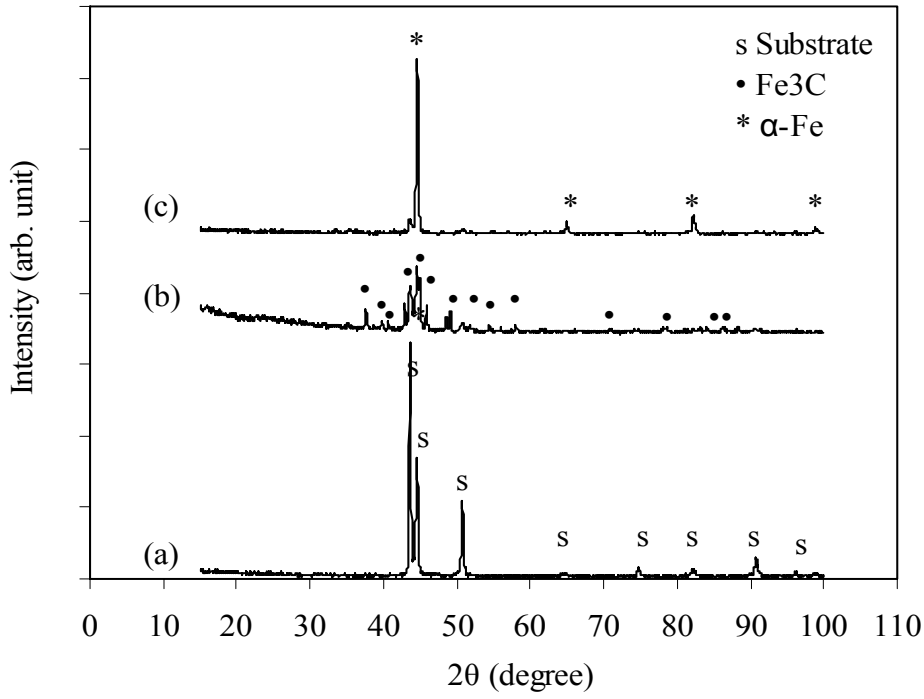

Figure 5.13 XRD patterns of films deposited on steel substrate at 700°C: (a) clean stainless steel substrate, (b) as-deposited film, (c) film after treatment with H_2.

substrates, and they corresponded to the crystalline iron alpha phase (α-Fe).

SEM top view images of as-deposited film on silicon substrate for 60 min at 700°C are shown in Figure 5.14. Carbon Nanotubes (CNT) clearly appeared as seen in image (b) with magnification of 50000K.

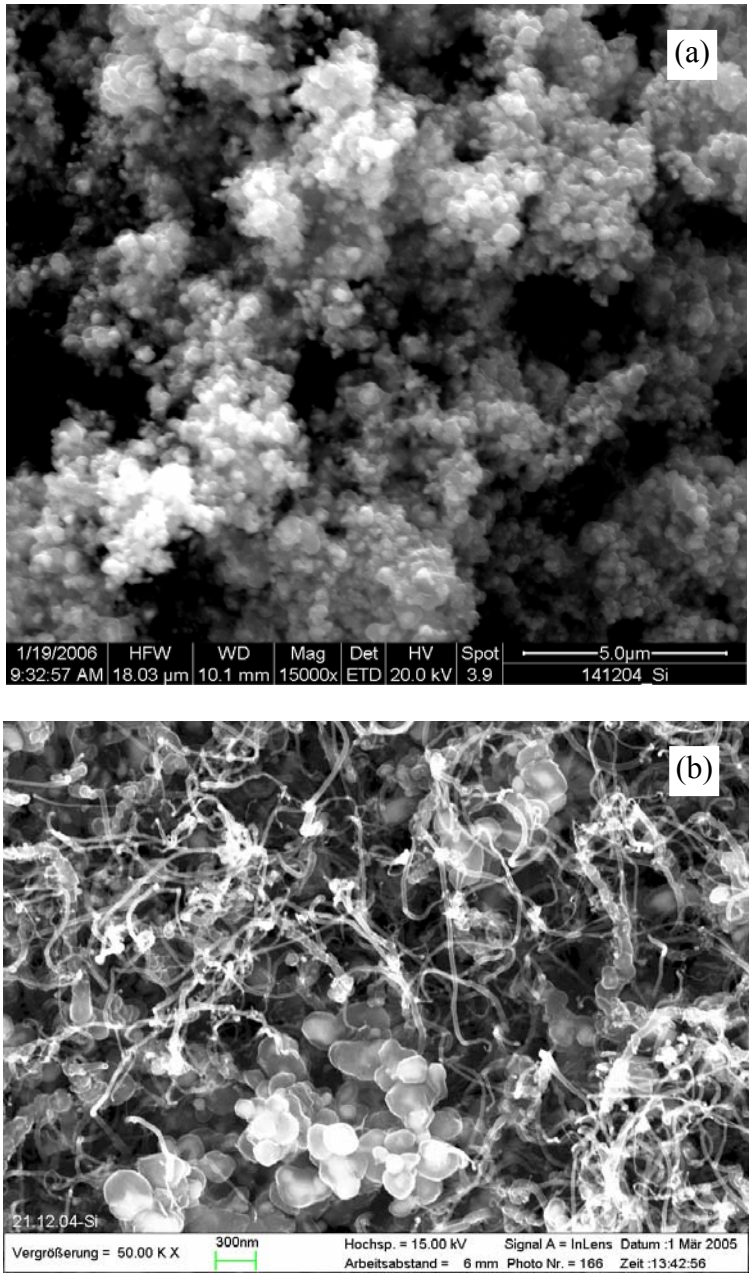

Figure 5.14 SEM image of a black powder film deposited on silicon substrate at 700°C, (a) 15000K and (b) 50000K.

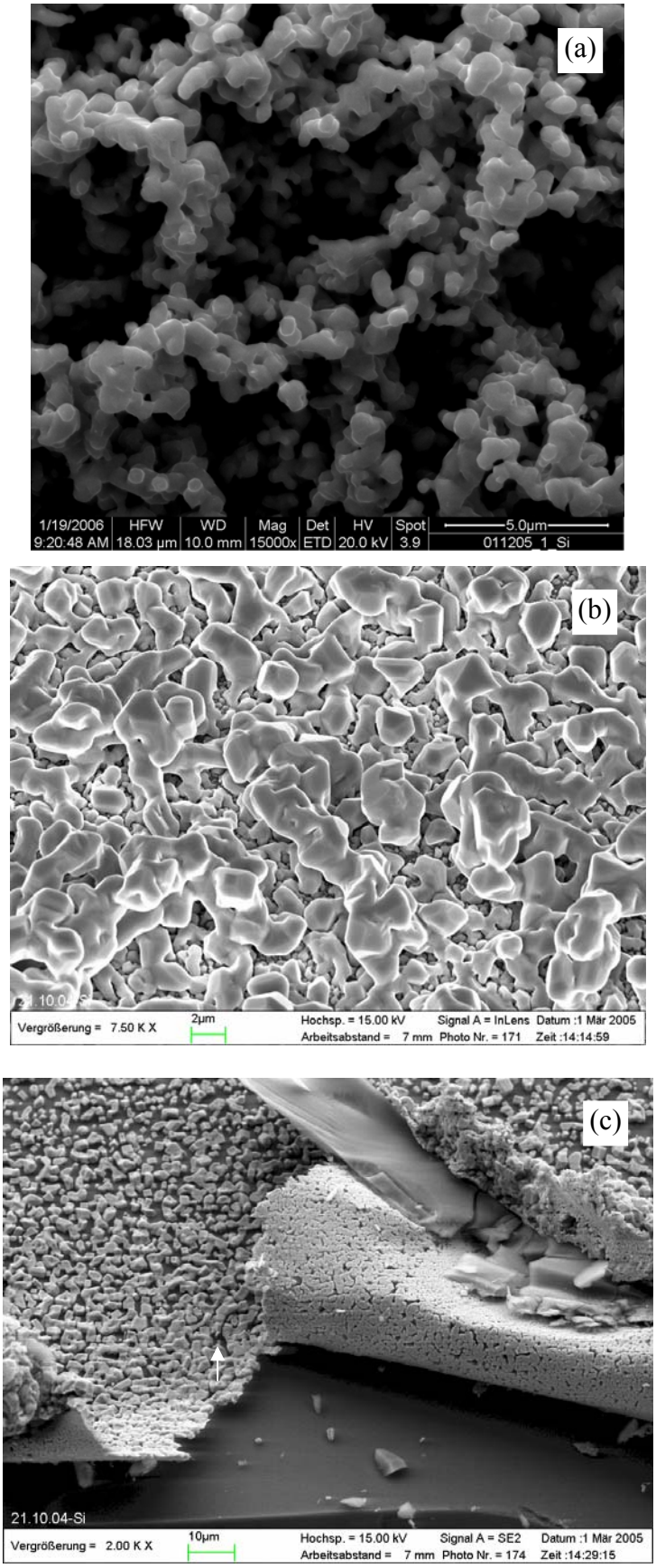

Figure 5.15 SEM image of an iron film deposited on silicon substrate after treatment with H_2, (a) 15000K, (b) 7500K and (c) 2000K.

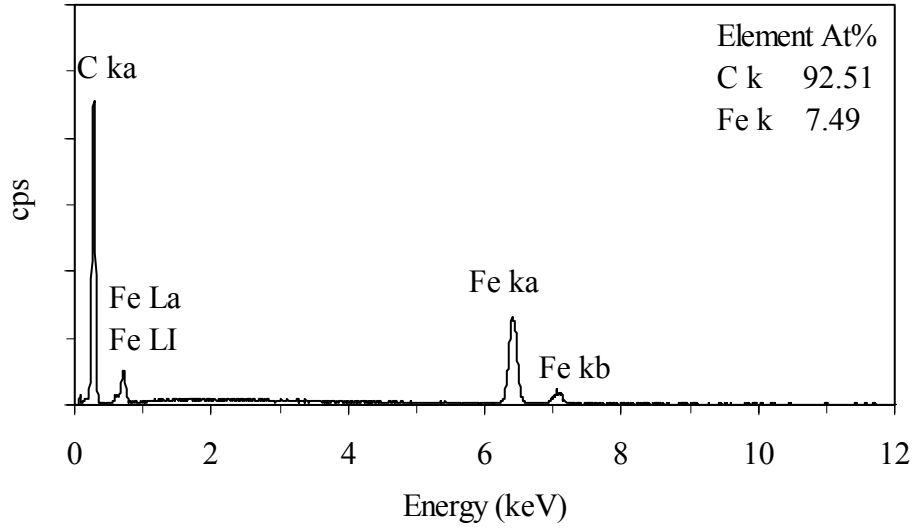

Figure 5.16 EDX spectrum of a black powder film deposited on silicon substrate at 700°C.

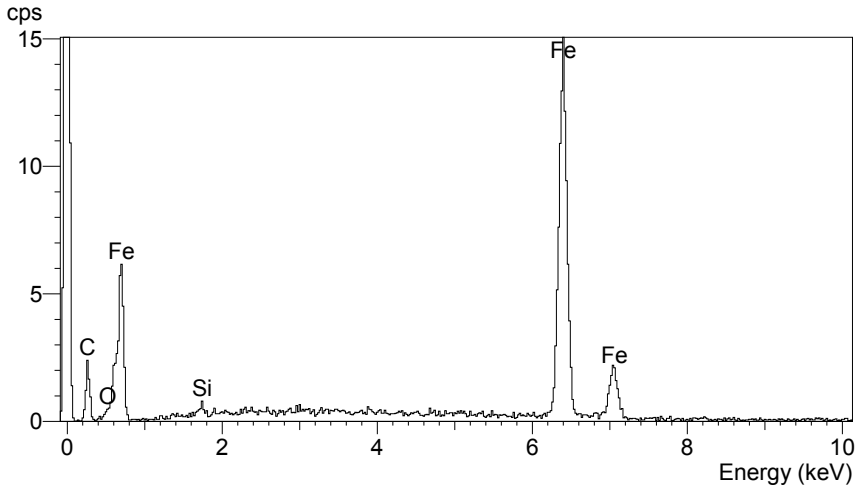

Figure 5.17 EDX spectrum of an iron film deposited on silicon substrate after treatment with H_2.

The cubic phase of alpha iron can also be recognized in the structure of the film even at the low magnification of 15000X, (image (a)). Atomic percentage of iron and carbon in the film was analyzed by EDX, only 7.5 % of the film consisted of iron and the rest was carbon as shown in Figure 5.16.

SEM top view images of treated films grown on silicon substrates, Figure 5.15, shows

clearly the cubic structure of α-Fe films. The thickness of the film might also be evaluated from a broken film shown in Figure 5.15 (c); it is around 1.3 microns. The calculated thickness of the same broken film based on the density of bulk pure iron was 1.1 microns. Both results are in good agreement.

The chemical composition of the treated films on the silicon substrates were analyzed with EDX. The iron content strongly increased related to the carbon content. Figure 5.17 shows the spectrum of the elements in the film.

Pure iron films could be prepared from as-deposited films from ferrocene on silicon and steel substrates. As-deposited films, which are mixture of carbon, iron and iron carbide, were treated with 300 to 500 sccm hydrogen flow at treatment temperature of 700°C and a reactor pressure of 100 mbar. A treatment time, which is equal to the deposition time, is sufficient for film purification.

5.3.2.2 Deposition of Silicon Films:

Silicon films were deposited from TMS on steel substrate using the HLR-CVD system. Steel substrates were cleaned and weighed before loading them into the reactor. The deposition temperature was 800°C. The reactor pressure was set to 30 mbar. TMS as a silicon precursor was evaporated at room temperature. A TMS vapor flow of 5 to 40 sccm, (9.1 to 44.444 mol %), was mixed with hydrogen flow of 50 sccm, both flows were controlled by mass flow controller before mixing. They are transported to the reactor through the nozzle. After 60 min of deposition the substrate was cooled under vacuum and analyzed using XRD, SEM and EDX.

5.3.2.2.1 Deposition Results and Film Analysis:

The deposits were transparent films at all used TMS flow rates, the substrate color

was changed from the clean stainless steel, shining silver, to rainbow colored interferences. The deposition growth rates were evaluated from the mass changes of the substrates. Figure 5.18 shows the depositions grow rates at 5, 15, 20 and 40 sccm, (9.1, 23.077, 28.571, 44.444 mol %), of TMS in 60 min deposition time. The deposition growth rate is directly proportional to the flow of TMS, thus thicker films can be grown by increasing the flow rate of TMS.

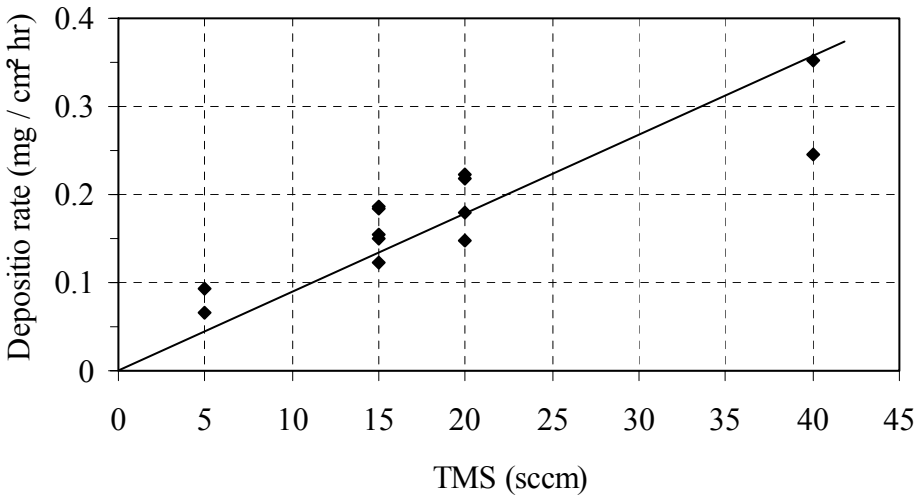

Figure 5.18 Deposition rates of silicon films deposited on steel substrates from TMS.

Films deposited at 800°C using 15 sccm TMS for 60 min, were analyzed to identify the phase composition, morphology and chemical composition. Some silicon peaks appeared in the XRD patterns as shown in Figure 5.19, also some peaks of steel substrate are still visible. The other peaks, which can be recognized in the patterns, are related to Cr_2O_3. This result indicated that the deposited film was just about to change from the amorphous to the crystalline phase. Figure 5.20 shows SEM images at two different magnification of 7500X and 50000X and compare the substrate surface before and after deposition. It can be recognized that the film is homogenous

and covers the entire substrate surface area.

Comparing Figure 5.21 of a clean steel substrate with Figure 5.22 of the deposited one shows that the deposit was a silicon film. Around 27 % atomic percentage of Si was detected by EDX analysis compared to the very low atomic percentage of Si in a clean stainless steel substrate, which is less than 1%. The detected amount of carbon in the film was approximately same as the amount detected in the clean substrate. The high percentage of oxygen presents in the deposited film might come from atmosphere contamination during the storage period of the deposited substrate.

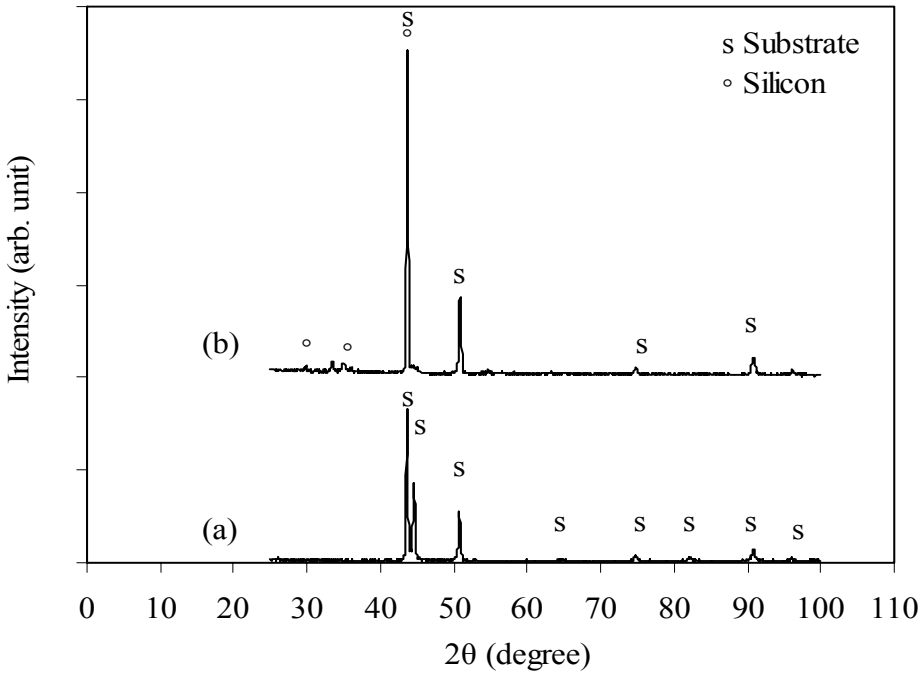

Figure 5.19 XRD patterns of: (a) a clean steel substrate, (b) as deposited silicon film from TMS.

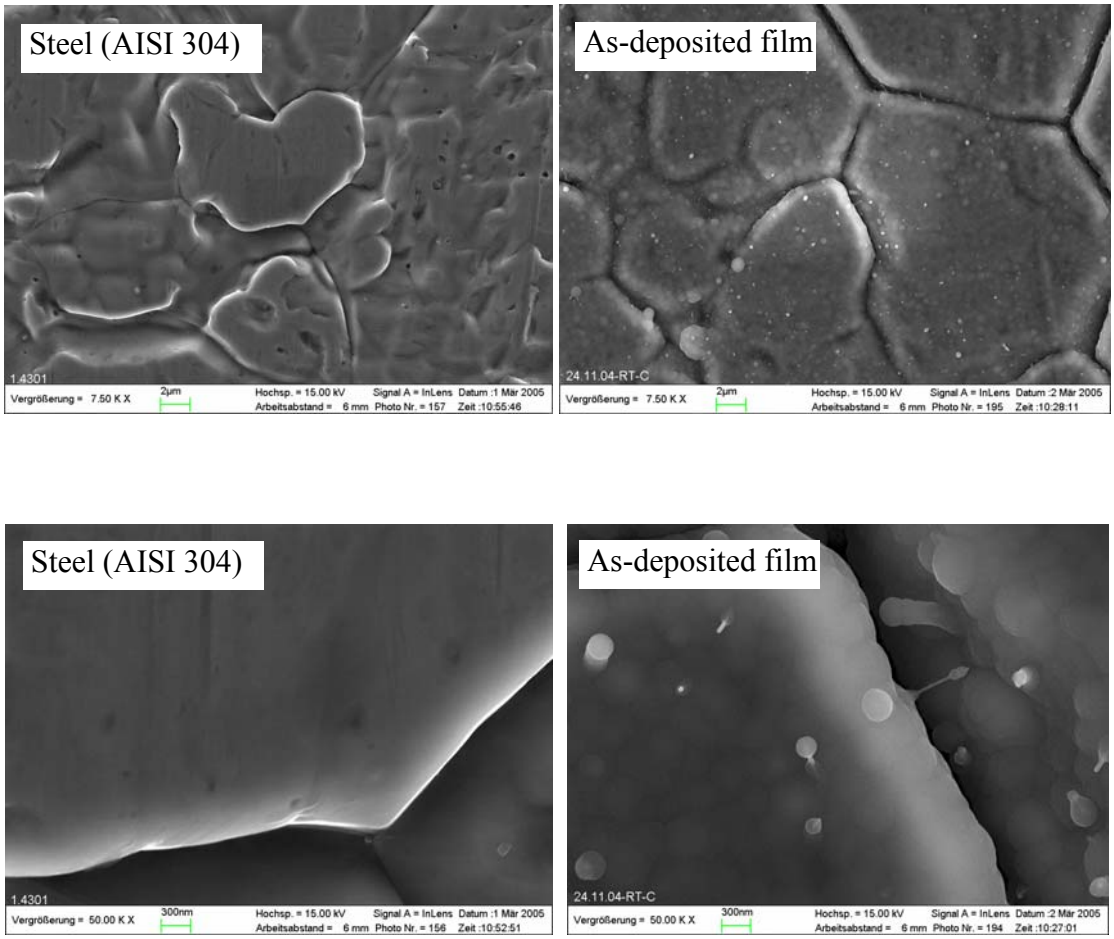

Figure 5.20 SEM image of a silicon film deposited on steel substrate from TMS.

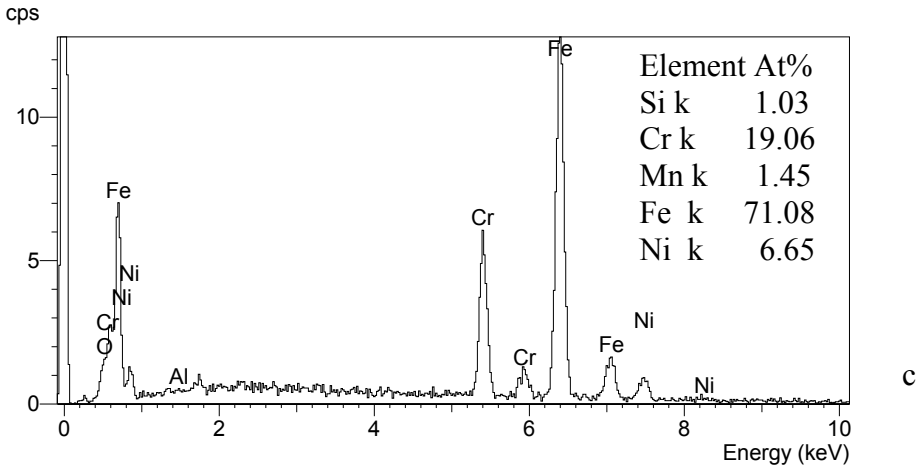

Figure 5.21 EDX spectrum of a clean stainless steel substrate.

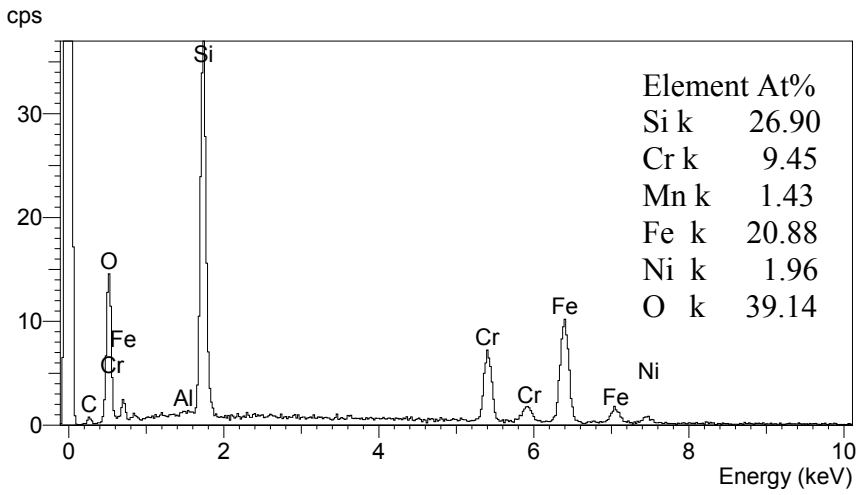

Figure 5.22 EDX spectrum of a silicon film deposited on steel substrate from TMS.

5.3.2.3 Deposition of Beta Iron Disilicide Films:

Beta iron disilicide films were deposited on silicon substrates in HLR-CVD system using a step deposition technique (SDT). From the results presented in section 5.3.2.1 and section 5.3.2.2, the deposition procedures and deposition conditions required for deposition of iron and silicon films were established and could now be used to prepare beta iron disilicide films. The film was prepared from deposition of pure iron film on the substrate followed by deposition of silicon film on the surface of the iron film. Ferrocene vapor was carried by 50 sccm of argon for 20 min at 700°C. The black powder film was treated with 500 sccm hydrogen flow for 20 min at the same deposition temperature. The silicon film was deposited for 60 min at 800°C from 30 sccm flow rate of TMS mixed with 50 sccm of hydrogen flow. Figure 5.23 shows the growth sequence of beta iron disilicide films in a HLR.

5.3.2.3.1 Deposition Results and Film Analysis:

The final deposited film was a transparent and well adhering film. The mass of the

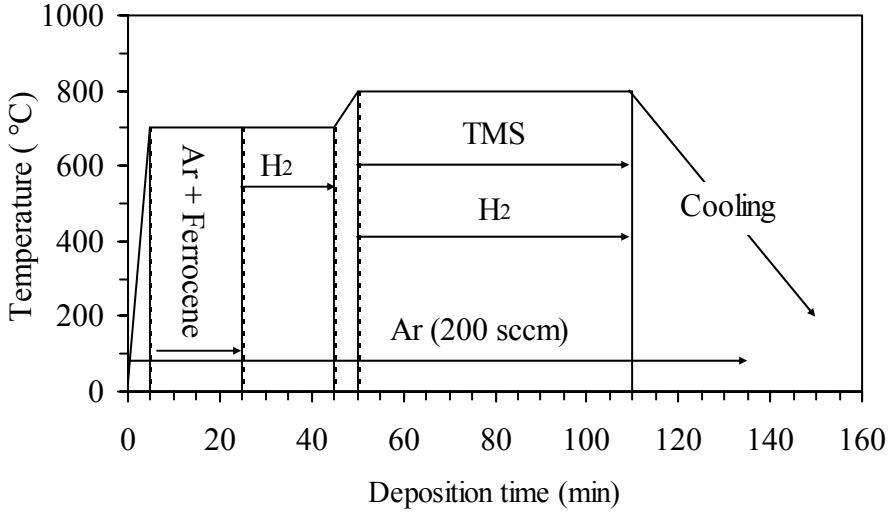

Figure 5.23 Growth sequences of beta iron disilicide films in HLR.

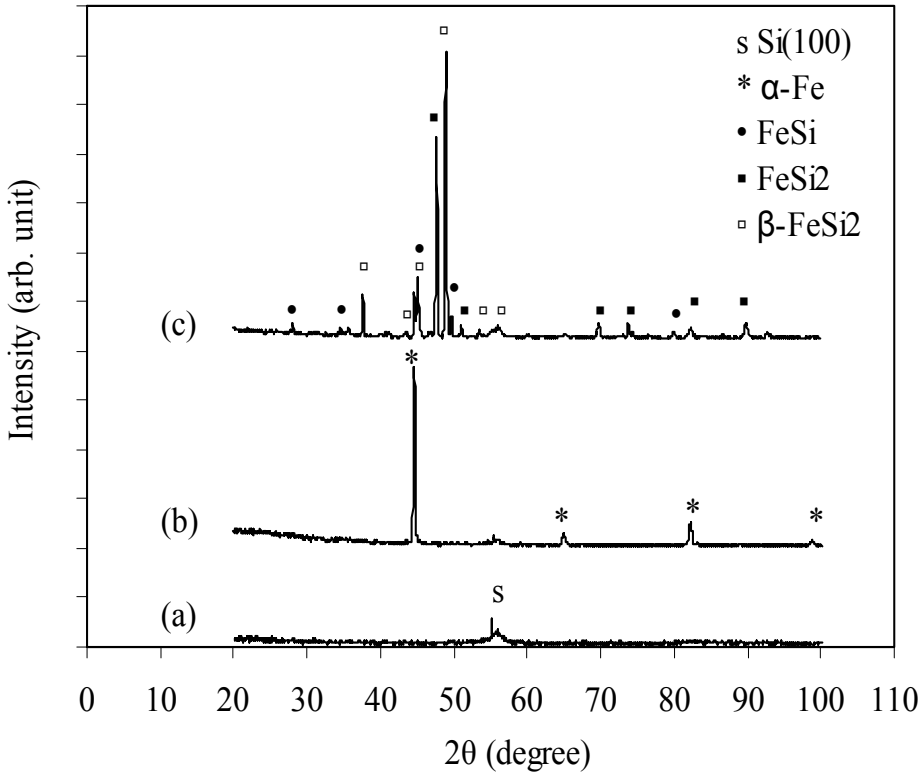

Figure 5.24 XRD patterns of iron disilicide film deposited from ferrocene and TMS using SDT: (a) clean Si(100), (b) film before annealing, (c) film after annealing.

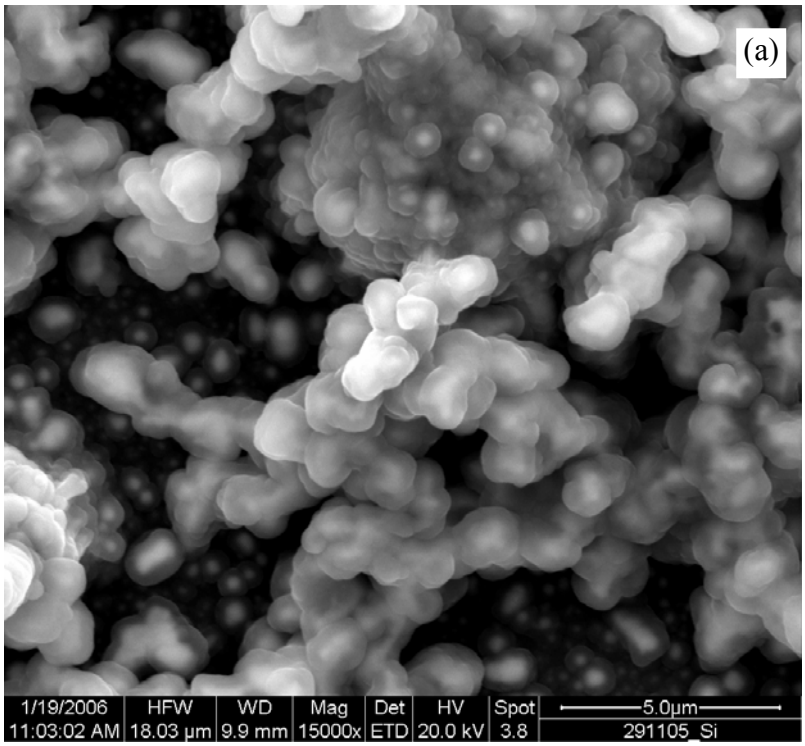

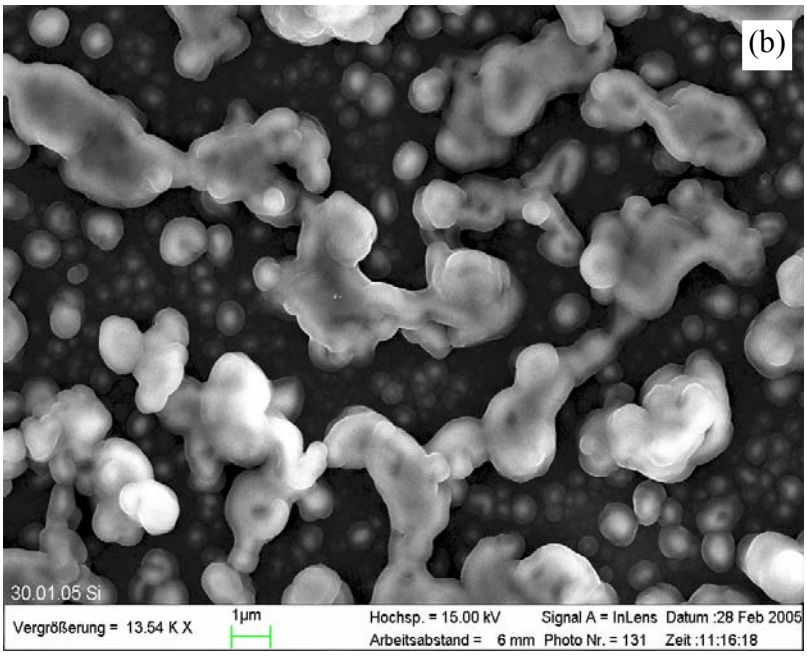

Figure 5.25 SEM image of iron disilicide film deposited on silicon substrate from ferrocene and TMS using SDT, (a) film before annealing (15000K) and (b) film after annealing (13540K).

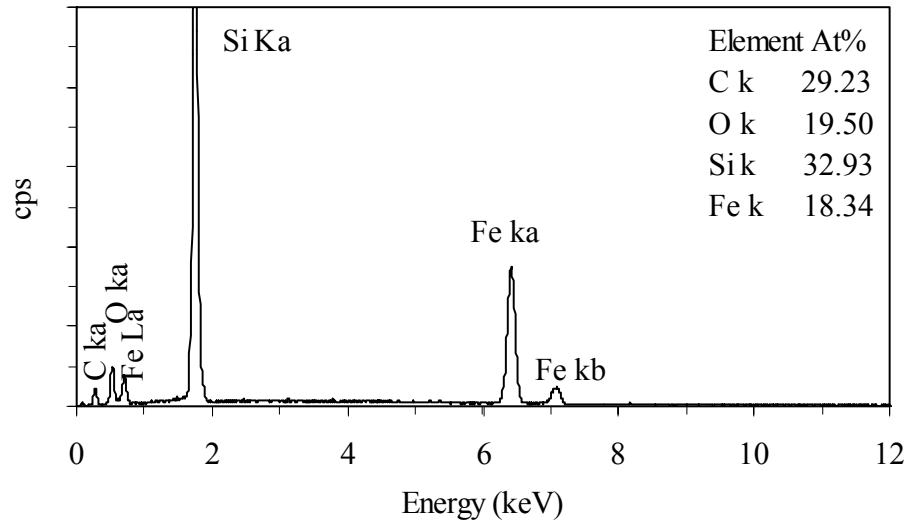

Figure 5.26 EDX spectrum of iron disilicide film deposited from ferrocene and TMS on silicon substrate using SDT (before annealing).

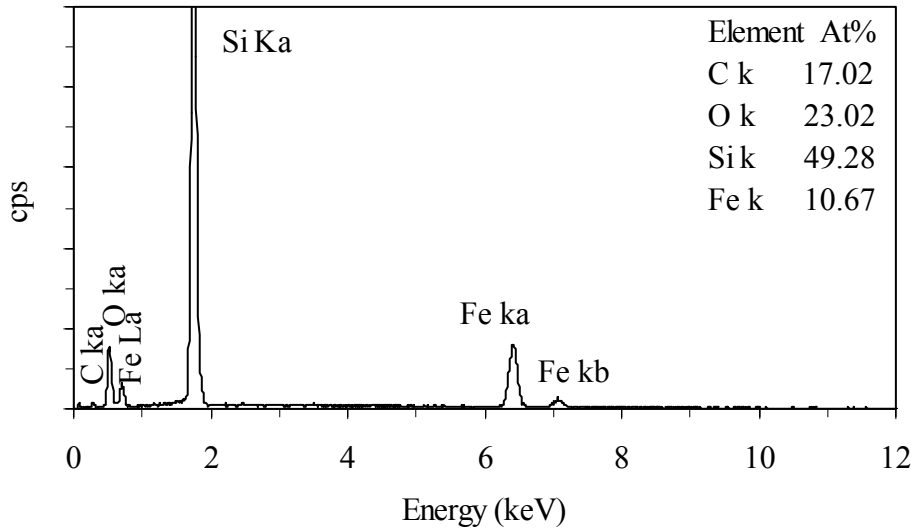

Figure 5.27 EDX spectrum of iron disilicide film deposited from ferrocene and TMS on silicon substrate using SDT (after annealing).

film was calculated from the change in substrate weight before and after deposition. Some films were analyzed without further heat treatment by XRD, SEM and EDX. No XRD peaks related to iron disilicide were detected; only peaks of α-Fe crystalline film appeared, also indicating that the silicon film deposited on iron film was

amorphous. Figure 5.24 (b) shows the patterns of as-deposited film. However, after annealing the film at 930°C for 2 hr in 1.3 mbar and 100 sccm flow of nitrogen, a crystalline film of iron silicide was formed. XRD peaks of iron disappeared while peaks of crystalline FeSi, $FeSi_2$ and β-$FeSi_2$ were clearly observed. Figure 5.24 shows the composition of deposited film before and after annealing.

From the SEM image shown in Figure 5.25 (a), it seems that a silicon film was growing on the cubic structure of the iron film, this can be clearly observed by comparing this image with the image (a) in Figure 5.16. In addition, the crystalline structure of annealed film is visible in image (b) of Figure 5.25.

The chemical compositions of the film before and after annealing were analyzed by EDX. The atomic percentage of iron to silicon elements in the film before annealing was 1:2, and for the annealed film it was 1:4.5. Other elements such as carbon and oxygen were presented in the film too. Figure 5.26 and 5.27 show the result of EDX analyses for deposited films before and after annealing respectively.

5.4 Summary:

A reactor with lamp heating was constructed and successfully used to deposit thin films. This appropriate design provides good advantages of varying and controlling the substrate temperature even during the deposition process. The usage of the relatively cheap and easy to handle materials, TMS and ferrocene as precursors, is also an advantage of using this CVD setup. The deposition of iron films at 700°C, treated with hydrogen for purification at 700°C followed by the deposition of silicon at 800°C in a continues deposition process was successful in the deposition of $FeSi_2$. The direct deposition of β-$FeSi_2$ was not possible. In the direct deposition experiments, a very low percentage of iron was detected in the films compared to

silicon. This might be due to the difficulty of a direct deposition of pure iron films from ferrocene. It is possible to deposit amorphous beta iron disilicide films from ferrocene and TMS by using the SDT. Crystalline iron films were deposited firstly on the silicon substrate and followed by deposition of silicon film. Crystalline β-$FeSi_2$ mixed with other phases of iron silicide was successfully prepared by heat treatment of the deposited amorphous film for 2 hr at 900-950°C. In future a further optimization of the procedure concerning the relative deposition times of the two films should lead to even pure silicide deposition.

Chapter 6

Conclusions

Two reactors were constructed and used for CVD studies. The first one is a Hot Wall Reactor (HWR). It is used for the deposition of aluminium oxide films. Thin films of Al_2O_3 were deposited by using a low cost CVD set-up. The deposition was performed on stainless steel (AISI 304) substrate at ambient pressure that avoids the usage of an expensive vacuum system. Amorphous Al_2O_3 films were successfully deposited by using aluminium acetylacetonate and synthetic air as precursors. At temperature of 360°C, the film started to grow. Up to 450°C, a quite homogeneous deposition was achieved in the reactor center for about 20 cm. The maximum deposition rate was achieved at furnace temperature of 500°C at the center of the furnace as the decomposition of $Al(acac)_3$ becomes too fast. The deposition rate is related to the substrate position and the furnace control temperature. As the furnace temperature increase, the position of maximum deposition rate was shifted towards the entrance of the reactor. Behind that position, the depletion of the precursor in the gas phase controls the growth rate; at higher furnaces temperatures deposition rates are reduced. Nevertheless, thicker films were deposited by increasing the deposition time. The film thickness increases nearly linearly with deposition time (at 2 hr deposition time it is ~0.6 μm and ~2.1μm at 8 hr).

The deposited films at 500°C are transparent and adhesive. As shown by XRD, SEM and EDX analyses, the films are amorphous, completely closed and consist of aluminium and oxygen. Crystalline alumina films, forming at T>>600°C, could not be directly deposited by increasing the furnace control temperature using this setup. Thus crystalline phases are prepared by annealing the amorphous films, at 800°C the films

became (γ-Al_2O_3), and at 1115°C (α-Al_2O_3) was observed. As-deposited film were mechanically and chemically stable up to annealing temperature of 800°C but above this temperature the film can not survive, it is spalling.

The second reactor is a Halogen Lamp Reactor (HLR). The reactor was designed and build for the deposition of β-$FeSi_2$. Light from halogen lamps are used to heat the substrate. Fast heating ramp-up and cool-down (saving time), low thermal budget, reduced contamination, possibility of deposition of different films and many layers at different deposition temperatures and composition at the same experimental run are some advantages of using this efficient non-contact substrate heater. The maximum substrate temperature which can be achieved was slightly above 800°C. By this design a maximum set point temperature of 800°C and any temperature down to room temperature are easily achieved and controlled.

It has been shown that ferrocene and TMS can be used successfully as source materials of iron and silicon for deposition of β-$FeSi_2$, respectively. The deposition was performed in a HLR at low pressure and substrate temperature of 785-800°C by using two deposition techniques, direct deposition and step deposition techniques.

Films deposited using the direct deposition technique (DDT) were amorphous films mainly consists of silicon and very low percentage of iron as detected by EDX.

In SDT, iron films were deposited on silicon substrates followed by silicon deposition on the surface of the iron films. Both films iron and silicon were successfully deposited separately on silicon and stainless steel substrates respectively before forming β-$FeSi_2$ films by annealing using SDT. Crystalline iron films were prepared by two steps: growth of a black powder layer consisting of iron and carbon and converting this layer to pure iron by supplying hydrogen at the deposition temperature. The black powder layers were deposited on silicon substrates at 700°C

and 30 mbar and treated with 300 to 500 sccm hydrogen at same temperature and 100 mbar. The iron film purification depended on treatment time; longer treatment time lead to a higher reduction of the carbon contamination level. Amorphous silicon films were deposited on stainless steel substrates at 800°C and 30 mbar.

Amorphous β-$FeSi_2$ was formed by using two step deposition technique (SDT). Crystalline iron films were deposited on the substrate at 700°C and silicon films were deposited on the iron films at 785-800°C. Crystalline β-$FeSi_2$ could be formed by a heating treatment of these films for 2 hr at 900-950°C. XRD and EDX show that the film is transformed to a crystalline β-$FeSi_2$ mixed with other phases of iron silicide. This step deposition seems to be more effective technique than the direct deposition. Deposition of β-$FeSi_2$ using ferrocene and TMS as precursors was successfully achieved.

Further properties, like adhesion strength of thin alumina films and thermo-electrical property of iron disilicide films could not be addressed in the present work; these should be studied in future. The composition of the formed iron silicide films should also depend on the deposition thicknesses of the iron and silicon films, here is a further potential for improvement.

References

1. H. O. Pierson, "*Handbook of Chemical Vapor Deposition (CVD)*", Noyes Pub. / W. Andrew Pub., LLC, Norwich New York, USA. 1999.
2. D. L. Smith, "*Thin-Film Deposition*", McGraw Hill, 1995.
3. M. Ohring, "*Material Science of Thin Films*", 2nd Ed. AP, 2001.
4. J. L. Vossen and W. Kern, "*Thin film Processes*", AP, 1978.
5. K. L. Choy, "*Chemical Vapor Deposition of Coatings*", Progress in Material Science 48, 57-170, 2003.
6. D. M. Dobkin and M. K. Zuraw, "*Principles of Chemical Vapor Deposition*", Kluwer Academic Publishers, 2003.
7. F. Incropera and D. DeWitt, "*Fundamentals of Heat and Mass Transfer*", John Willy & Sons, 5th.ed. , 2001.
8. Matthew Sweetland, John H. Lienhard V, "*Rapid IR Heating of Electronic Components in the Testing Cycle*", Proc. 35th National Heat Transfer Conf., California, 2001.
9. P. P. Apte and K. C. Saraswat, "*Rapid Thermal Processing Uniformity Using Multivariable Control of a Circularly Symmetric 3 Zone Lamp*", IEEE Trans. Semiconductor Manufacturing, vol. 5, pp.180-188, Aug. 1992.
10. J. Y. Choi, H. M. Do, "*A learning Approach of Wafer Temperature Control in Rapid Thermal Processing System*", IEEE Trans. Semiconductor Manufacturing, vol. 14, No. 1, Feb. 2001.
11. K. A. Conrad, R. K. Sampson, H. Z. Massoud, E. A. Irene, "*Design and Construction of a Rapid Thermal Processing System for in Situ Optical Measurements*", Rev. Sci. Instruments, 67(11), Nov. 1996.
12. P. Xu, J. Shao, Y. Yen, "*Experimental Study of Substrate Temperature*",

Applied Optics, Vol. 28, No. 14, July 1989.

13. S. Hung, C. Chao, C. Hsu, "*Lamp Design for Fast Cooling of Rapid Thermal Processes with a Two-Zone Lamp Using a Step Cooling Process*", Semicond. Sci. and Technol. 20, 72-79, 2005.
14. R. Singh, M. Fakhruddin, K. Pool, "*Rapid Photothermal Processing as a Semiconductor Manufacturing Technology for the 21st Century*", Applied Surface Science 168, 198-203, 2000.
15. A. Bouteville, "*Numerical Simulation Applied to Chemical Vapor Deposition Process. Rapid Thermal CVD and Spray CVD*", J. Optoelectron. Adv. Mater. Vol. 7, No. 2, 599-606, April 2005.
16. M. Lindstam, M. Boman, K. Piglmayer, "*Halogen Lamp-assisted High Rate Deposition of both Hard and Elastic Carbon Films from CH_2I_2*", Nucl. Instr. and Meth. In Phys. B 192, 274-279, 2002.
17. P. Logerais, M. Girtan. A. Bouteville, "RTLPCVD *Modeling: Steady-state Simulations*", (EUROCVD-15, Bochum, Germany), ECS Proceeding Vol. 2005-09, 49-56, 2005.
18. S. Krumidieck and H. Jung, "*Substrate Heater Design Investigation for Uniform Temperature in a Cold-Wall Low Pressure Reactor*", (EUROCVD-15, Bochum, Germany), ECS Proceeding Vol. 2005-09, 13-20, 2005.
19. Travis L. Turner and Robert L. Ash, "*Numerical and Experimental Analyses of the Radiant Heat Flux Produced by Quartz Heating Systems*", NASA Technical Paper 3387, March 1994.
20. R. Singh, "*Rapid Isothermal Processing*", J. Appl. Phys., 63 (8), R59-R114, 1988.
21. S. A. Norman, C. Schaper, and S. Boyd, "*Improvement of Temperature*

Uniformity in Rapid Thermal Processing Systems using Multivariable Control", Mat. Res. Soc. Proc., 1991.

22. M. Pettersson, S. Stenstrom, "*Modeling of an electric IR heater at transient and steady state conditions Part II: Modeling a paper dryer*", Intl. J. Heat Mass Trans., 43, 1223-1232, 2000.
23. H. Chang, R. A. Adomaitisa, J. Kidder and G. Rubloff, "*Influence of gas composition on wafer temperature in a tungsten chemical vapor deposition reactor: Experimental measurements, model development, and parameter identification*", J. Vac. Sci. Technol. B, Vol. 19, No. 1, Jan./Feb 2001.
24. M. Lindstam, O. Wanstrand, M. Boman and K. Piglmayer, "*Mechanical and tribological aspects on a-C films deposited by lamp assisted chemical vapor deposition*", Surf. Coat. Technol. 138, 264-268, 2001.
25. A. T. Fiory "*Methods in Rapid thermal Annealing*", Proceedings of RTP 2000, 8th. Int. Conf. on Advanced Thermal Processing of Semiconductors, Sept. 20 - 22, 15-25, 2000.
26. S. Moralesi and B. Dahhous, "*Temperature uniformity in RTP using MIMO Adaptive Control*", Int. J. Adapt. Control Signal Process. 12, 227-245, 1998.
27. T. Kobayashi, M. Okamura, E. Yamaguchi, Y. Shinoda, Y. Hirota, "*Effect of pyrolytic Al_2O_3 deposition temperature on inversion-mode InP metal-insulator-semiconductor field–effect transistor*", J. Appl. Phys. 2, 6734-6436, 1981.
28. R. H. Niska, A. P. Constant, T. Witt, and O. J. Gregory, "*Chemical Vapor deposition of Alpha Aluminum Oxide for High-Temperature Aerospace Sensors*", J. Vac. Technol. A 18(4), 1653-1658, 2000.
29. B. E. Yoldas, "*Investigations of porous oxides as an antireflective coating for glass surfaces*", Appl. Optics 19, 1425-1429, 1980.

30. J. E. Sundgren, H.T.G. Hentzell, "*A review of the Present State of Art in Hard Coatings Grown from the Vapor Phase*", J. Vac. Sci. Technol. A 4, 2259-2279, 1986.

31. T. Maruyama and S. Arai, "*Aluminum Oxide Thin Films Prepared by Chemical Vapor Deposition from Aluminum acetylacetonate*", Appl. Phys. Lett. 60(3), 322-323, 1992.

32. A.R. Barron "*Insulating Materials*" in W.S. Rees, Jr., "*CVD of Nonmetals*", VCH, Weinheim 1996.

33. A. M. Huntz, M. Andrieux, M. Herdst-Ghysel, C. Huet, C. Vahlas, D. Samelor, M. Sovar, and A. Gleizes, "*De-hydration and Phase Transformations of MOCVD Processed Alumina coatings Investigated by Temperature-Induced Deflection of dissymmetrical samples*", (EUROCVD-15, Bochum, Germany), ECS Proceeding Vol. 2005-09, 1037-1044, 2005.

34. N. Bahlawane, S. Blittersdorf, K. Kohse-Höinghaus, B. Atakan, J. Müller, "*Investigating of CVD Processes to Perform Dense α-Alumina Coating on Superalloys*", J. ECS, 151, C182-186, 2004.

35. S. K. Pranhan, P. J. Reucroft and Y. Ko, "*Crystallinity of Al_2O_3 Films Deposited by Metalorganic Chemical Vapor Deposition*", Surf. Caot. Technol. 176, 382-384, 2004.

36. J. Müller, M. Schierling, E. Zimmermann, D. Neuschütz, "*Chemical Vapor Deposition of Smooth α-Al_2O_3 Films on Nickel Base Superalloys as diffusion Barriers*", Surf. Coat. Technol. 16, 120-121, 1999.

37. S. Blittersdorf, N. Bahlawane, K. Kohse-Hoinghaus, B. Atakan and J. Muller, "*CVD of Al_2O_3 Thin Films Using Aluminum Tri-isopropoxide*", Chem. Vap. Deposition, 9, No. 4, 194-198, 2003.

38. J. M. Schneider, W.D. Sproul, A. Matthews, "*Reactive Ionized Magnetron Sputtering of Crystalline Alumina coatings*", Surf. Coat. Technol. 98, 1473-1476, 1998.

39. M. P. Singh and S.A. Shivashankar, "*Low –pressure MOCVD of Al_2O_3 Films Using Aluminium Acetylacetonate as Precursor: Nucleation and Growth*", Surf. Coat. Technol. 161, 135-143, 2002.

40. J. von Hoene, R.G. Charles, W.M. Hickam," *Thermal Decomposition of Metal Acetylacetonate Mass Spectrometer Studies*", J. Phys. Chem., 62, 1098-1101, 1958.

41. B. D. Fahlman, A.R. Barron, "*Substituent effects on the volatility of metal β-diketonates*", Adv. Mater. Opt. Electron. 10, 223-232, 2000.

42. NIST Chemistry Web Book, Online-Database, *http://webbook.nist.gov.*

43. M.A. Siddiqi, B. Atakan, to be published.

44. B. Schrader, "*Raman/Infrared Atlas of Organic Compounds*", VCH, Weinheim, 1989.

45. R. A. Lula, "*Stainless Steel*", American Society for Metals, Ohio, 1993.

46. V. A. Haanappel, D. vendel, H. Metselaar, H. Van Corbach, T. Fransen and P. Gellings, "*The Mechanical Properties of Thin Alumina Films Deposited by Metal-Organic Chemical Vapor Deposition*", Thin Solid films, 254, 153-163, 1995.

47. Landolt-Bornstein, New Series, Group IV, Vol. 5.a, Vol. 7, Springer, Berlin.

48. A. Muhsin, C. Pflitsch, U. Bergmann and B. Atakan, "*Growth of Thin Aluminium Oxide films on Stainless Steel by MOCVD at Ambient Pressure*", (EUROCVD-15, Bochum, Germany), ECS Proceeding Vol. 2005-09, 1045-1050, 2005.

49. C. Pflitsch, A. Muhsin, U. Bergmann and B. Atakan, "*Growth of Thin Aluminium Oxide films on Stainless Steel by MOCVD at Ambient Pressure and by using a Hot-Wall CVD-Setup*", Surf. Coat. Technol. 1-2, Vol.201, 73-81, 2006.

50. M.A. Siddiqi, B. Atakan, *"Vapor-Liquid Equilibrium of Ferrocene in some Organic Solvents Using Spectroscope Methods"* J. Chem. Eng., 51, 1092-1096, 2006.

51. M.C. Bost, J.E. Mahan, "*Optical Properties of Semiconducting Iron Disilicide Thin films*", J. Appl. Phys. 58(7), 2696-2703, Oct. 1985.

52. M. Milosavljevic, G. Shao, N. Bibic, C.N. McKinty, C. Jeynes and K.P. Homewood, "*Amorphous-Iron Disilicide: A promising Semiconductor*", Appl. Phys. Lett., Vol. 79, No. 10, 1438-1440, Sep. 2001.

53. J. Schumann, H. Griessmann and A. Heinrich, "*Doped β-$FeSi_2$ as Thin Film Thermoelement Sensor Material*", 17th International conference on Thermoelectrics, p.221-225, 1998.

54. E. Arushanov, "*Possible New Material Candidate for Solar Cell Application*", Moldavian J. of the Phys. Sci., Vol. 1, N4, 2002.

55. X.B. Zhao, T.J Zhu, S.H Hu, B.C. Zhou and Z.T. Wu, "*Transport Properties or Rapid Solidified Fe-Si-Mn-Cu Thermoelectric Alloys*", J. Alloys Comp. 306, 303-306, 2000.

56. O. Wan T.H. Wang and C.L. Lin, "*Synthesis and Optical Properties of Semiconducting beta-$FeSi_2$ Nanocrystals*", App. Phys. Lett. Vol.82, 19, 32243226, May 2003.

57. U. Sstarke, W. Weiss, M. Kutschera, R. Bandorf, and K. Heiny, "*High Quality Iron Silicide Films by Simultaneous Deposition of iron and Silicon on Si(111)*",

J. Appl. Phys. 91, 6154-6161, May 2002.

58. P. Muret, I. Ali and M. Brunel, "*Semiconducting Iron Silicide Thin Films on Silicon (111) with Large Hall Mobility and Low Residual electron Concentration*", Semicond. Sci. Technol. 13, 1170-1179, 1998.
59. J.H. Je, H.K. Kim and D.Y. Noh, "*Amorphous Silicide and Crystalline Fe Film Grown on Si(001) by Radio-Frequency magnetron Sputtering*", J. Mater. Res., Vol. 14, No 4, 1658-1663, Apr. 1999.
60. A. H. Reader, J.P.W.B. Duchateau, J. Timmers and F.J.G. Hakkens, "*Epitaxial β-$FeSi_2$ formed by Fe Deposition on Hot Si(001)*", Appl. Sur. Sci. 73, 131-134, 1993.
61. J.L. Regolini, F.Trincat, I. Berbezier, and Y. Shapira, "*Selective and Epitaxial Deposition of β-$FeSi_2$ on Silicon by Rapid Thermal Processing-Chemical Vapor Deposition Using a Solid Iron source*", Appl. Phys. Lett, 60(8), 956-958, Feb. 1992.
62. H. Chen, P.Han, X.D. Huang and Y.D. Zheng, "*Solid Phase Epitaxy of β-$FeSi_2$ on Si (100)*", J. Vac. Sci. Technol. A 14(3), 905-907, 1996.
63. J.H. Oh, S.K. Lee, K.P. Han, K.S. An, C.Y. Park, "*Effects of the Heat Treatments on the Growth and Formation of Iron Silicide on Si(100)*", Thin Solid Films, 341, 160-164, 1999.
64. G. Molnar, L. Dozsa, G Peto, Z. Vertesy, A.A, Koos, Z.E. Horvath, E. Zsoldos, "*Thickness Dependent Aggregation of Fe-Silicide Islands on Si Substrate*", Thin Solid Films, 459, 48-52, 2004.
65. M. Takauji, N. Seki, T. Ssuemasu, F. Hasegawa and M. Ichida, "*Growth of Si/ β-$FeSi_2$/Si double-heterostructures on Si(111) Substrate by Molecular-Beam Epitaxy and Photoluminescence using Time-Resolved Measurements*", J. Appl.

Phys. Vol.96,No 5, 2561-2565, Sep. 2004.

66. K. Akiyama, S. Ohya, H. takano, N. Kieda and H. Funakubo, "*Growth of β-$FeSi_2$ Thin Film on Si(111) By Metal-Organic Chemical vapor Deposition*", Jpn. J. Appl. Phys. Vol. 40, L 460- L 462, 2001.
67. K. Akiyama, S. Ohya, S. Konuma, K. Numata and H. unakubo, "*Composition Dependence of Constituent Phase of Fe-Si Thin Film Prepared by MOCVD*", J. Crys. Growth 237-239, 1951-1955, 2002.
68. T. Kimura, K. Akiyama, T. Watanabe, K. Saito and H. Funakubo, "*Crystal Structure Analysis of metalorganic chemical Vapor Deposition-β-$FeSi_2$ Thin Film by X-Ray Diffraction measurement*", Jap. J. Phys. Vol.42, 4943-4948, 2003.
69. K. Akiyama, S. Ohya and H. Funakubo, "*Preparation of β-$FeSi_2$ Thin Film by Metal Organic Chemical Vapor deposition using Iron-Carbonyl and Mono-Silane*", Thin Solid Films 461, 40-43, 2004.
70. K. Akiyama, T. Kimura, T. Suemasu, M. hasegawa, Y. Maeda, and H. Funakubo, "*Growth of Epitaxial β-$FeSi_2$ Thin Film on Si (001) by Metal-Organic Chemical Vapor deposition*", Jpn. J. Appl. Phys. Vol. 43, L 551- L 553, 2004.
71. M. Mukaida, I. Hiyama, T. Tsunoda and Y. Imai, "*Preparation of Fe-Si Thin Films by Chemical Vapor Deposition*", 17th International conference on Thermoelectrics, p.237-240, 1998.
72. M. Mukaida, I. Hiyama, T. Tsunoda and Y. Imai, "*Preparation of β-$FeSi_2$ Thin Films by Chemical Vapor Deposition*", Thin Solid Films 381, 214-218, 2001.
73. T. Yoshitake, M. Yatabe, M. Itakura, N. Kuwana, Y. Tomokiyo and K. Nagayama, "*Semiconducting Nanocrystalline Iron Disilicide Thin Films*

Prepared by Pulsed-Laser Ablation", App. Phys. Lett. Vol. 83, No. 15, 3057-3059, Oct. 2003.

74. H. Kakemoto, Y. Makita, S. Sakuragi, T. Tsukamoto, "*Synthesis and Properties of Semiconducting Iron Disilicide β-$FeSi_2$*", Jpn. J. Appl. Phys. Vol.38, 5192-5199, 1999.
75. K.C. Kim, K.S. Nahm, Y.B. Hahn, Z.S. Lee and H. Byun, "*Kinetic Study of 3C-SiC Growth on Si by Pyrolyzing Tetramethylsilane in Low Pressure Radio Frequency-Induction Heated Chemical Vapor Deposition Reactor*", J. Vac. Sci. Technol. A 18(3), 891-899, May/Jun 2000.
76. F.D. Duminica, F. Maury, C. Vahlas, F. Sencocq and T. Delsol, "*Growth of iron Thin Films by AP-MOCVD Starting From Ferrocene and H_2O*", (EUROCVD-15, Sep. (5-9) 2005, Bochum, Germany), ECS Proceeding Vol. 2005-09,644-651, 2005.
77. T. Delsol, F. Maury and F. Senocq, "*Thin Films of Iron from Fe(CO)5 under Atmospheric Pressure*", (EUROCVD-15, Sep. (5-9) 2005, Bochum, Germany), ECS Proceeding Vol. 2005-09, 638-643, 2005.
78. M. Milosavljevic, G. Shao, M. Lourenco, R. Gwilliam, K. Homewood, S. Edwards, R. Valizadeh and J. Colligon, "*Transition from Amorphous to Crystalline Beta Phase in Co-Sputtered $FeSi_2$ Films as a Function of Temperature*", J. Appl. Phys. 98, 123506(1-6), 2005.

Mechanical Drawing of HLR

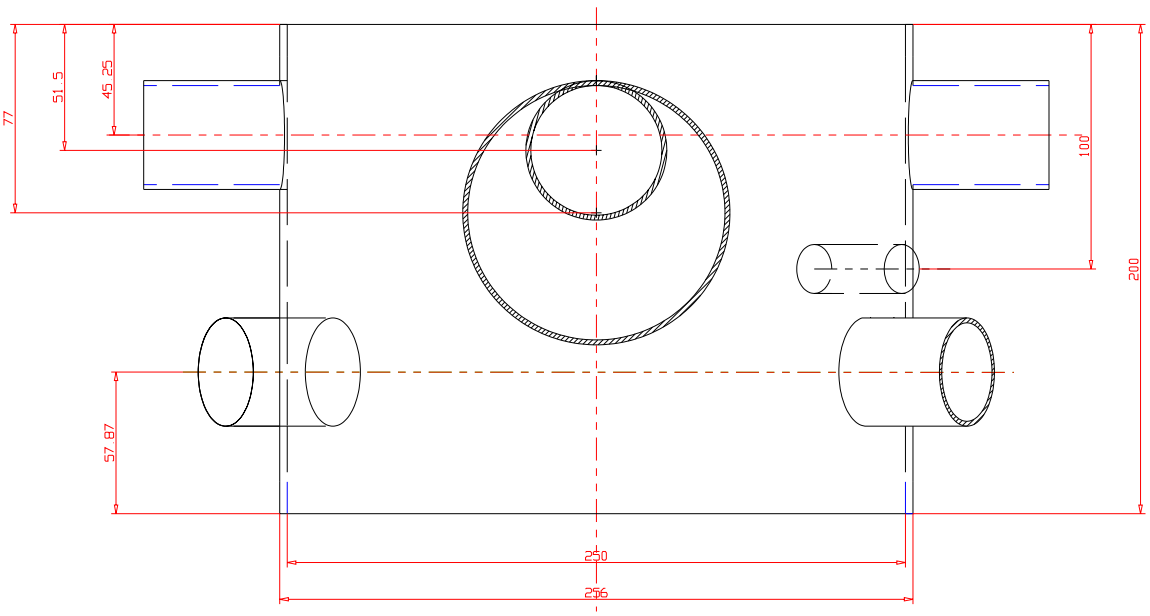

University of Duisburg -Essen Department of Mechanical Engineering		
Job Title: Halogen lamp reactor		
Drg. Title: DN 250 Body of the Reactor		
Drg. No.:	Rev.:	Issued:
Scale:	Date:2003	Drawn by: Ali Muhsin
Approved: Prof. Atakan		

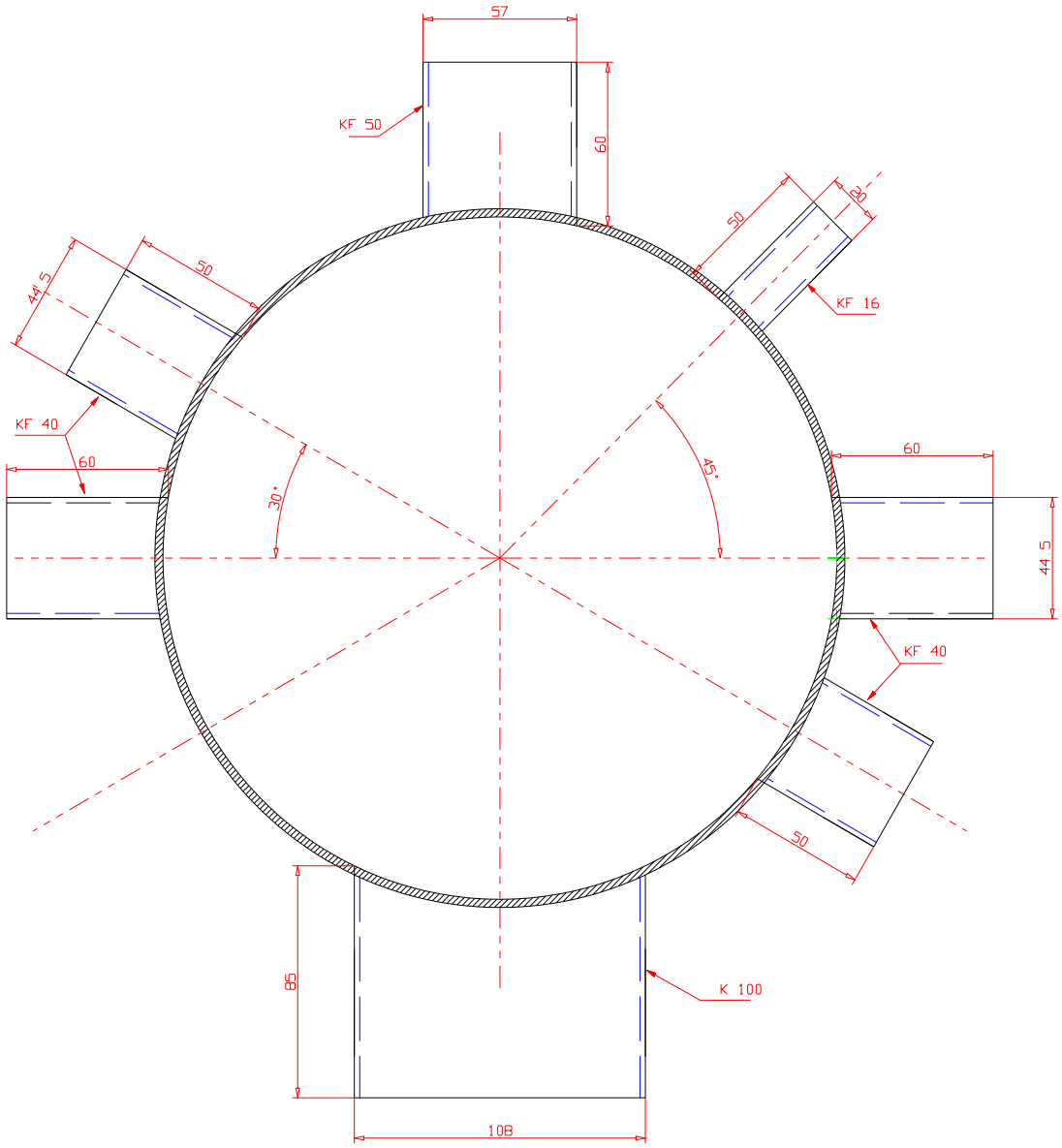

University of Duisburg -Essen Department of Mechanical Engineering		
Job Title: Halogen lamp reactor		
Drg. Title: DN 250 Body of the Reactor		
Drg. No.:	Rev.:	Issued:
Scale:	Date:2003	Drawn by: Ali Muhsin
Approved: Prof. Atakan		

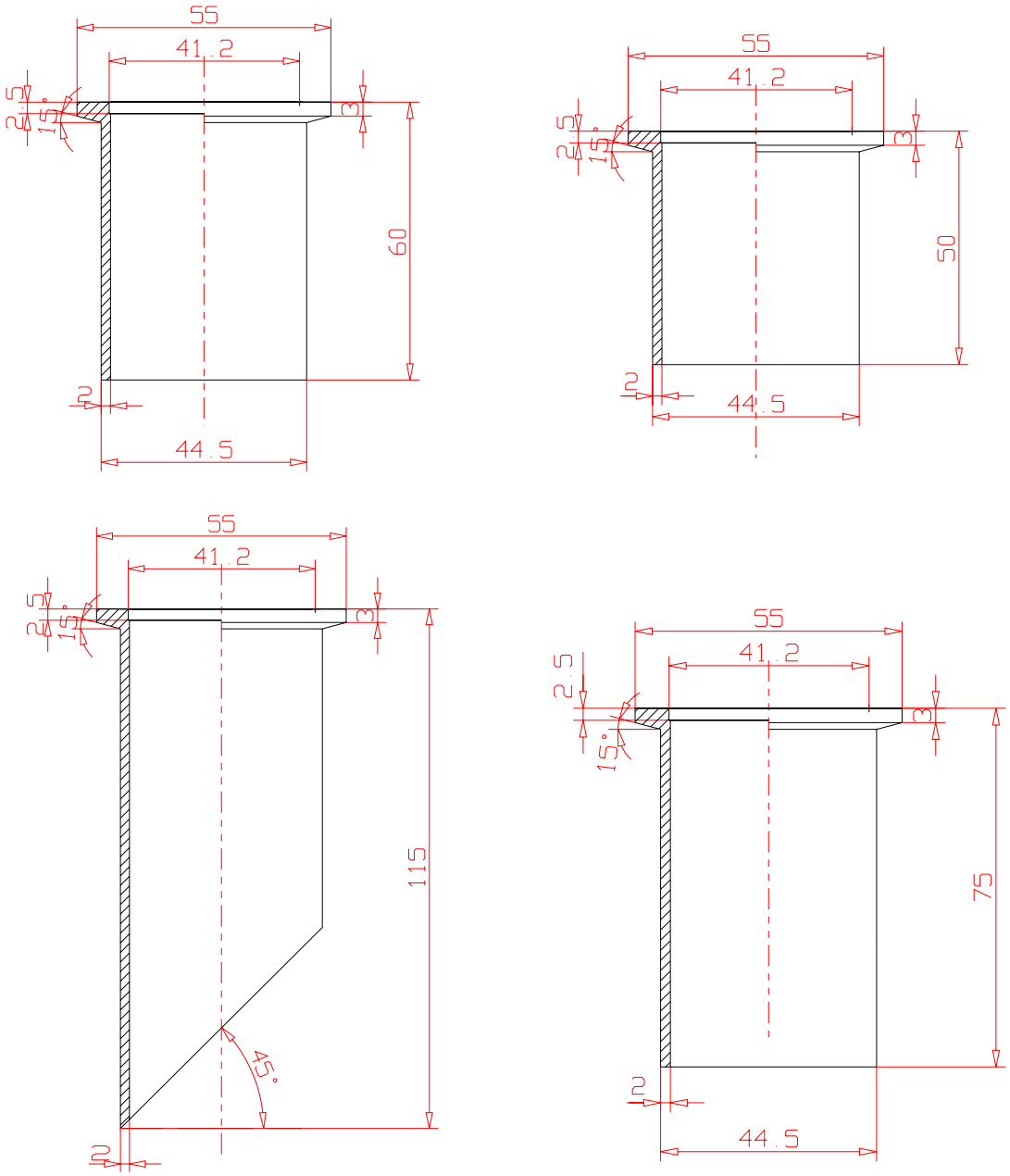

University of Duisburg -Essen Department of Mechanical Engineering		
Job Title: Halogen lamp reactor		
Drg. Title: DN 50 ISO-KF Flanges		
Drg. No.:	Rev.:	Issued:
Scale:	Date:2003	Drawn by: Ali Muhsin
Approved: Prof. Atakan		

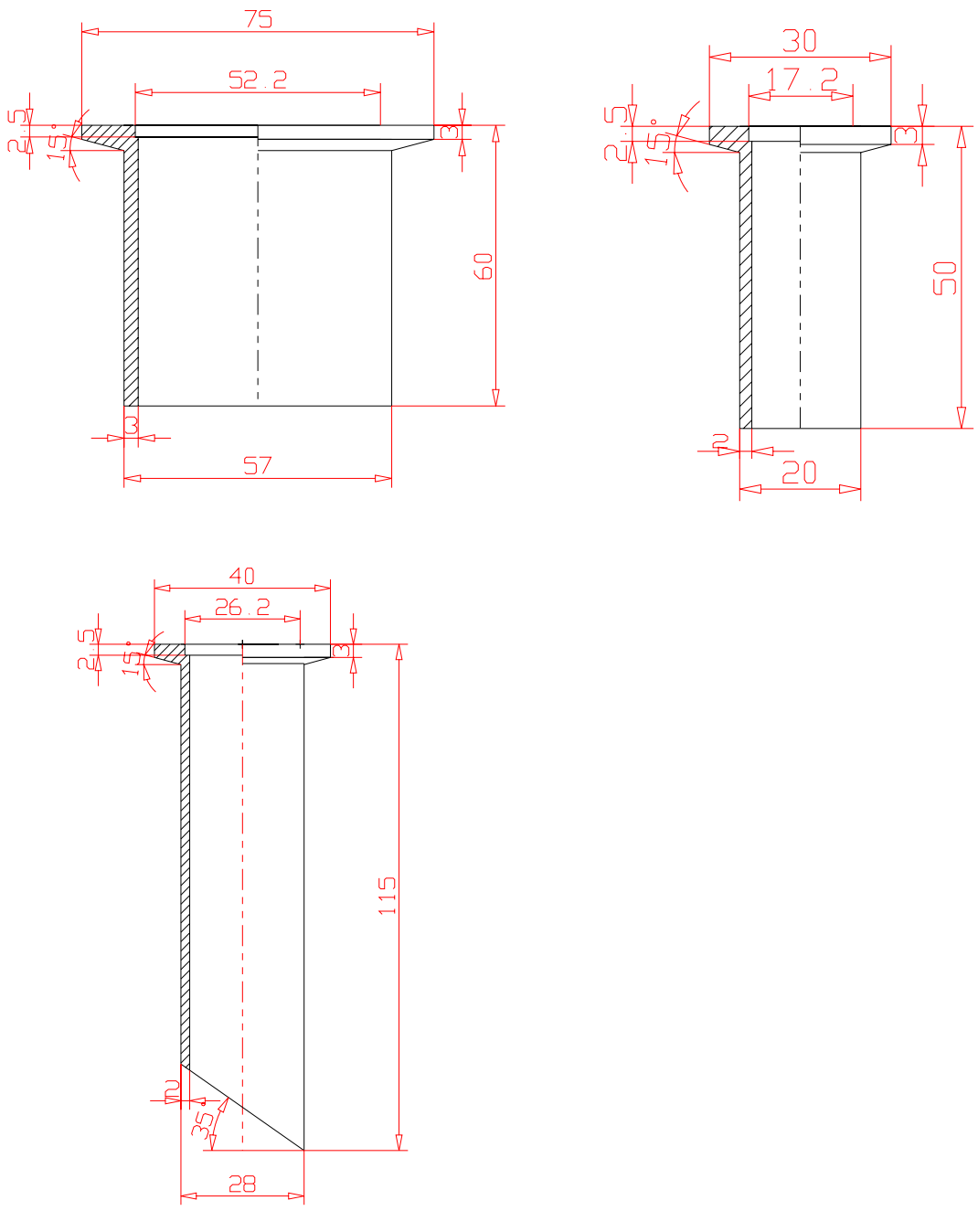

University of Duisburg -Essen Department of Mechanical Engineering		
Job Title: Halogen lamp reactor		
Drg. Title: DN 16,25,50 ISO-KF		
Drg. No.:	Rev.:	Issued:
Scale:	Date:2003	Drawn by: Ali Muhsin
Approved: Prof. Atakan		

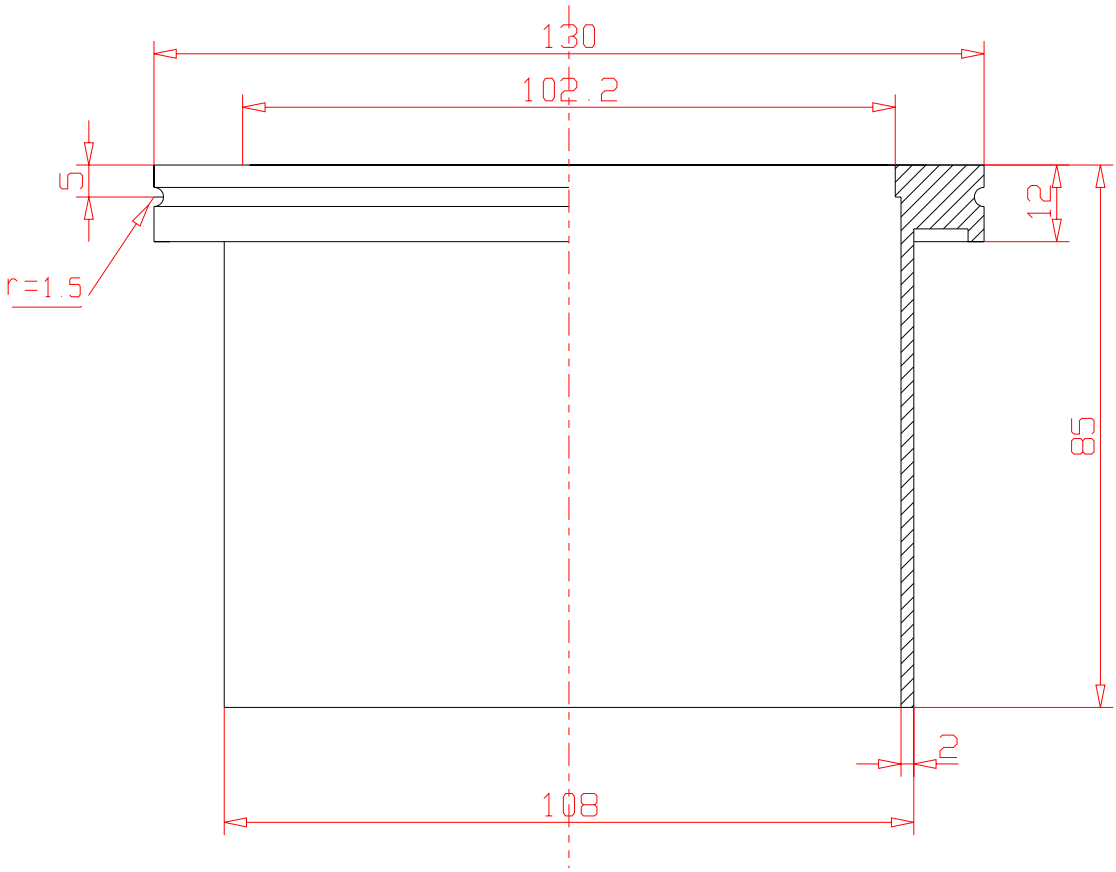

University of Duisburg -Essen Department of Mechanical Engineering		
Job Title: Halogen lamp reactor		
Drg. Title: DN 100 ISO-K		
Drg. No.:	Rev.:	Issued:
Scale:	Date:2003	Drawn by: Ali Muhsin
Approved: Prof. Atakan		

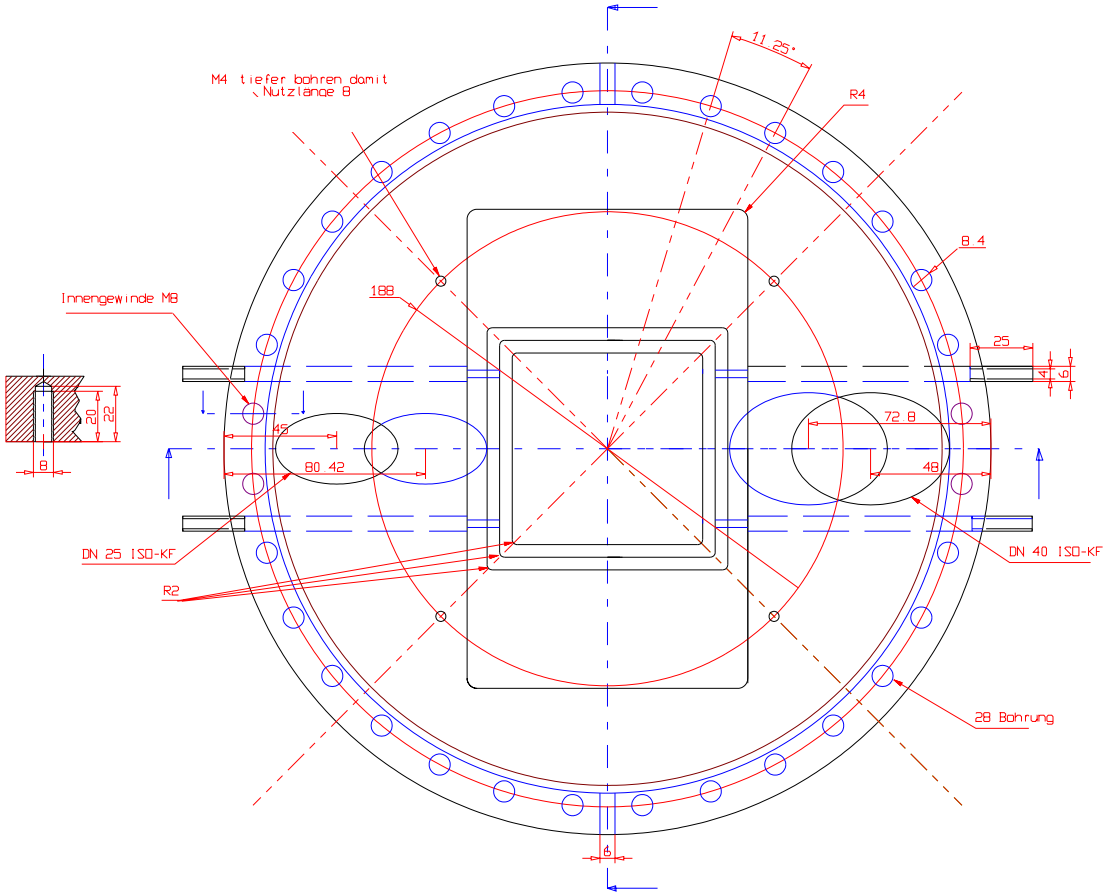

University of Duisburg -Essen Department of Mechanical Engineering		
Job Title: Halogen lamp reactor		
Drg. Title: DN 250 ISO-CF Top Flange		
Drg. No.:	Rev.:	Issued:
Scale:	Date:2003	Drawn by: Ali Muhsin
Approved: Prof. Atakan		

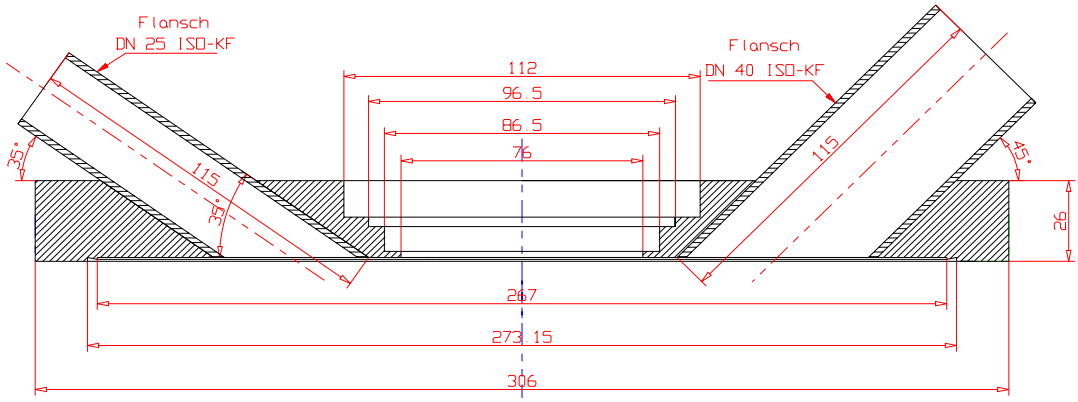

University of Duisburg -Essen Department of Mechanical Engineering		
Job Title: Halogen lamp reactor		
Drg. Title: DN 250 ISO-CF Top Flange Cross-Section		
Drg. No.:	Rev.:	Issued:
Scale:	Date:2003	Drawn by: Ali Muhsin
Approved: Prof. Atakan		

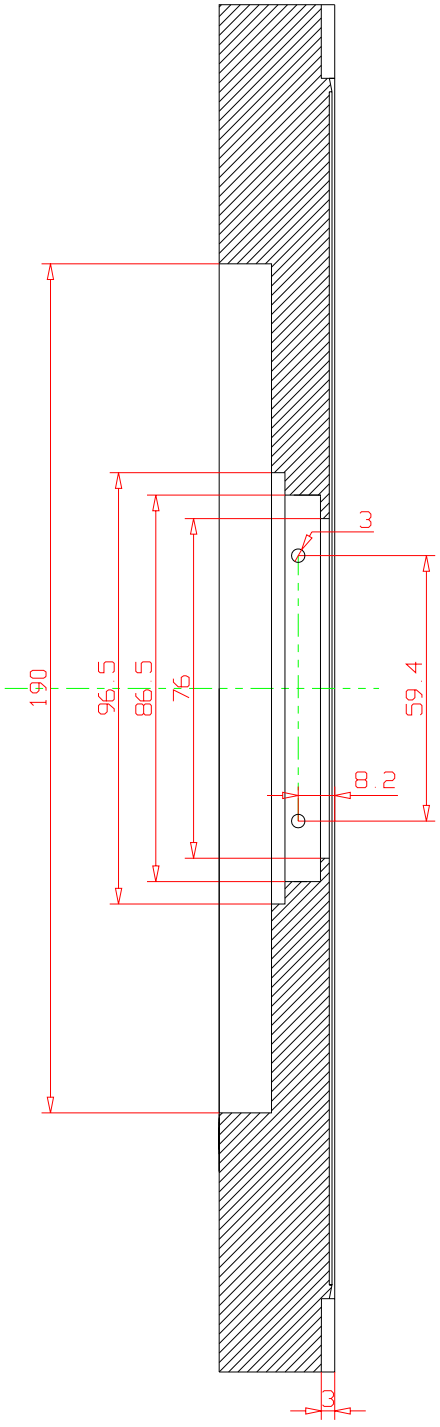

University of Duisburg -Essen Department of Mechanical Engineering		
Job Title: Halogen lamp reactor		
Drg. Title: DN 250 ISO-CF Top Flange Cross-Section		
Drg. No.:	Rev.:	Issued:
Scale:	Date:2003	Drawn by: Ali Muhsin
Approved: Prof. Atakan		

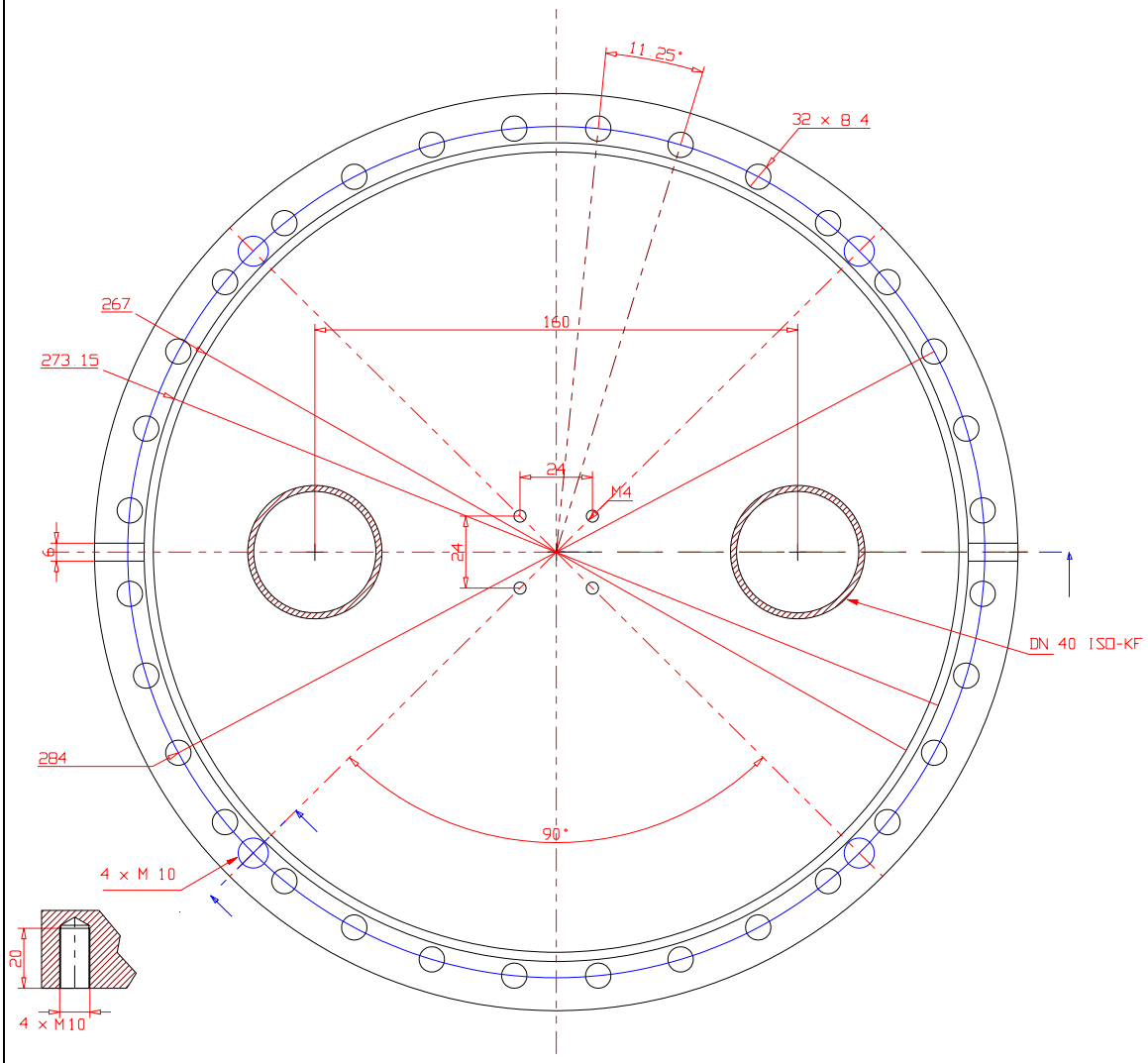

University of Duisburg -Essen Department of Mechanical Engineering		
Job Title: Halogen lamp reactor		
Drg. Title: DN 250 ISO-CF Bottom Flange		
Drg. No.:	Rev.:	Issued:
Scale:	Date:2003	Drawn by: Ali Muhsin
Approved: Prof. Atakan		

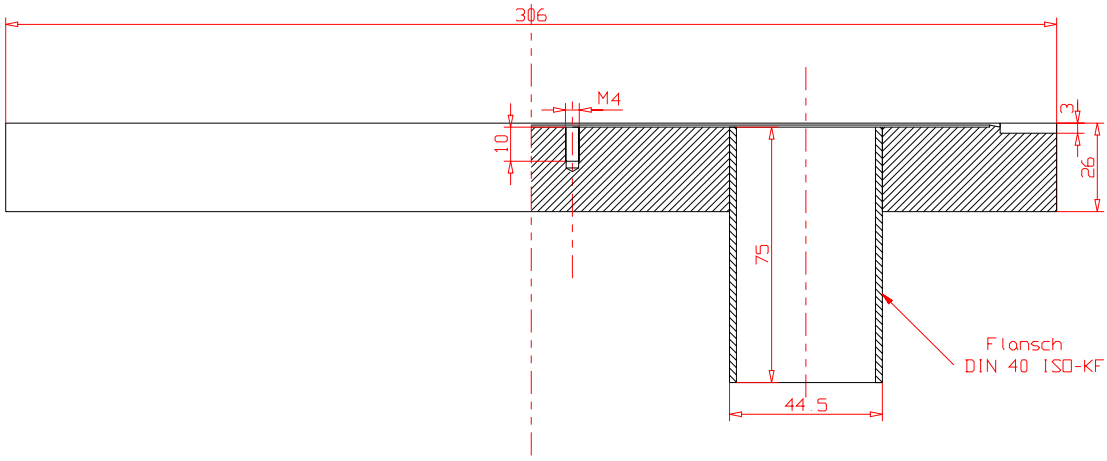

University of Duisburg -Essen Department of Mechanical Engineering		
Job Title: Halogen lamp reactor		
Drg. Title: DN 250 ISO-CF Bottom Flange-Cross Section		
Drg. No.:	Rev.:	Issued:
Scale:	Date:2003	Drawn by: Ali Muhsin
Approved: Prof. Atakan		

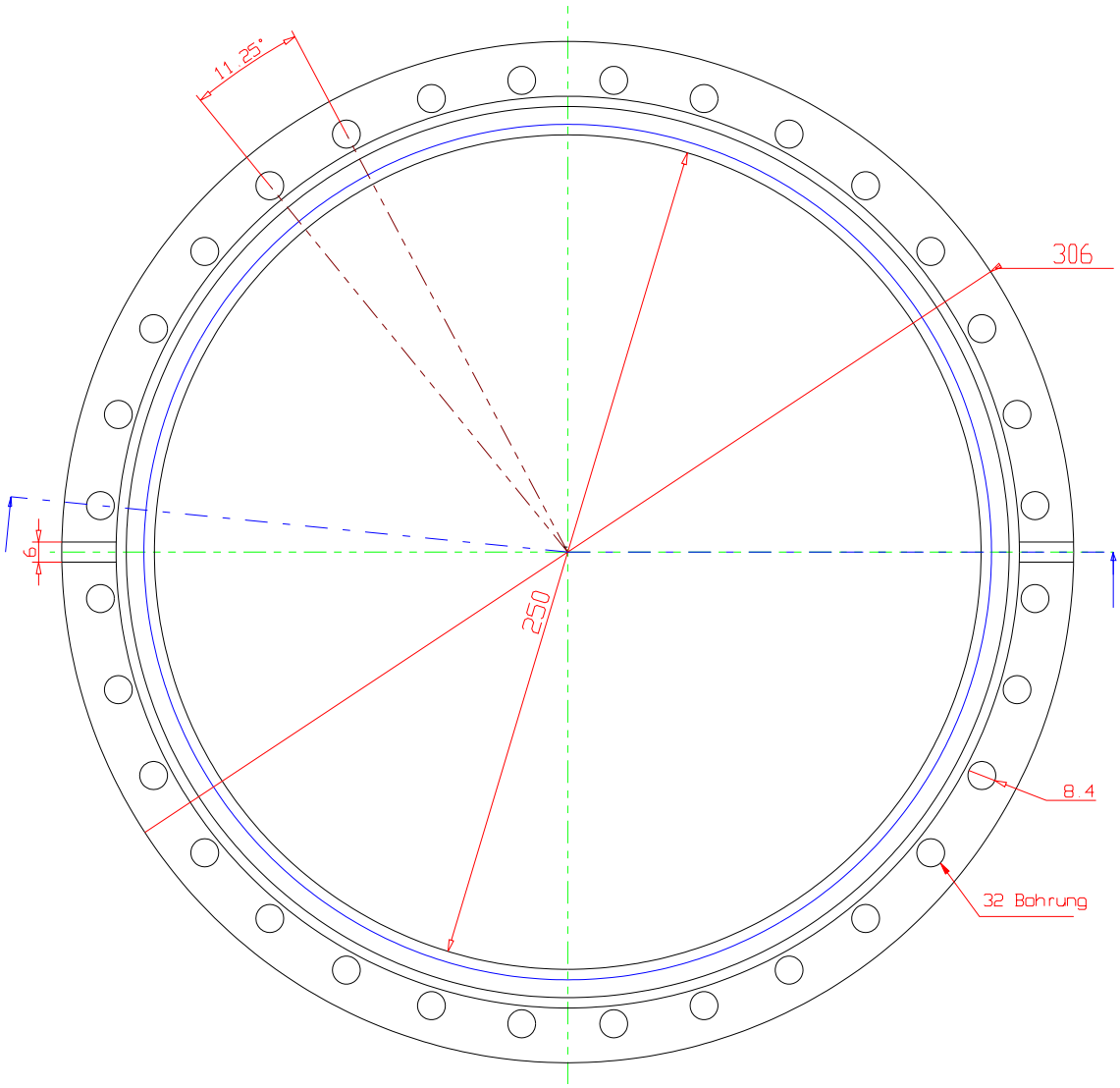

University of Duisburg -Essen Department of Mechanical Engineering		
Job Title: Halogen lamp reactor		
Drg. Title: DN 250 ISO-CF Flange		
Drg. No.:	Rev.:	Issued:
Scale:	Date:2003	Drawn by: Ali Muhsin
Approved: Prof. Atakan		

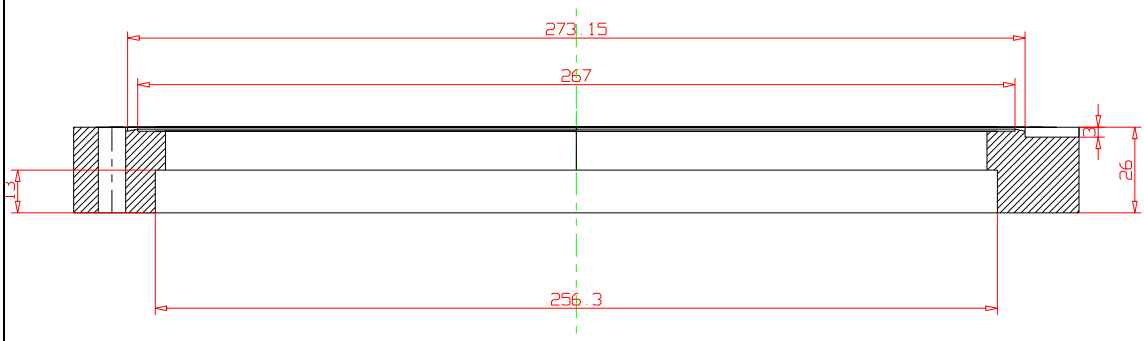

University of Duisburg -Essen Department of Mechanical Engineering		
Job Title: Halogen lamp reactor		
Drg. Title: DN 250 ISO-CF Flange Cross-Section		
Drg. No.:	Rev.:	Issued:
Scale:	Date:2003	Drawn by: Ali Muhsin
Approved: Prof. Atakan		

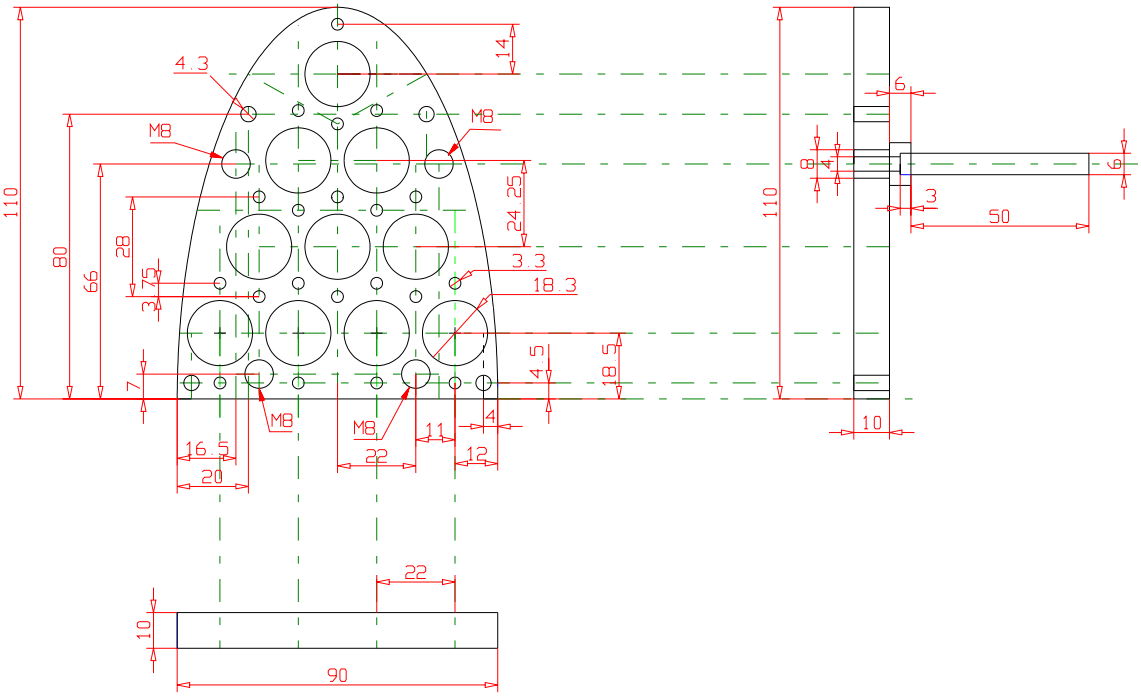

University of Duisburg -Essen Department of Mechanical Engineering		
Job Title: Halogen lamp reactor		
Drg. Title: Halogen lamps holder		
Drg. No.:	Rev.:	Issued:
Scale:	Date:2003	Drawn by: Ali Muhsin
Approved: Prof. Atakan		

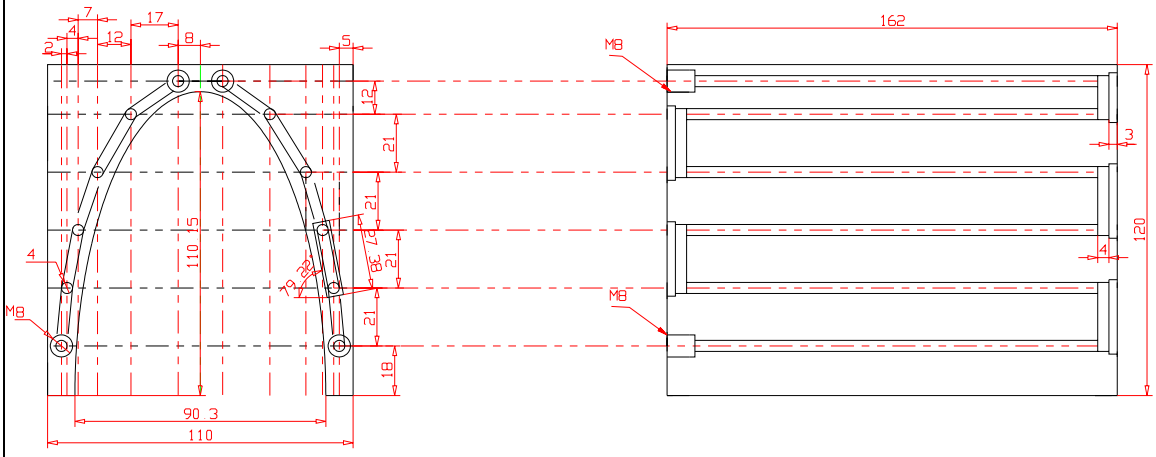

University of Duisburg -Essen Department of Mechanical Engineering		
Job Title: Halogen lamp reactor		
Drg. Title: Aluminium reflector		
Drg. No.:	Rev.:	Issued:
Scale:	Date:2003	Drawn by: Ali Muhsin
Approved: Prof. Atakan		

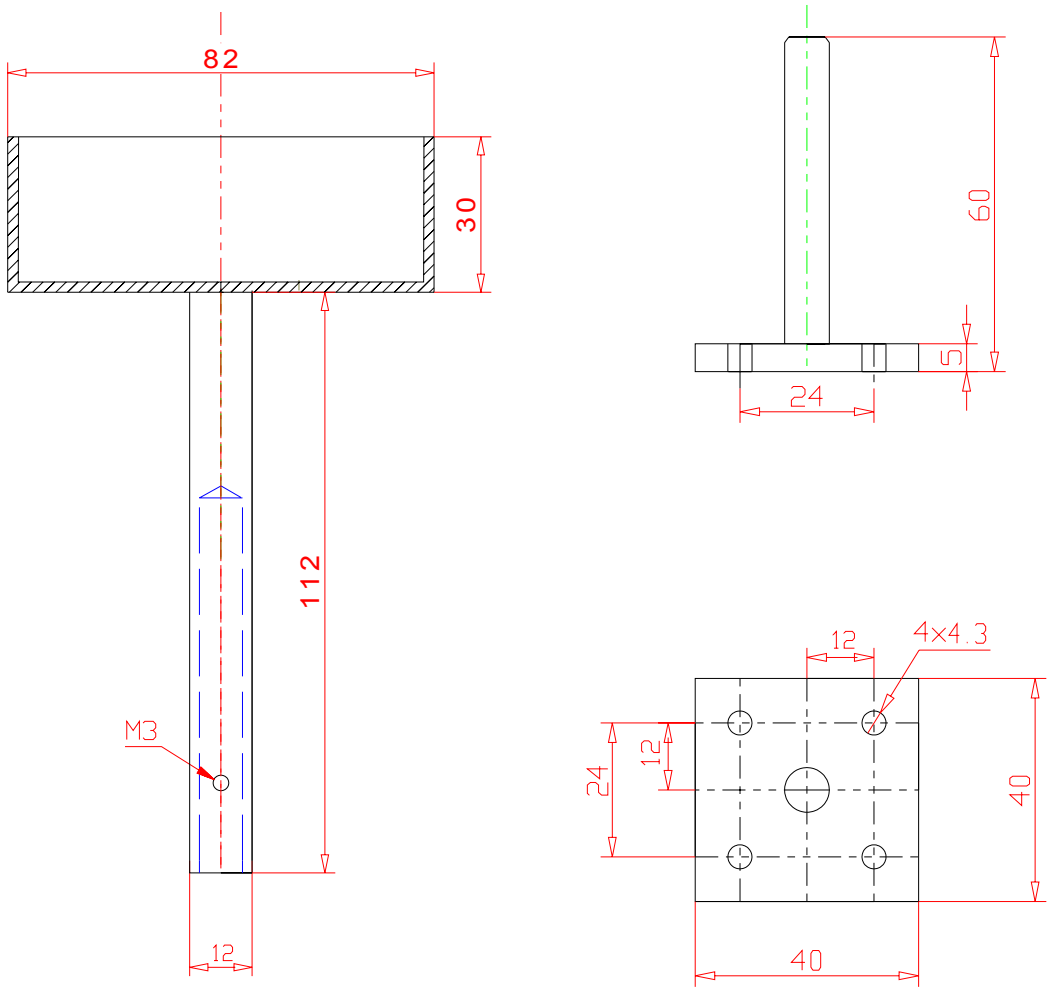

	University of Duisburg -Essen Department of Mechanical Engineering		
	Job Title: Halogen lamp reactor		
	Drg. Title: Substrate Holder		
	Drg. No.:	Rev.:	Issued:
	Scale:	Date:2003	Drawn by: Ali Muhsin
	Approved: Prof. Atakan		

Pictures of HWR-CVD and HLR-CVD Systems

Hot-wall reactor (HWR)

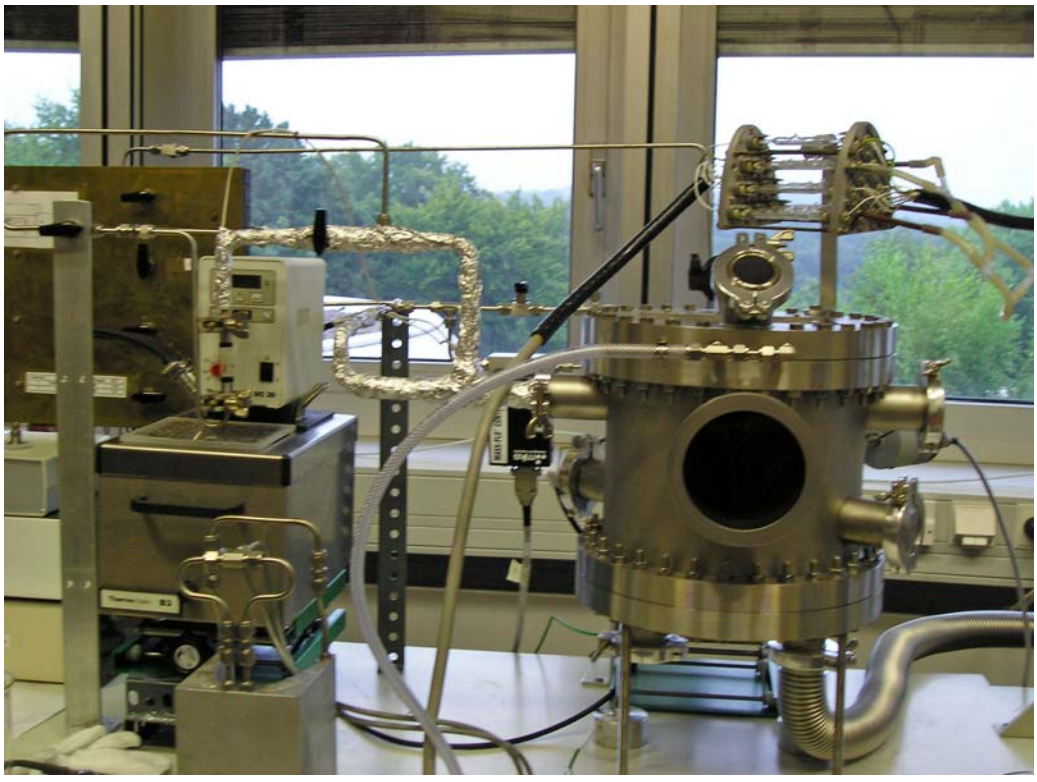

Halogen lamp reactor (HLR)

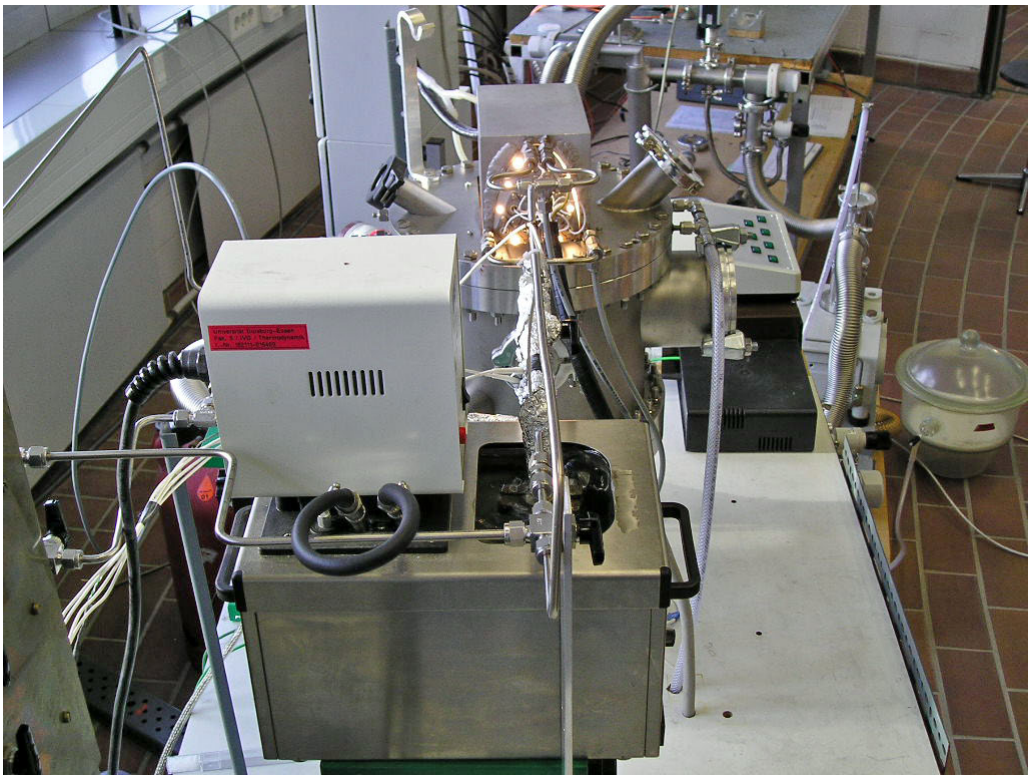

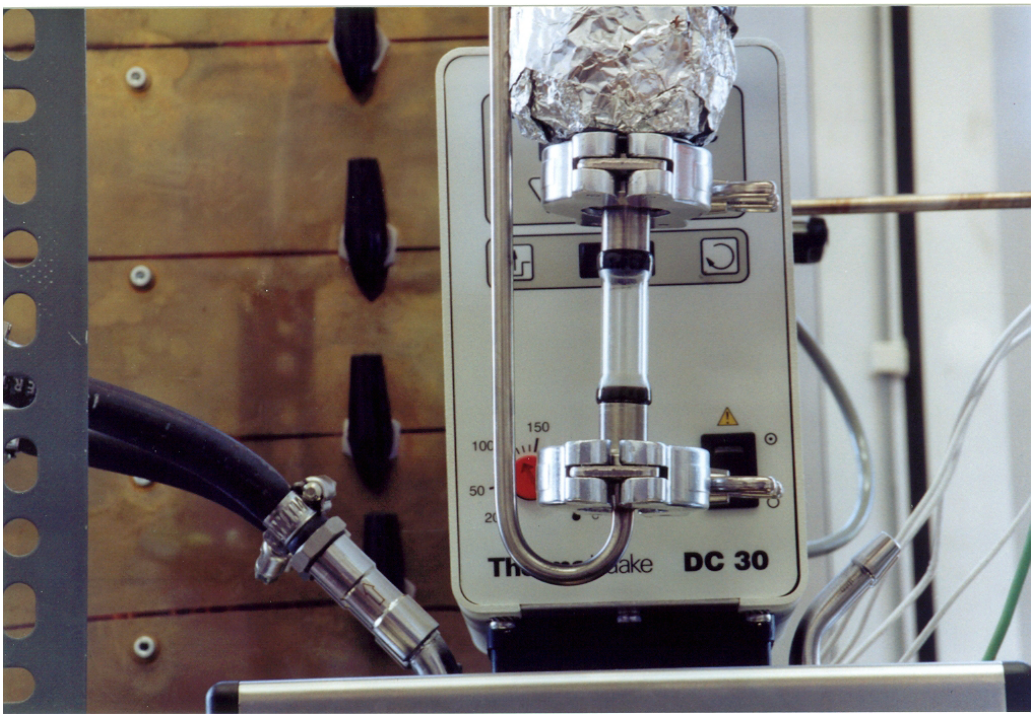

Thermal evaporation system for solid precursors (ferrocene and aluminium acetylacetonate)

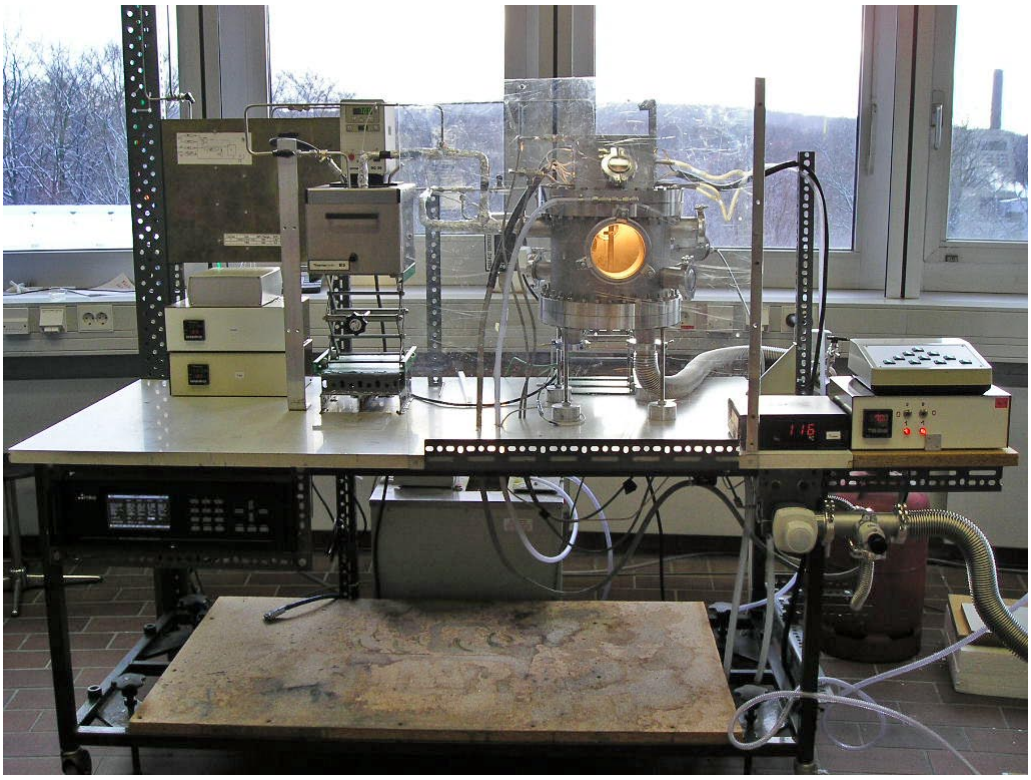

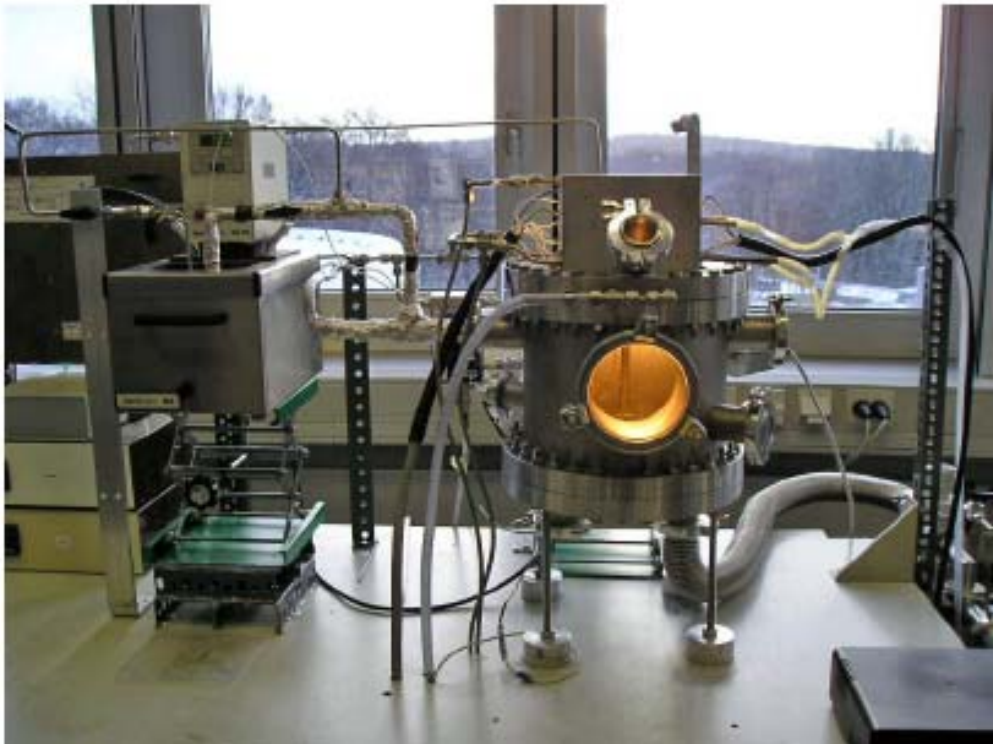

Halogen lamp reactor during deposition process

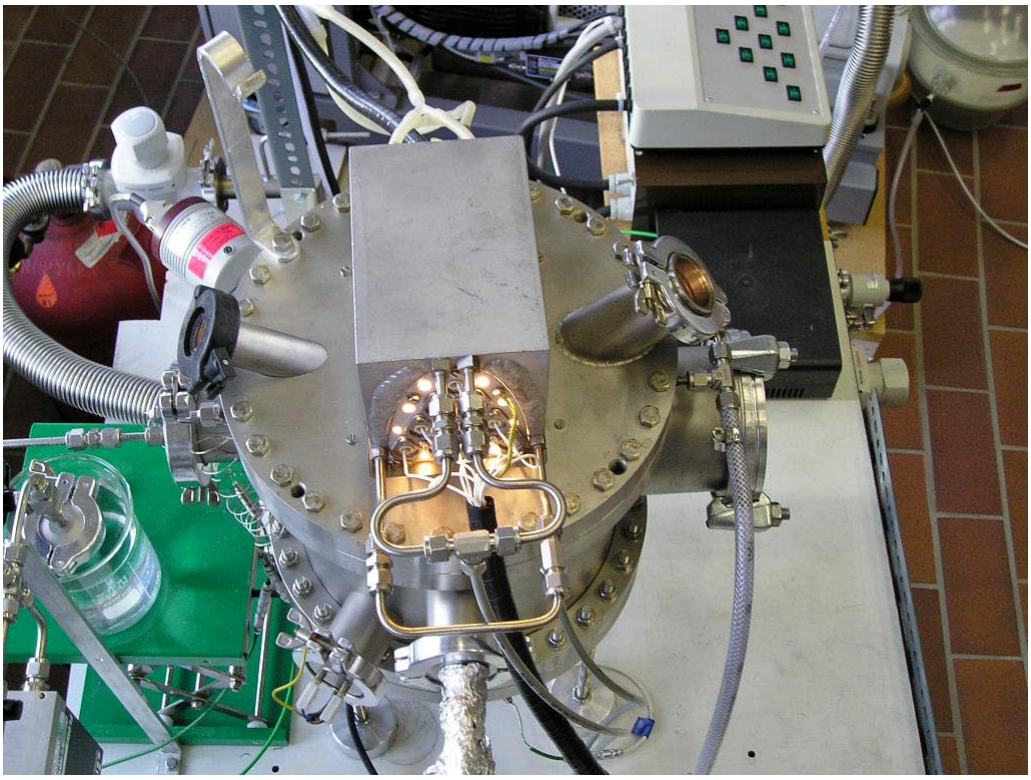

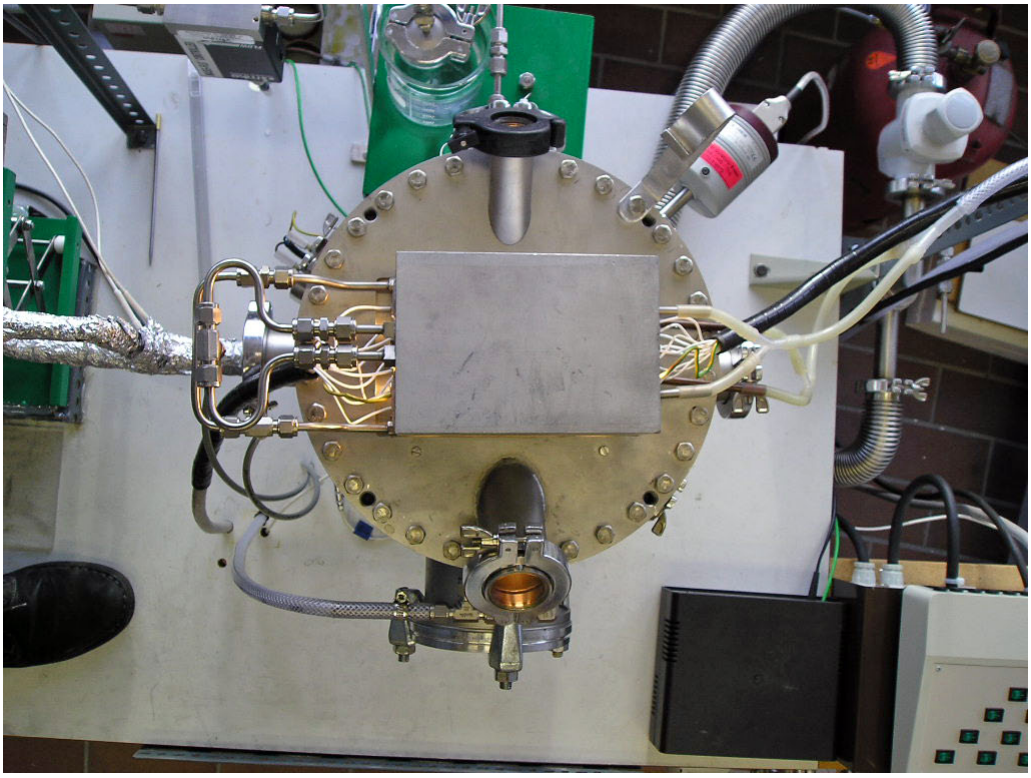

Heater position

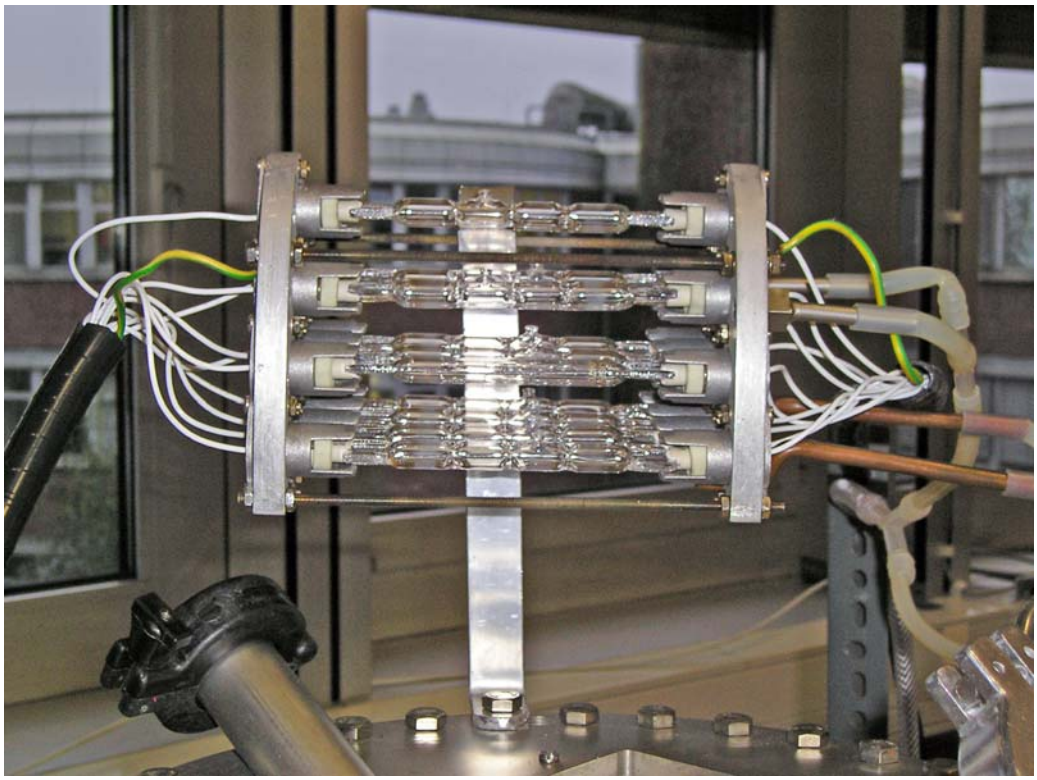

Halogen lamp heater

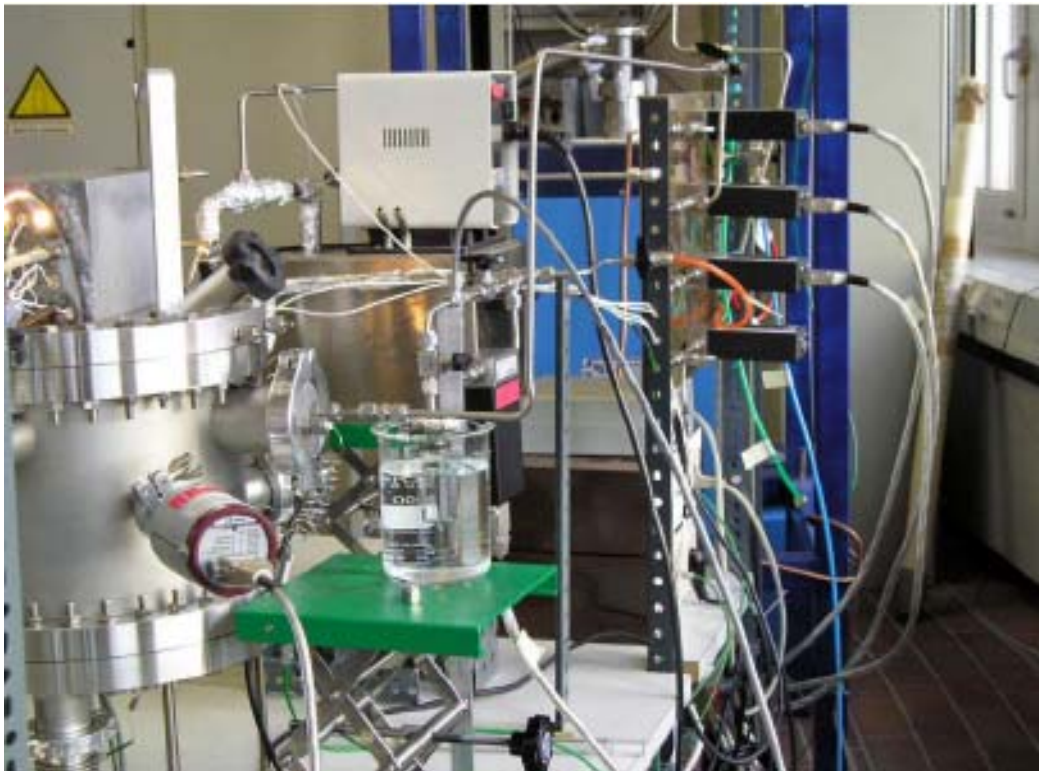

Evaporating system for TMS

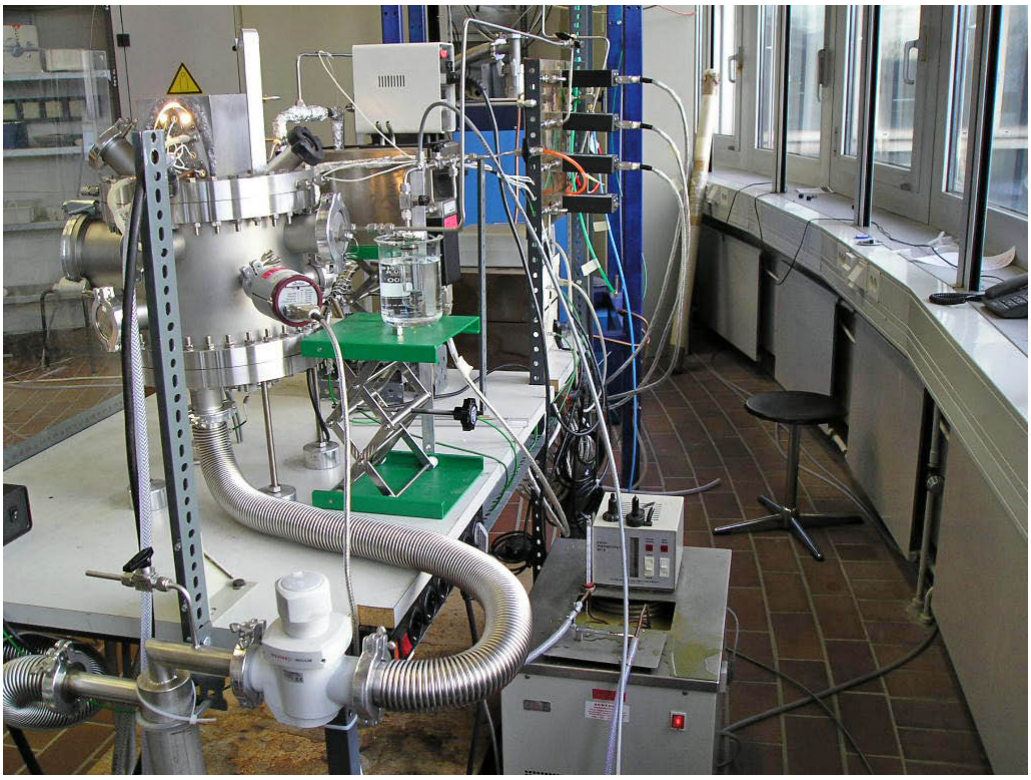

Other components of HLR system

Pictures of deposited Al_2O_3, Fe, Si and β-$FeSi_2$ Films

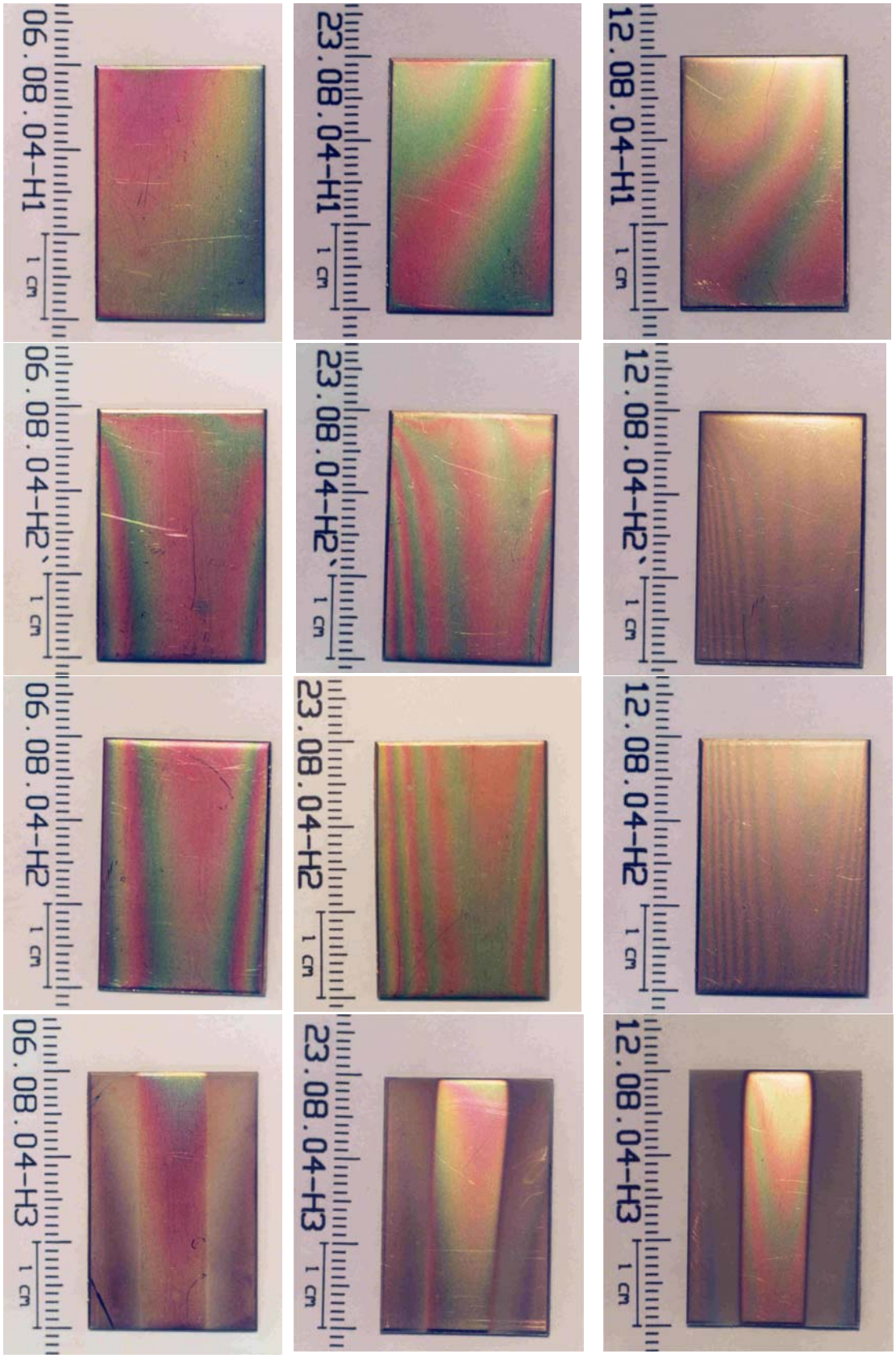

2 hours deposition time | 4 hours deposition time | 8 hours deposition time

Al_2O_3 films

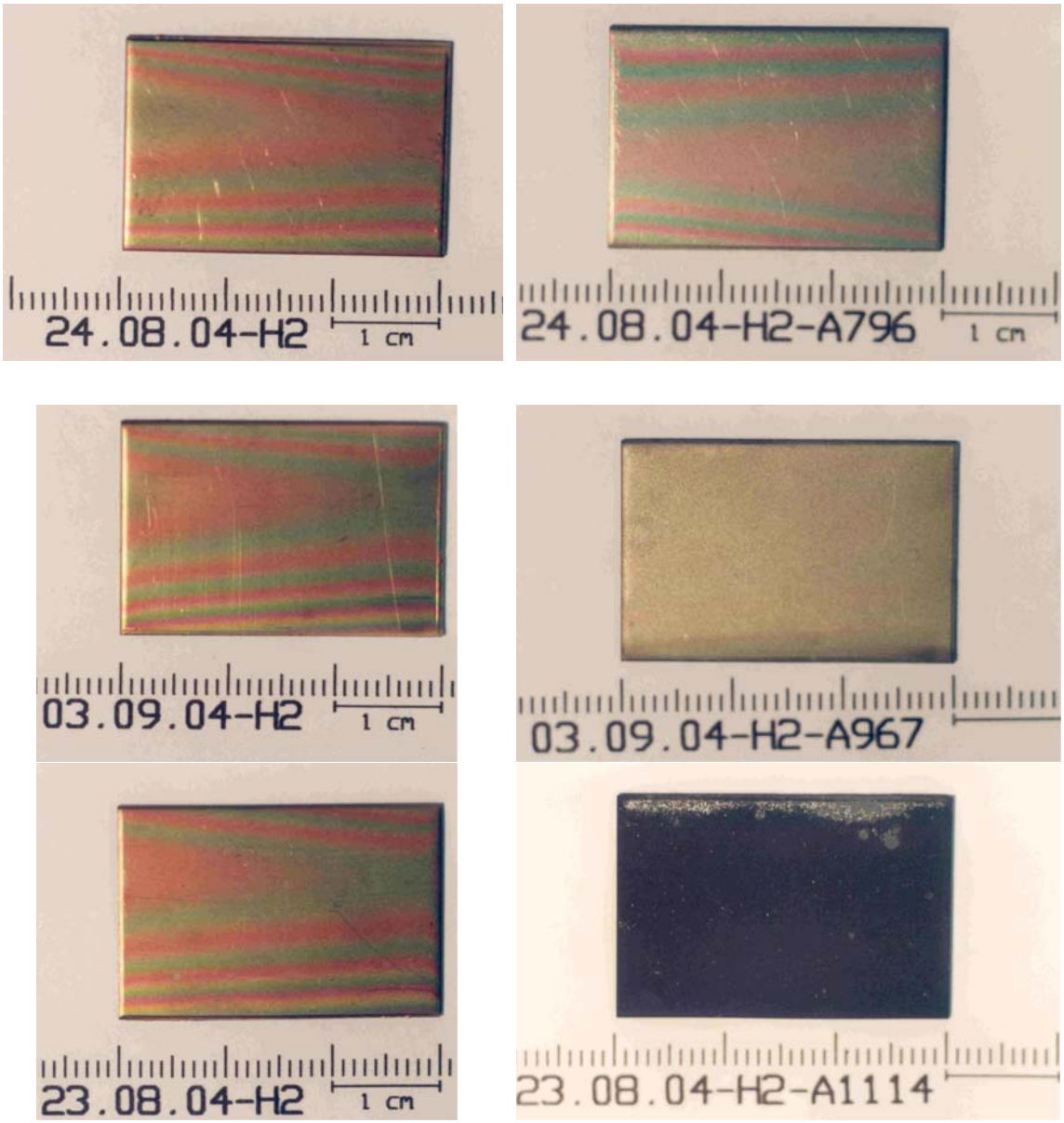

As-deposited films

Films after annealing

Al_2O_3 films

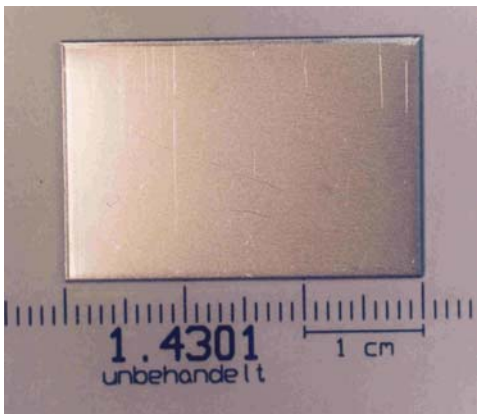

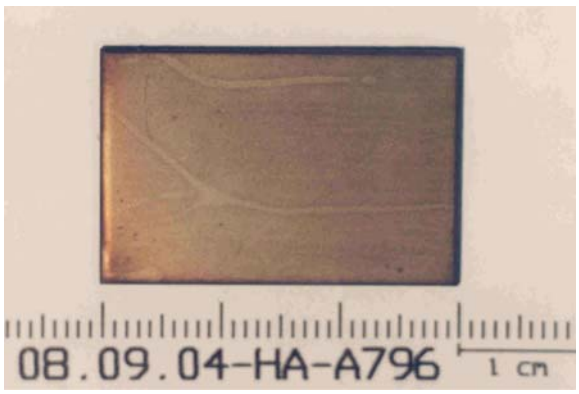

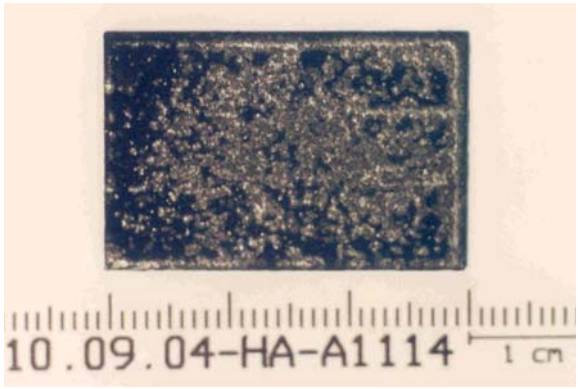

Clean stainless steel substrate before and after annealing

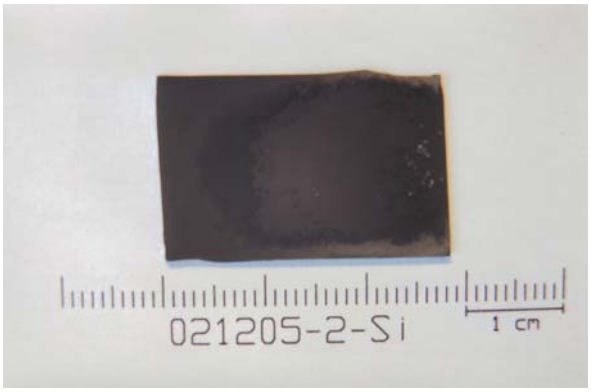

As-deposited film (black powder film)

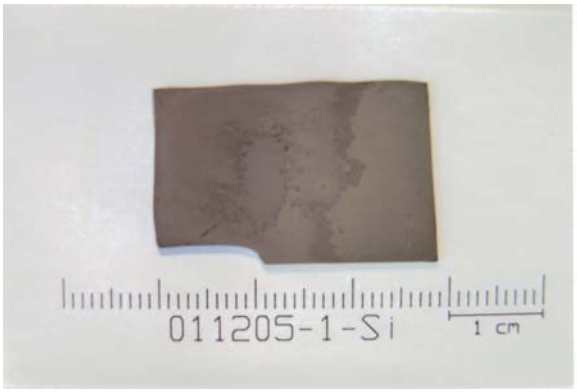

Iron film after treatment with H_2 flow

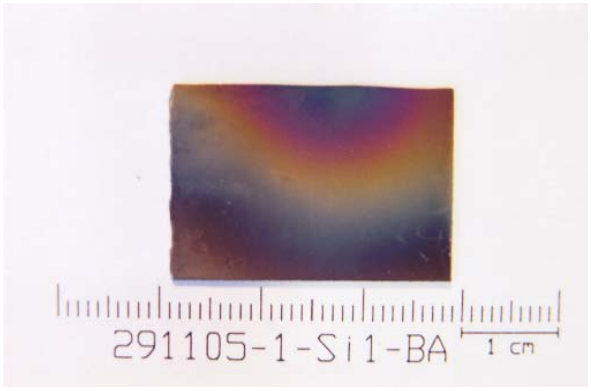

Iron disilicide film (As-deposited by SDT)

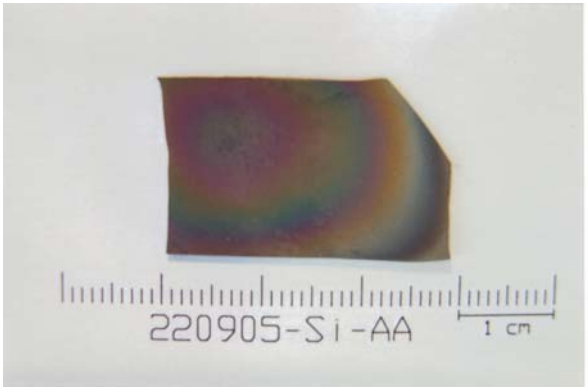

Iron disilicide film (after annealing)

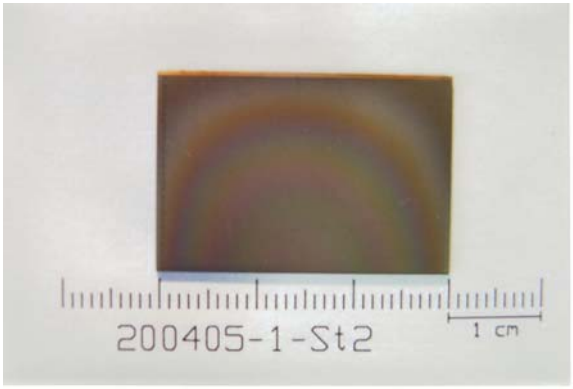

Silicon film